Mathematical modelling of the human cardiopulmonary system

Lin, Jinhuai

Award date:
2007

Awarding institution:
University of Bath

MATHEMATICAL MODELLING OF THE HUMAN CARDIOPULMONARY SYSTEM

Submitted by

Jinhuai Lin

for the degree of Ph.D.

October 2007

COPYRIGHT

ProQuest LLC
789 East Eisenhower Parkway
P.O. Box 1346
Ann Arbor, MI 48106-1346

SUMMARY

This thesis describes the developments of a comprehensive human cardiopulmonary model that combines respiratory and cardiovascular aspects and their associated control actions.

A literature survey indicated a wide variation in the approaches used to model the cardiopulmonary system. The objective of the research reported in this thesis is to develop a comprehensive human cardiopulmonary model with detailed models of the respiratory and cardiovascular systems which is capable of modelling the interaction of the two systems and their responses under different physiological conditions.

The mathematical model developed for the cardiovascular system contained 13 segments including blood vessels and heart chambers. The heart serves as a hydraulic pump and the vessels are distensible pipes configured in a serial and parallel arrangement. The accurate representation of the hemodynamics in various parts of the system and the good fit to published pressure and flow waveforms provided confidence for the incorporation of the baroreflex control model and the respiratory model.

An improved baroreceptor reflex model was developed in this research as a three-compartment model - afferent compartment, central compartment and efferent compartment. A sigmoid function was included in the efferent compartment to produce sympathetic and parasympathetic nerve outflow to the effector sites. The baroreflex action was modelled in a physiological manner and provides a clearer picture of how the baroreflex system works. Simulation results presented show the ability of the model to predict the static and dynamic hemodynamic responses to environmental disturbances.

A respiratory model including the mechanics of breathing, gas exchange process and the regulation of the system was then developed and integrated with the cardiovascular model to form a complete cardiopulmonary model. The cardiopulmonary model was then validated using a number of different test conditions. Possible applications of the model were demonstrated and good agreement was obtained with published data.

ACKNOWLEDGEMENTS

This research has been sponsored by the Department of Mechanical Engineering at the University of Bath.

A huge thank you to Dr. Derek Tilley and Dr. Roger Ngwompo for their excellent supervision and guidance during the course of my research. It was their encouragement and patience that helped me through the highs and lows of my PhD.

I would like to thank Professor Adrian Wilson from the University of Warwick for his assistance in the medical and physiological fields. Thanks as well to Dr. P Pfeffer who gave me the confidence and courage to start my PhD.

I would like to thank my parents who always believe in me and love me (感谢永远相信我和爱我的父母). And also my brother who kept my parents company while I was away from home.

A big thank you to my boyfriend for putting up with me during the final and toughest year of my PhD. Last but not least, thanks goes to Ying Chen, Wan-Jung Chou, Woon-Yik Yong, and the many friends who support me.

This work is dedicated to my dearest grandparents (谨以此献给我最亲爱的爷爷奶奶外公外婆).

CONTENTS

NOTATION

Chapter 2 and Chapter 3

A	Heart valve area (cm^2)
b_v	Bernoulli's resistance (mmHg/ $(ml/s)^2$)
C	Compliance/Capacitance (ml/mmHg)
e	Time varying elastance (mmHg/ml)
$\hat{e}$	Effective time varying elastance with septal coupling (mmHg/ml)
E	Elastance (mmHg/ml)
Es	Elastance of interventricular septum (mmHg/ml)
E_{va}	Amplitude component of exponential Elastance of ventricles (mmHg/ml)
E_{vb}	Baseline component of exponential Elastance of ventricles (mmHg/ml)
E_{aa}	Amplitude component of exponential Elastance of atria (mmHg/ml)
E_{ab}	Baseline component of exponential Elastance of atria (mmHg/ml)
k_{lr}	Left-to-right ventricular pressure gain
k_{rl}	Right-to-left ventricular pressure gain
K_{pc}	Pericardial pressure coefficient (mmHg)
L	Inertance (mmHg/ (ml/s^2))
LV	Left ventricle
P	Pressure (mmHg)
P_v	Ventricular pressure (mmHg)
P_a	Atrial pressure (mmHg)
p_v	Ventricular pressure without considering interventricular septum (mmHg)
PE	Parallel elastic element in Hill's muscle model
P-V	Pressure-volume
Q	Flow (ml)
Q_v	Flow across heart valve (ml/s)
R	Resistance (mmHg/(ml/s))
RV	Right ventricle
R_v	Valve resistance (mmHg/(ml/s))
SE	Series elastic element in Hill's muscle model
t_{ac}	Time atrium begins to contract (s)
t_{ar}	Time atrium begins to relax (s)

t_{ee}	Time of end-ejection at maximum e_v (s)
$T_1 \sim T_{10}$	Time steps in a cardiac cycle (s)
Tr	Time period of cardiac cycle (s)
V	Blood volume (ml)
V_o	Left ventricular volume intercept (ml)
β	changes in venous volume (ml)
Φ	Volume constant (ml)
μ	Viscosity of blood
ρ	Density of blood (g/ml)
τ_{ac}	Time constant for atrial contraction (s)
τ_{ar}	Time constant for atrial relaxation (s)
τ_{vc}	Time constant for ventricular contraction (s)
τ_{vr}	Time constant for ventricular relaxation (s)
Ω	Viscoelastance (mmHg · s/ml)
suffix	
a	Atrium
aa	Aorta
h	Thickness of vascular walls
it	Intrathoracic
l	Length for vascular segment
lv	Left ventricle
pc	Pericardial
r	Radius for vascular segment
rv	Right ventricle
v	Ventricle
vlv	Heart valves

Chapter 4 and Chapter 5

a	Coefficient for heart rate control
CO	Cardiac output (l/min)
f	Nerve frequency (Hz)
G	Gain
H^+	Hydrogen ion
k	Coefficient
MAP	Mean arterial pressure (mmHg)
P_{CO2}	Partial pressure of carbon dioxide (mmHg)
P_{demand}	Arterial pressure at the baroreflex operating point (mmHg)
P_{error}	Pressure difference between demanding and actual pressure (mmHg)
P_{O2}	Partial pressure of oxygen (mmHg)
SNA	Sympathetic nerve activity (Hz)
S	Slopes for the sigmoid function
SV	Stroke volume (ml)
s	Complex variable for Laplace transformation
T	Pure time delay (s)
TPC	Total peripheral conductance ((ml/s)/mmHg)
TPR	Total peripheral resistance (mmHg/(ml/s))
ΔHR	Heart rate change (beats/min)
HR	Heart rate (beats/min)
HR_0	Intrinsic heart rate (beats/min)
τ	Time constant for first order filter (s)
suffix	
aff	Afferent compartment
eff	Efferent compartment
c	Central compartment
s	Sympathetic nerve activity
sv	Interaction between sympathetic and parasympathetic nerve activity
v	Parasympathetic (vagal) nerve activity

Chapter 6 and Chapter 7

A	Area (m^2)
B	Bulb modulus (N/m^2)
C	Gas concentration in the blood
$\hat{C}$	Saturated gas capacity of blood
C_l	Lung compliance (mmHg/ml)
CO_2	Carbon dioxide
D_i	Dispensability (l/bar)
D	Gas diffusion capacity
F_{th}	Thoracic force (N)
F_c	Coulomb resistance force (N)
f	Viscous friction
f_{dv}	Frational dead space
fsh	Frational veno-arterial shunts
G	Gain
k	Stiffness (N/m)
$k_1 \sim k_4$	Chemoreceptor controller constant
M	Mass (kg) / gas molecular weight (kg/mole)
m	Gas mass (kg)
n	Polytropic index
n_e	Number of extra-pulmonary airways
O_2	Oxygen
P	Pressure (bar / mmHg)
PH	pH level
Q	Flow (L/s)
Q_{alv}	Blood flow through the alveolar
q	Mass flow rate (kg/s)
R	Specific gas constant (J/kg K)
Re	Reynolds number
R_o	Universal gas constant (J/mol K)
RQ	Ratio between CO_2 production rate and O_2 consumption rate
S	Gas solubility coefficient L/(L N/m^2)
T	Temperature (K)

t	Time (s)
$\dot{U}$	Gas mass flow rate (kg/s)
V	Volume (L)
V_{frc}	Lung functional residual capacity (L)
$\dot{V}/Q$	Ventilation/perfusion ratio
x	Displacement (l)
$x_1(t)$	Effect of the central chemoreflex on the ventilation
$x_2(t)$	Effect of the peripheral chemoreflex on the ventilation
$y(t)$	Ventilation response (L/s)
ρ	Density (kg/m^3)
ΔG_{SNA}	Percentage change of sympathetic nerve activity gain (%)
ΔMAP	Change of baroreflex operating point (mmHg)
suffix	
alv	Alveolar
aw	Airway
b	Brain artery
cy	Respiratory cycle
Danat	Anatomical dead space
dem	Demand
e	Effective
exp	Expiration
H	H^+ ion
i	Gas constituents
insp	Inspiration
l	Lung
m	Mouth
n	Nose
pl	Pleural
pua	Pulmonary artery
puc	Pulmonary capillaries

Q	Flow
T	Tidal
th	Thoracic

Chapter 8

Dm	Fraction damage of the lung
P	Pressure (mmHg)
suffix	
alv	Alveolar
puc	Pulmonary capillaries

GLOSSARY

acute: lasting a relatively short time

afferent pathway: component of reflex arc that transmits information from receptor to integrating centre

airway: tube through which air flows between external environment and lung alveoli

alveolar dead space: volume of fresh inspired air that reaches alveoli but does not undergo gas exchange with blood

alveolar pressure: air pressure in pulmonary alveoli

alveolus: thin-walled, air-filled outpocketing from terminal air passageways in lungs

anatomic dead space: space in respiratory tract airways where gas exchange does not occur with blood

anemia: reduction in total blood haemoglobin

anemic hypoxia: hypoxia resulting from a decreased concentration of hemoglobin

aneurysm: an aneurysm (or aneurism) is localized, blood-filled dilation (bulge) of a blood vessel caused by disease or weakening of the vessel wall.

angiotensin II: a protein that has two forms: angiotensin I and angiotensin II. Angiotensin I is derived from a plasma protein and released by the action of renin from the kidneys. It forms angiotensin II which has two amino acid units less than angiotensin I. Angiotensin II increases the output of aldosterone from the adrenal cortex. Angiotension II can also cause blood vessels to constrict thus raising blood pressure.

aorta: largest artery in body; carries blood from left ventricle of heart to thorax and abdomen

aortic arch baroreceptor / arterial baroreceptor / carotid sinus baroreceptor: nerve endings sensitive to stretch or distortion produced by arterial blood pressure changes; located in carotid sinus or aortic arch

aortic valve: valve between left ventricle of heart and aorta

arrhythmia: any variation from normal heartbeat rhythm

arteriole: blood vessel between artery and capillary, surrounded by smooth muscle

artery: thick-walled elastic vessel that carries blood away from heart to arterioles

atrioventricular valve: valve between atrium and ventricle of heart

atrium: chamber of heart that receives blood from veins and passes it on to ventricle on same side of heart

autonomic nervous system: component of efferent division of peripheral nervous system that consists of sympathetic and parasympathetic subdivisions

autoregulation: ability of an individual organ to control its vascular resistance independent of neural and hormonal influence

baroreceptor: receptor sensitive to pressure and to rate of change in pressure

bradycardia: a resting heart rate of under 60 beats per minute

brainstem: brain subdivision consisting of medulla oblongata, pons and midbrain and located between spinal cord and forebrain

bronchiole: small airway distal to bronchus

bronchus: large-diameter air passage that enters lung

capillary: smallest blood vessels

carbamino compound: Any of various carbamic acid derivatives formed by the combination of carbon dioxide with an amino acid or a protein, such as hemoglobin forming carbaminohemoglobin

carbonic acid: H_2CO_3

cardiac: pertaining to the heart

cardiac output (CO): blood volume pumped by each ventricle per minute

cardiovascular center: neuron cluster in brainstem medulla oblongata that serves as a major integrating center for reflexes affecting heart and blood vessels

cardiovascular system: heart and blood vessels

carotid artery: an artery that supplies the head and neck with oxygenated blood

central chemoreceptor: receptor in brainstem medulla oblongata that responds to H^+ concentration changes of brain extracellular fluid

central nervous system (CNS): brain plus spinal cord

cerebellum: subdivision lying behind forebrain and above brainstem

cerebral cortex: cellular layer covering the cerebrum

cerebrospinal fluid: fluid that fills cerebral ventricles and the subarachnoid space surrounding brain and spinal cord

cerebrum: part of the brain that forms the forebrain

chemoreceptor: afferent nerve ending sensitive to concentrations of certain chemicals

Cheyne–Stokes respiration: An abnormal type of breathing seen especially in comatose patients, characterized by alternating periods of shallow and deep breathing

chronic: persisting over a long time

chronic obstructive pulmonary disease: Chronic obstructive pulmonary disease (COPD) is comprised primarily of two related diseases - chronic bronchitis and emphysema. In both diseases, there is chronic obstruction of the flow of air through the airways and out of the lungs, and the obstruction generally is permanent and progressive over time.

contractility: force of heart contraction

contraction: operation of the force-generating process in a muscle

coronary blood flow/coronary circulation: blood flow to heart muscle

diabetic neuropathy: a complication of diabetes causing damage to the nerves

diaphragm: dome-shaped skeletal-muscle sheet that separates the abdominal and thoracic cavities

diffusion: occurs from a region of higher concentration to a region of lower concentration

dyspnea: perceived difficulty breathing or painful breathing

edema/ oedema / œdema: swelling due to generation of interstitial fluid

effector: cell or cell collection whose change in activity constitutes the response in a control system

efferent pathway: component of reflex arc that ransmits information from integrating center to effector

electrocardiogram (ECG): recording at skin surface of the electric currents generated by cardiac muscle action potentials

end-diastolic volume: amount of blood in ventricle just prior to systole

end-systolic volume: amount of blood remaining in ventricle after ejection

expiration: movement of air out of lungs

functional residual capacity: lung volume when lung pressure is atmospheric

heart rate (HR): number of heart contractions per minute

haemoglobin: located in erythrocytes and transports most blood oxygen

haemoglobin saturation: percent of haemoglobin molecules combined with oxygen

hemorrhage: bleeding

hypercapnia: condition where there is too much carbon dioxide (CO2) in the blood

hypertension: chronically increased arterial blood pressure

hypotension: abnormally decreased arterial blood pressure

hyperventilation: increase in ventilation that causes an decrease in arterial P_{CO2}

hyperpnea: increased ventilation due to lack of oxygen

hypoventilation: decrease in ventilation that causes an increase in arterial P_{CO2}

hypoxemia: an abnormal deficiency in the concentration of oxygen in arterial blood

hypoxia: Deficiency in the amount of oxygen reaching body tissues

hypoxic hypoxia: hypoxia resulting from defective oxygenation of the blood in the lungs

inspiration: air movement from atmosphere into lungs

intracardiac phonocardiogram (PCG): the graphic recording of heart sounds and murmurs

intrapleural pressure/intrathoracic pressure: pressure in pleural space; also called intrapleural pressure

interventricular septum: the stout wall separating the lower chambers (the ventricles) of the heart from one another

intrinsic: situated entirely within a part

ischemia: reduced blood supply

isocapnic: a state in which the arterial carbon dioxide pressure remains constant or unchanged

larynx: part of air passageway between pharynx and tranchea;contains the vocal cords

lung compliance: change in lung volume caused by a given change in transpulmonary pressure

lung lavage: washing out of the lungs with saline or mucolytic agents for therapeutic purposes

mean arterial pressure: average blood pressure during cardiac cycle

mechanoreceptor: sensory receptor that responds preferentially to mechanical stimuli such as bending, twisting or compressing

medulla: innermost portion of an organ

membrane: cellular structures composed of lipids and proteins; provide selective barrier to molecule and ion movement and structural freamework to which enzymes, fibers and ligands are bound

metabolic rate: total body energy expenditure per unit time

metabolism: chemical reactions that occur in a living organism

myocardium: cardiac muscle, which forms heart walls

neuron/nerve cell: cell in nervous system specialized to initiate, integrate, and conduct electric signals

nucleus: cluster of neuron cell bodies in CNS

nucleus tractus solitarius: grey matter located in the dorsomedial part of the medulla oblongata associated with the solitary tract; receives inputs from most organ systems including the terminations of the facial, glossopharyngeal, and vagus nerves; major coordinator of autonomic nervous system regulation of cardiovascular, respiratory, gustatory, gastrointestinal, and chemoreceptive aspects of homeostasis

Oleic acid injection : process induced pulmonary edema

Orthostatic stress: physical tension that results from upright standing position

Oscillographic: study of the records of oscillations in electric current waveform

parasympathetic division: portion of autonomic nervous system whose preganglionic fibers leave CNS from breainstem and sacral portion of spinal cord

paraventricular nucleus: an aggregation of neurons in the brain which produces many hormones

partial pressure: part of total gas pressure due to molecules of one gas species among more than one constituent

pericardium: connective-tissue sac surrounding heart

peripheral chemoreceptor: carotid or aortic body responds to changes in arterial blood P_{O2} and P_{CO2}

pharynx: throat

plasma: liquid portion of blood

pons: a structure located on the brain stem above the medulla, below the midbrain

postganglionic: a autonomic-nervous-system neuron or nerve fiber whose cell body lies in a ganglion

preganglionic: autonomic-nervous-system neuron or nerve fiber whose cell body lies in CNS and whose axon terminals lie in a ganglion

pulmonary circulation: circulation through lungs

pulmonary stretch receptor: afferent nerve ending lying in airway smooth muscle and activated by lung inflation

pulmonary valve: valve between right ventricle of heart and pulmonary trunk

reflex: biological control system linking stimulus with response and mediated by a reflex arc

renal: pertaining to kidneys

residual volume: air volume remaining in lungs after maximal expiration

respiration: oxygen and carbon dioxide exchange between organism and external environment

respiratory rate/breathing frequency: number of breaths per minute

stenosis: an abnormal narrowing in a blood vessel or other tubular organ or structure.

stroke volume: blood volume ejected by a ventricle during one heartbeat

sympathetic pathway/sympathetic division: portion of autonomic nervous system whose preganglionic fibers leave CNS at thoracic and lumbar portions of spinal cord

systole: period of ventricular contraction

tachycardia: a form of rapid beating of the heart

tidal volume: air volume entering or leaving lungs with single breath during any state of respiratory activity

total peripheral capacitance (TPC): reciprocal of TPR

total peripheral resistance (TPR): total resistance to flow in systemic blood vessels from beginning of aorta to ends of vena cava

trachea: single airway connecting larynx with bronchi

tricuspid valve: valve between right atrium and right ventricle of heart

vagus nerve: major parasympathetic nerve

Valsalva manoeuvre: a technique for increasing the intrathoracic and intra-abdominal pressure by trying to breathe out forcibly (using the diaphragm and abdominal muscles) when the glottis (the opening between the vocal cords) is closed.

vein: any vessel that returns blood to heart

vena cava: large veins that returns systemic blood to heart

venous return: blood volume flowing to heart per unit time

ventilation: air exchange between atmosphere and alveoli

ventricle: lower chamber of heart

ventrolaterla: Both ventral and lateral

venule: a small blood vessel that allows deoxygenated blood to return from the capillary beds to the larger blood vessels called veins.

Chapter 1 Introduction

1.1 Computer simulation of the cardiopulmonary system

In the past four or five decades, modelling of the cardiovascular system and respiratory system has received a lot of interest with the possibility that such an approach could be useful in understanding the function and effects of the diseases associated with these two systems. With this purpose in mind, the models that have been developed to date are only specified in certain aspects and are usually limited to a particular function or disease. Some authors have developed very complicated cardiovascular models without fully considering the effect of respiratory system (Avula & Oestreicher 1978;Boyers et al. 1972;Heldt et al. 2002;Hyndman 1972;Jaron et al. 1984;Leaning et al. 1983;Melchior et al. 1992;Pennati et al. 1997;Sud et al. 1993;Sun et al. 1997;Ursino & Magosso 2003;Zacek & Krause 1996). Other researchers have concentrated on the development of the respiratory model but have ignored the important contribution of the cardiovascular system (Ben-Tal 2006;Grodins et al. 1967;Liu et al. 1998;Tilley et al. 2006;Tomlinson et al. 1994a). Only recently has there been a move to producing a comprehensive cardiopulmonary model so as to investigate the interaction between these two systems (Ben-Tal 2006;Lu et al. 2001;Ursino et al. 2001a;Ursino et al. 2001b). This significantly broadens the application of the cardiopulmonary model.

The objective of the research reported here is to develop a comprehensive human cardiopulmonary model, including detailed representations of the detailed respiratory and cardiovascular systems, which is capable of predicting the complex interactions between the two systems and their responses under different physiological conditions. An improved cardiovascular model including baroreflex is firstly developed. The model is then integrated with a respiratory model that includes the complex gas exchange process and the antagonistic interaction of the baroreflex and the chemoreflex.

At the University of Bath, Tomlinson et al (Tomlinson et al. 1993) developed a human respiratory system model in 1993, using the Bath*fp* simulation package (Fluid Power Centre, University of Bath). Lo (Lo 1995) subsequently applied this model to the simulation of underwater breathing apparatus. In order to enhance the human respiratory

system, a simple cardiovascular system was developed and later integrated into Lo's model (Horton 2001;Rajabally 1999). Tilley et al (Tilley et al. 2006) modified the lung model into a more physiological model rather than a mechanistic model which simulates patients who has lung disease in an Intensive Care Unit.

It is anticipated that the research reported in this thesis will extend the models developed at University of Bath to form a more complete cardiopulmonary system model. This should prove to be a powerful tool in clinical demonstration and education as well as supporting research in areas including sport sciences.

1.2 Overview of the cardiopulmonary system

A brief description of the respiratory and cardiovascular systems is given in this section as background knowledge of physiology.

1.2.1 Cardiovascular system

In engineering terms, the cardiovascular system (Figure 1-1) consists of a dual pump (heart), a series of distributing and collecting tubes (arteries and veins), and an extensive system of thin vessels that permit rapid gas exchange between the tissues and the vascular channels (capillaries). The heart consists of two pumps in series: one to propel blood through the lungs for exchange of oxygen (O_2) and carbon dioxide (CO_2) (the pulmonary circuit) and the other to propel blood to all other tissues of the body (the systemic circuit). Unidirectional flow through the heart is achieved by the appropriate arrangement of effective flap valves. Although the cardiac output is intermittent, continuous flow to the periphery occurs by distension of the aorta and its branches during ventricular contraction (systole) and elastic recoil of the walls of the large arteries with forward propulsion of the blood during ventricular relaxation (diastole). Blood moves rapidly through the aorta and its arterial branches. The branches become narrower in the more peripheral arteries, and their walls become thinner and change histologically. From a predominantly elastic structure in the aorta, the peripheral arteries become more muscular until at the arterioles the muscular layer predominates.

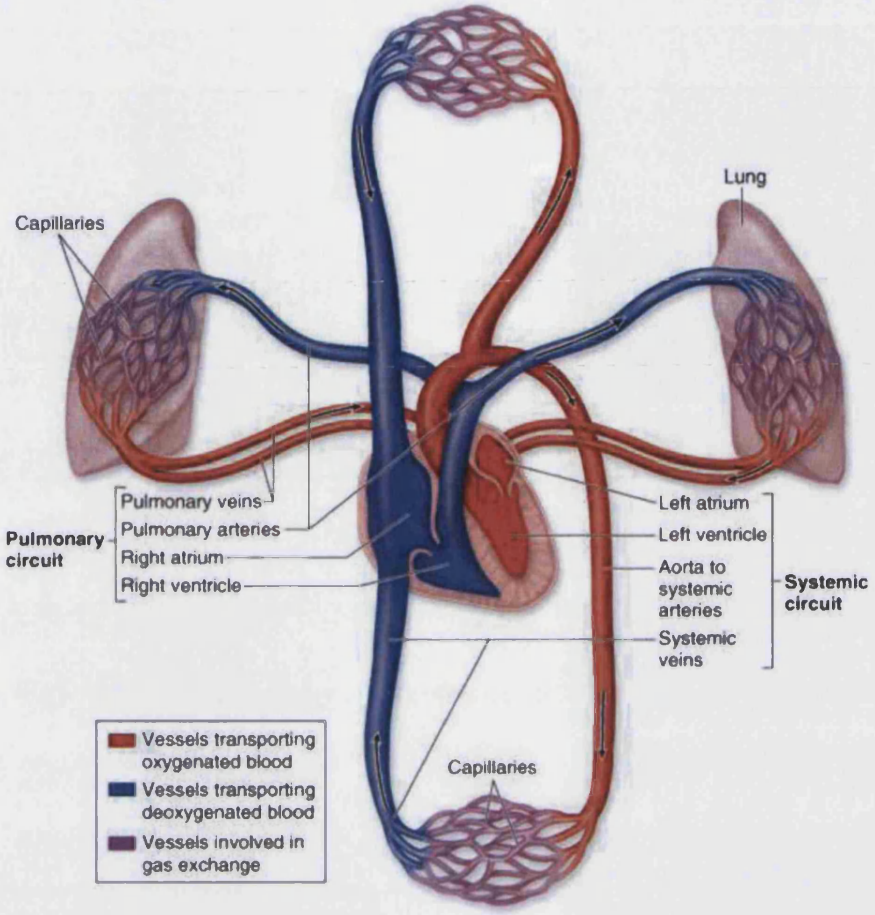

Figure 1-1Overview of the cardiovascular system (McKinley & O'loughlin 2005)

The frictional resistance to blood flow between the arteries and capillaries is relatively small. The arterioles, the stopcocks of the vascular tree, are the principal points of resistance to blood flow in the circulatory system. Due to this large resistance, there is a considerable fall in pressure from the arterioles to capillaries. Adjustment in the degree of contraction of the circular muscle of these small vessels permits regulation of tissue blood flow and aids in the control of arterial blood pressure.

In addition to a sharp reduction in pressure across the arterioles, a change from pulsatile to steady flow also occurs. The pulsatile arterial blood flow, caused by the intermittency of cardiac ejection, is damped at the capillary level by the combination of distensibility of the large arteries and frictional resistance in the arterioles. Each arteriole supplies many capillaries so that the total cross-sectional area of the capillary bed is very large,

despite the fact that the cross-sectional area of each capillary is less than that of each arteriole. As a result, blood flow reduces to a low level in the capillaries, analogous to the decrease in flow rate seen at the wide regions of a river. Since the capillaries consist of short tubes whose walls are only one cell thick, and since the flow rate is slow, the conditions in the capillaries are ideal for the exchange of diffusible substances between blood and tissue.

On its return to the heart from the capillaries, blood passes through venules and then through veins of increasing size. As the heart is approached, the number of veins decreases, the thickness and composition of the vein walls change, the total cross-sectional area of the venous channels reduces, and the velocity of blood flow increases. Most of the circulating blood is located in the venous vessels.

The arterial baroreflex contributes importantly to the short-term regulation of blood pressure and cardiovascular variability. Baroreceptors which are located at the aortic arch and carotid arteries sense systemic blood pressure. Changes in arterial baroreceptor afferent discharge transmitted to the central nervous system trigger reflex adjustments that buffer or oppose the changes in blood pressure: a rise in pressure elicits reflex parasympathetic activation and sympathetic inhibition, with subsequent decreases in heart rate (HR), cardiac contractility, vascular resistance, and venous return. Conversely, a decrease in arterial pressure reduces baroreceptor afferent discharge and triggers reflex increases in HR, cardiac contractility, vascular resistance, and increased venous return. Thus the baroreflex, by affecting blood pressure and HR control, provides powerful beat-to-beat negative feedback regulation of arterial blood pressure that minimizes short-term fluctuations in pressure.

1.2.2 Respiratory system

The major responsibility of the respiratory system is to ventilate the lungs. This provides an ongoing source of fresh gas (normally air) to the gas-exchanging surfaces to allow the addition of oxygen (O_2) and the removal of carbon dioxide (CO_2) from the blood passing through the lungs. From a functional standpoint, the respiratory system can be considered to be a control system. The system adjusts the rate of ventilation as

environmental conditions vary, as metabolic demands are altered, or as the physical characteristics of the ventilatory apparatus are modified by growth, aging, or disease.

The respiratory system consists of the upper airways, trachea and branch airways to the two lungs (Figure 1-2). Air is inhaled following this path and then exhaled through the same path in reverse. This process (termed ventilation) is the first step in the respiratory process. In the lung, there are approximately 300 million alveoli which is the site of gas exchange. The gas exchange process is an important procedure to exchange nutrients (O_2) and waste products (CO_2). O_2 must also be transported to other parts of the body by the blood.

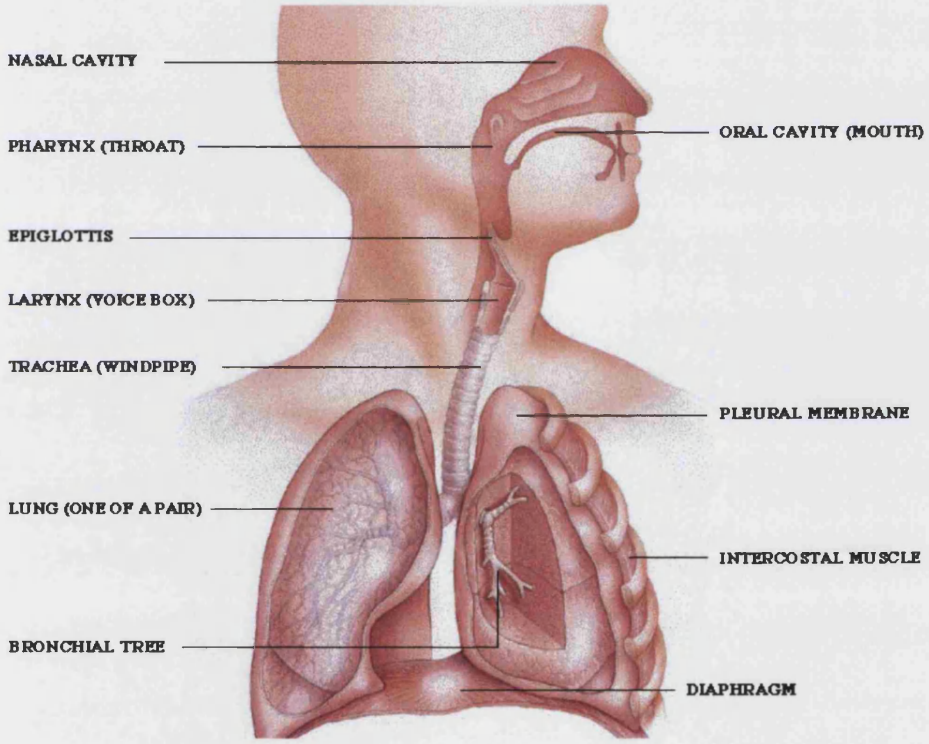

Figure 1-2 Overview of the respiratory system (Sherwood 2001)

The system controller consists of a network of neurons in the medulla and pons. The discharges of the neurons set the cyclic inspiratory and expiratory pattern of breathing. The activity of brain stem respiratory neurons, however, may be influenced by inputs from other brain centres, such as the cerebral cortex and cerebellum. Examples of the cerebral cortical influence on breathing are the cessation of respiratory activity that accompanies voluntary breath holding and the modulation of respiration during speech.

Inputs that influence the automatic behaviour of brain stem respiratory neurons arise from chemoreceptors that sense the partial pressure of O_2 and CO_2 in the blood and brain and from mechanoreceptors in the lung and chest wall that monitor lung inflation and chest expansion. Signals from central medullary chemoreceptors and peripheral chemoreceptors in the carotid and aortic bodies increase neuronal inspiratory activity in the brain stem. Also, afferent impulses from lung stretch receptors are relayed back to the brain stem via the vagus nerves. These receptors play an important role in the determination of breathing frequency and tidal volume.

1.2.3 Interactions between the respiratory system and the cardiovascular system

Interactions between the respiratory and cardiovascular systems include the gas exchange process, intrathoracic pressure on the veins and arteries in the thoracic cavity, and alveolar pressure in pulmonary capillaries. The gas exchange process is the predominant mechanism supporting energy consumption in the human body. The other two have relatively smaller effects on system performance.

The blood entering pulmonary capillaries has a high CO_2 content and a low O_2 content. The differences in the partial pressures of oxygen (P_{O2}) and carbon dioxide (P_{CO2}) on the two sides of the alveolar-capillary membrane result in the net diffusion of oxygen from alveoli to blood and of carbon dioxide from blood to alveoli. As this diffusion occurs, the capillary blood P_{O2} rises and its P_{CO2} falls. The net diffusion of these gases ceases when the capillary partial pressures become equal to those in the alveoli.

The cardiac response to peripheral or arterial chemoreceptor stimulation is worth special consideration because it shows the complexity of two reflex control systems. Neurophysiologic studies have identified areas of the brain stem where afferent inputs from peripheral baroreceptors and chemoreceptors converge, including the nucleus tractus solitarius (NTS) and paraventricular nucleus (PVN) (Tjen et al. 1997).

Figure 1-3 shows the interactions of chemoreceptor reflex and baroreflex. Chemoreceptors are activated by changing P_{O2} and/or P_{CO2} in the brain and arterial blood. Activation of chemoreceptors produces an increase in sympathetic outflow (Du & Chen 2007) and a decrease in parasympathetic outflow (Davidson et al. 1976;Kollai

et al. 1994) to peripheral organs. This inhibits baroreflex which leads to the increase of blood pressure. The activation of the baroreflex by the increased blood pressure weakens the increase of sympathetic outflow and the decrease of parasympathetic outflow.

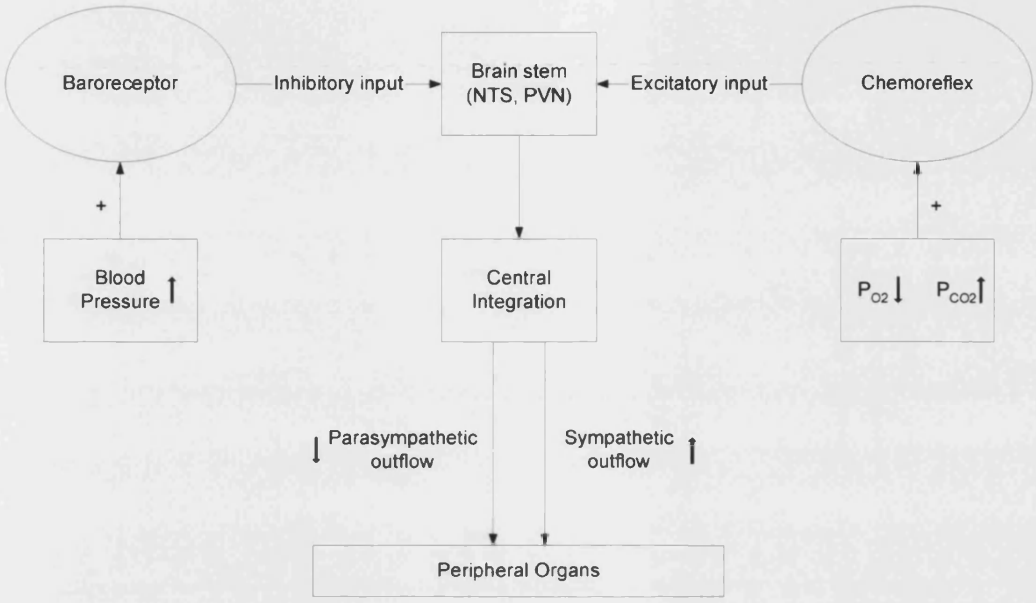

Figure 1-3 Schematic overview of the interactions among chemoreceptor reflex, and baroreflex adapted from (Du & Chen 2007) and (Davidson et al. 1976). +: activation; PVN: paraventricular nucleus; NTS: nucleus tractus solitarius (↑: increase; ↓: decrease)

1.3 Introduction to the Bathfp simulation package

The cardiopulmonary model will be developed using the Bath*fp* dynamic simulation package developed at the University of Bath which had been previously used to develop physiological models (Tomlinson et al. 1993). This package provides an environment which has been targeted towards the user who is involved in either the design or assessment of physical systems. The following facilities are provided by the package (Lo 1995):

1. Automatic linking of the component models together to form the system simulation program.
2. A library of models representing the behaviour of particular of components
3. Utilities to assist the user in creating new models
4. An inbuilt facility for displaying simulation results in graphical form
5. A facility which allows for changes in dimensional and performance data or circuit configuration

Bath*fp* uses a sophisticated integration method, based on the LSODA package developed by Petzold (1983), to solve all the nonlinear ordinary differential equations in the overall model. The algorithm has been modified to enable it to be incorporated with the Bathfp as follows:

1. The development of communication protocols between the component models and the integrator.
2. Special procedures allowing physical discontinuities to be handled efficiently.

1.4 The scope of the thesis

The thesis is divided into nine chapters.

Chapter 2 describes the development of an improved cardiovascular model conducted under this research. A review of previous cardiovascular models is given. It includes a description of detailed features of the cardiovascular models and the interactions between them. Based on the findings obtained, a cardiovascular model is developed which has novel features developed by the author. Attention is also paid to the compatibility of the model with the requirements of a respiratory model.

Chapter 3 validates the cardiovascular model described in Chapter 2. The results are justified by the accuracy of the hemodynamics representation in various parts of the system and a good fit to measured pressure and flow waveforms.

Chapter 4 reviews previous baroreceptor reflex control models and describes the development of an improved baroreflex model conducted under this research that includes afferent, central and efferent compartments and effector sites. Improvements

are made to the efferent compartment and heart effector site of the model in order to give most of the parameters physiological explanations.

Chapter 5 validates the baroreflex model described in Chapter 4. Tests are performed to assess the static and transient responses of the baroreflex control model.

Chapter 6 describes the integration of the cardiovascular model and the respiratory system. Firstly, a brief overview of the previous respiratory models is given followed by a description of the respiratory model development. Modifications required by the integration of the cardiovascular and respiratory models, including gas exchange and gas transportation due to the pulsatile blood flow, autoregulation of cerebral blood flow and the combination of chemoreceptor and baroreceptor reflex model, are described.

Chapter 7 details tests performed to demonstrate the capability of the cardiopulmonary model to simulate the interactions of the respiratory and cardiovascular systems which include the gas exchange process, the effect of breathing on cardiovascular system and the blood gas contents on the hemodynamics. The interaction between the chemoreceptors and baroreceptors is also demonstrated.

Chapter 8 demonstrates some possible applications of the cardiopulmonary model, including simulations of the cardiopulmonary responses of patients with lung and cardiovascular disease, together with those of healthy people during exercise.

Chapter 9 draws conclusions from the research described in this thesis and suggests some areas for future work.

Chapter 2 Cardiovascular model

The mathematical models that have been previously developed for the human cardiovascular system vary from very simplistic models to multi-segmental representations of the vascular tree. Melchior et al. (1992) split the models into three distinct groups. The first group includes models of the vascular network without any control aspects of circulation. The second group of models consists of certain specific vascular beds such as coronary and cerebral circulation. The third group includes models of the cardiovascular system, incorporating at least some central nervous system control.

Generally speaking, the cardiovascular system can be represented as two major blocks. The first is a hydraulic system with a numbers of distensible vessels in a serial and parallel arrangement with the heart as a pump. The second is a control system to regulate the arterial pressure and blood flow. This chapter describes the hydraulic model of cardiovascular system and the control model of the cardiovascular system will be presented in Chapter 4 and Chapter 5.

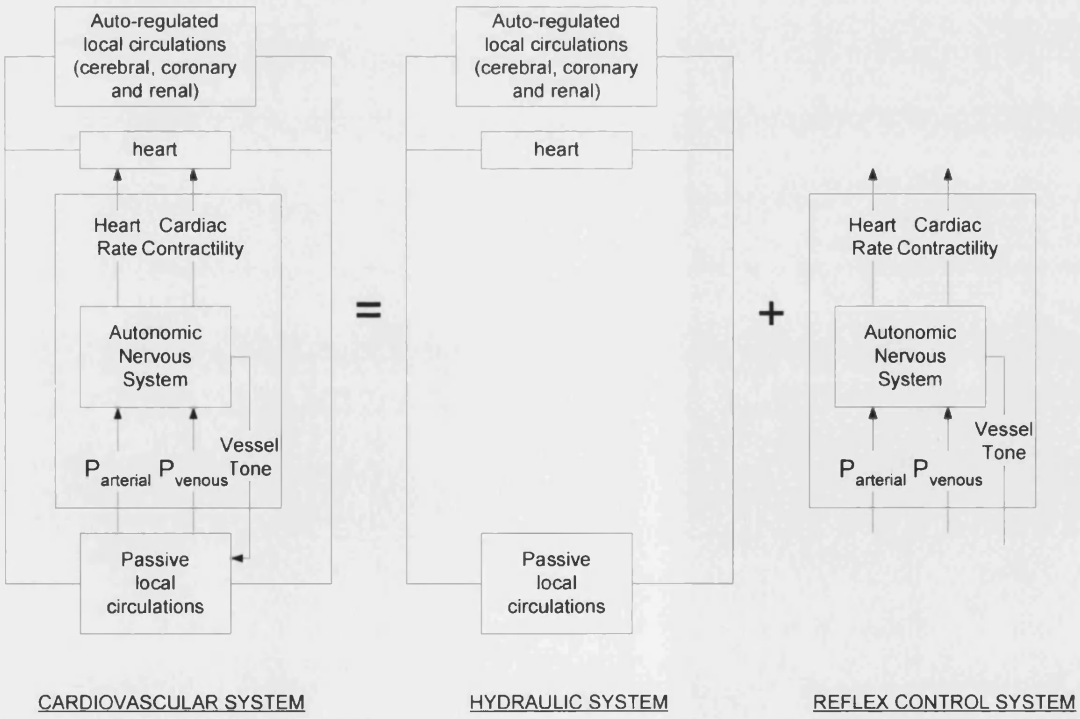

Figure 2-1Overall cardiovascular system (Melchior et al. 1992)

2.1 Hydraulic model of the cardiovascular system

2.1.1 Heart

The heart (Figure 2-2) is the most important component in the hydraulic cardiovascular system as it pumps blood into the pulmonary and systemic arteries. It consists of four chambers, two ventricles and two atria. The right and left sides of the heart is divided by the septum of the heart. The atria are separated by the atrial or inter-atrial septum while the ventricles are separated by the ventricular or interventricular septum. Each chamber has a unidirectional valve to prevent blood back flow. The heart muscles contract to pump blood out of the heart. The right and left atria contract first, and then the ventricles contract together to propel blood out of the heart. The heart muscles then relax to allow blood to fill up the heart before the cycle is repeated.

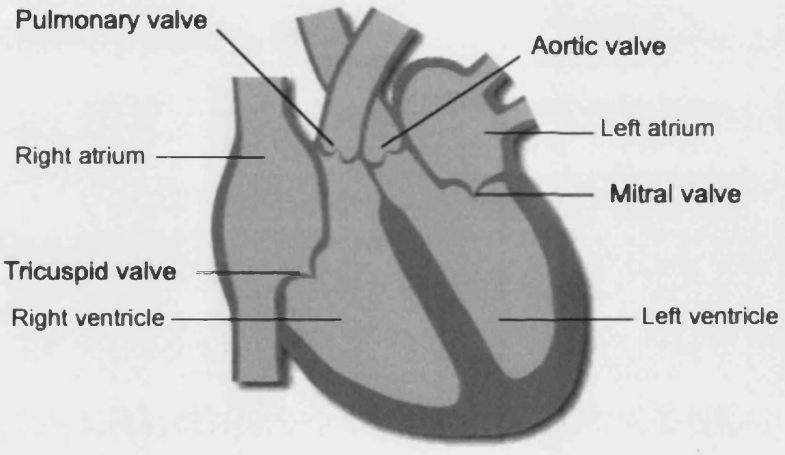

Figure 2-2 Anatomy of the human heart (Thomson Healthcare 2004)

Attention was first given to the most important chamber, the left ventricle. Suga (1971) defined the left ventricle as a 'time-varying elastic model'. He developed a left-ventricular pumping model, based on a left-ventricular systolic time-varying pressure/volume ratio (e(t)). By varying e(t), Suga compared the results to the established physiological properties of the left ventricle. Quantitative relationships among various hemodynamic parameters were obtained, and good agreement was observed with the physiological characteristics of the left ventricle.

The 'Time-varying elastic model' was applied to other chambers of the heart by assuming that they behaved in a similar manner (Beyar et al. 1987). There is evidence from animal studies to support the use of similar elastance characteristics for the two ventricles (Lausted & Johnson 1999) and it has been shown that the atria can be represented by the time-varying elastance concept (Beyar et al. 1987). In Figure 2-3, the symbols in panel A indicate 'isochronic' points on the different Pressure-Volume-loops, occurring at the moment during the cardiac cycle. These points line up and, stepping through the cardiac cycle (T_1, T_2, ...), the slope of the line (the elastance; panel B) varies in a cyclic way, while the intercept with the volume axis remains constant (V_o). The elastance curve can be normalized with respect to both its amplitude and the time at which the amplitude occurs (panel C) (Sun & Gewirtz 1988).

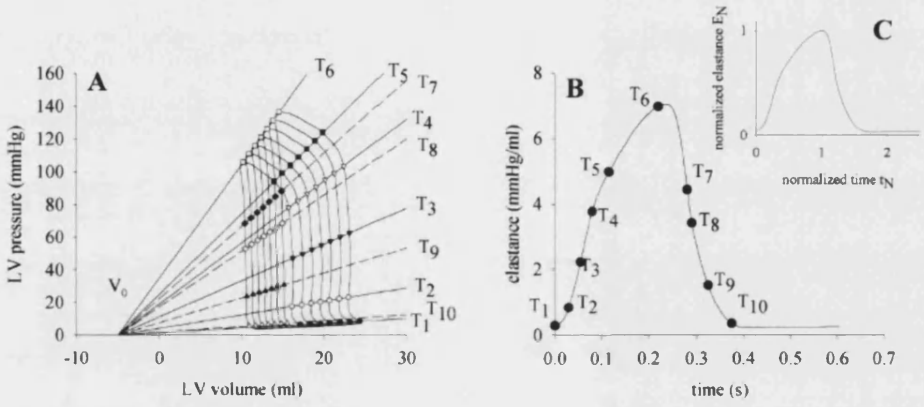

Figure 2-3 Time-varying elastance concept as elaborated by Suga and Sagawa; LV: left ventricle. (Segers et al. 2003)

Hill (Hill 1983) introduced a three-parametric model of heart muscle mechanics, which includes contractile, series elastic and parallel elastic elements as shown in Figure 2-4. Based on this theory, Grood et al (1974) presented a heart muscle model which successfully predicted the force development during both isometric and isotonic contractions. Zacek et al (1996) presented the relationship between pressure and volume in the ventricle model, based on this method. The contractile element simulates the force-velocity relationship due to stretching; the series elastic element relates to the quick changes in length while parallel elastic element simulates the filling phase. Using experimental results of the relationship between acting force and length of these muscle elements, it is possible to derive the Pressure-Volume (P-V) relationship for the ventricle.

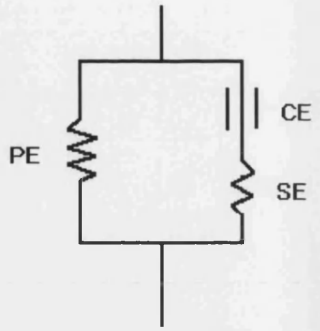

Figure 2-4 Hill's muscle model. CE – contractile element; SE – series elastic element; PE – parallel elastic element

Ventricular interaction describes a phenomenon where each ventricle's pressure-volume (PV) relationship is shifted to higher pressures, as the other ventricle is pressurized (Maruyama et al. 1982). A similar shift in the end-systolic P-V relationship is also used for the active heart (Janicki & Weber 1980). As a rough approximation, Beyar et al (1987) assumed that a certain fraction of the ventricular pressure is transmitted across the septum to the opposite ventricle. Shift of the septum has also been represented by an elastic compartment in Maughan et al.'s model (Maughan et al. 1987;Sun et al. 1997). Under this assumption, the left ventricular pressure is the sum of the effective left ventricular elastance times the volume and the "cross-talk" pressure from the right ventricle. Chung et al (Chung et al. 1997) present a more detailed and complicated model of the elastic septum. At end systole the septum is represented by the linear P-V relationship obtained by solving the traditional elastic formula.

In the heart, there are four valves (Figure 2-2): The tricuspid valve is between the right atrium and right ventricle; the pulmonary valve is between the right ventricle and the pulmonary artery; the mitral valve is between the left atrium and left ventricle; the aortic valve is between the left ventricle and the aorta. The cardiac valves consist of thin flaps of flexible, tough, endothelium-covered fibrous tissue firmly attached at the base to the fibrous valve rings. Movements of the valve leaflets are essentially passive, and the orientation of the cardiac valves is responsible for the unidirectional flow of blood through the heart.

Bernoulli's law is widely used to describe the pressure-flow relationship of heart valves. This approach suggests that the pressure drop caused by flow separations at the exit of the valve is proportional to the square of the flow rate. The most complicated form of the equation includes viscous resistance and an inertial term which is related to the acceleration and deceleration of the flow.

The physical understanding of the closure of the heart valves remains contentious after centuries of study by many different investigators (Baccani et al. 2002;Bowman et al. 2004;Fiore et al. 2002;Flanagan & Pandit 2003;King et al. 1996;Kono et al. 1984;Lai et al. 2002;Tsakiris et al. 1978). Most of models use simplified indications such as the valves close as soon as pressure gradient becomes negative. However experimental findings show the closure time is some time later. Hence the use of pressure differences is not reliable indicator of the direction of blood flow or of valve closure in the presence of rapidly changing or fluctuating flow velocity (Rushmere 1970).

2.1.2 Arterial segments

The arterial bed can be represented as a three-element Windkessel model as shown in Figure 2-5 (Maruyama et al. 1982). The inertance (L), resistance (R) and compliance (C) can be calculated from the geometric dimensions of the vessel. The inertance term represents the acceleration effect of the vessel. Non-linearity can be taken into account by specifying a nonlinear compliance (Sun 1991;Sun et al. 1995;Sun et al. 1997). Using this model, the effect of gravity or acceleration is easily accounted for by the inclusion of an electromotive force of appropriate strength (Maruyama et al. 1982). In Figure 2-5, P1(t) and P2(t) represent end pressures and ground, the pressure outside artery. Inductance (L) and capacitance (C) correspond, respectively, to inertance and compliance of a control volume. As indicated, resistance R, L, and C are related to vessel dimensions [length (l), radius (r) and thickness (h)], blood viscosity (μ), blood density(ρ) and Young's modulus of elasticity for the material of arterial walls (E)(Maruyama et al. 1982).

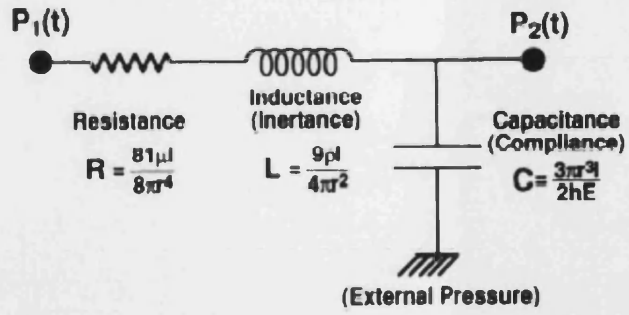

Figure 2-5 Electrical analog of arterial segment. (Maruyama et al. 1982)

Figure 2-6 shows the steady state relationship between the transmural pressure across the wall of an arterial segment and the volume of the segment arteries. Correlating the PV characteristics in the pressure range from 10 to 80 mmHg leads to an approximate constant slope with small concavity. In this range, the compliance can be treated as a constant parameter. However, the arterial pressures commonly go beyond this range, sometimes reaching as high as 180mmHg. Therefore, a nonlinear term is introduced for compliance into the arterial model using an exponential relationship (Sun et al. 1997).

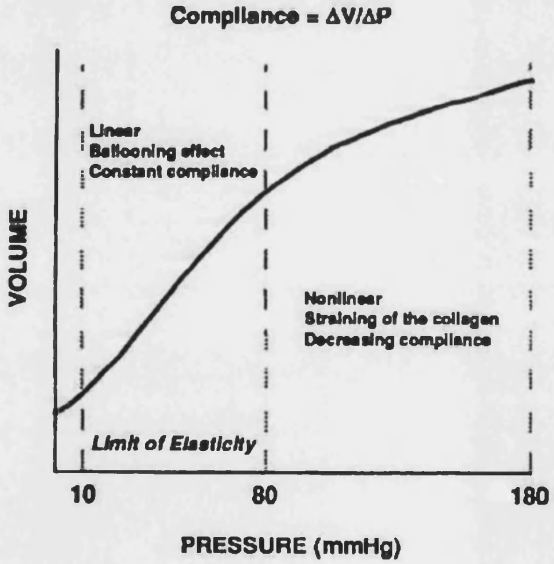

Figure 2-6 Pressure-volume relationship in arteries vessel(Melchior et al. 1992)

2.1.3 Vein segments

Models of the arterial bed can not readily be applied to venous segments due to veins and arteries having different elastic properties. Firstly, the veins may collapse if the transmural pressure decreases to a very low level. Secondly, valving in the veins prevents the flow from reversing and maintains pressure in the upper body. Thirdly, venous vessels have higher compliance so that the effect of changes in external vascular pressure is more pronounced. Finally, the local inertial force can be neglected because the low flow in the veins produces little pulsation. In order to model a human cardiovascular system in different postures, the phenomena of vein collapse should not be ignored.

The above features of the veins can be included in the arterial model with some modification. The most difficult aspect is that of venous collapse. A collapsible tube can be used as a mechanical model of the vein having the P-V relationship shown in Figure 2-7. This model mimics the behaviour of veins fairly well except at higher pressures. For pressures higher than 50 mmHg, the P-V curve will display different characteristics (broken line in Figure 2-7) due to the stiffening of vessel wall. Beyar et al (Beyar et al. 1987) include venous collapse by introducing a collapsible segment which is represented by a discontinuity resistance. The resistance increases at the very low transmural pressure to stimulate the cessation of flow during collapse. Alternatively, non-linear resistances of the vena cava can also effectively represent the collapse. Valving can be characterised by assigning the venous resistance high values for retrograde flow.

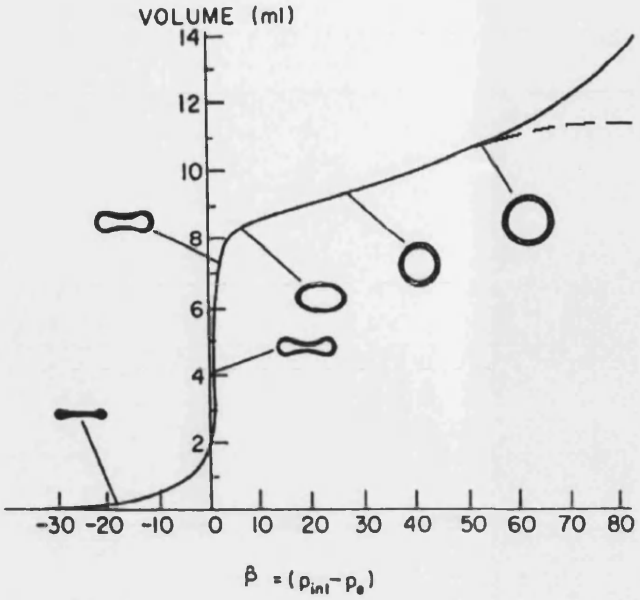

Figure 2-7 Changes in volume as a function of transmural pressure in a collapsible tube used as a mechanical model of a venous segment. (Melchior et al. 1992)

2.1.4 Extravascular pressure

Because blood vessels are not rigid tubes, the pressure outside the vessels will affect the flow by changing the vessel's diameter. This external pressure has a more significant effect on the veins than on the arteries since veins are relatively much more compliant (Maruyama et al. 1982). Intrathoracic pressure should also be included when respiratory manoeuvres are involved. Abdominal pressure and extravascular leg pressure are important factors when considering orthostatic stress (a condition that causes a person's blood pressure to drop when they rise from a seated or lying down position to standing).

2.1.5 Autoregulated local circulations

Autoregulated local circulations are discussed in the hydraulic system section because this is mostly independent of the central nervous system control. Most vascular beds of the cardiovascular system are known to be autoregulated. That is, the flow is maintained at a steady level by myogenic and metabolic reflexes for a wide range of changes in perfusion pressure (Fogliardi et al. 1996).

Autoregulation of cerebral and coronary arteries is of particular importance in the development of the cardiovascular system. Coronary flow supports the metabolic needs of the heart. However, coronary flow is always considered passive in modelling due to its small portion of cardiac output. On the other hand, cerebral blood flow accounts for 15% of cardiac output; therefore it is necessary to include the regulation of cerebral flow.

2.1.6 Mathematical models of the hydraulic system

Table 2-1 summarises the hydraulic system attributes of the published models indicating what aspects these models include. None of these models includes all the important phenomena of mathematical models due to different modelling purposes. As can be seen, autoregulation of local circulation have often been neglected. The modelling of the interventricular septum and pericardium has gained some attention only recently. Due to the relatively straight P-V curve, nonlinearity of the arterial compliance was often not considered. External vascular pressure appears only important when considering pulmonary dynamics or orthostatic stress.

Table 2-1Comparison of the cardiovascular models (included in the model)*

Investigators	Total Segments	Autoregulated local circulation	ventricle interaction	arterial bed		venous bed		
				Inertance	Nonlinear arterial compliance	Venous collapse	External vascular pressure	Venous valves
Beneken and DeWit (Beneken & DeWit 1967)	19			*		*	*	*
Snyder and Rideout(Snyder & Rideout 1969)	31			*		*	*	*
Boyers et al.(Boyers et al. 1972)	7	*						
Hyndman(Hyndman 1972)	10			*		*	*	
Croston et al.(Croston & Fitzjerrell 1974)	36			*	*	*	*	*
Green and Miller(Green & Miller 1973)	4							
Avula and Oestreicher (Avula & Oestreicher 1978)	5			*	*	*		
Leaning et al.(Leaning et al. 1983)	19			*		*		*
Jaron et al. (Jaron et al. 1984)	32			*			*	

.....continue

.....continue

Investigators	Total Segments	Autoregulated local circulation	ventricle interaction	arterial bed		venous bed		
				Inertance	Nonlinear arterial compliance	Venous collapse	External vascular pressure	Venous valves
Al-Dahan et al. (Al-Dahan et al. 1985)	8			*		*	*	*
Lu, K. et al. (Lu et al. 2001)	15		*	*				
Heldt, T. et al.(Heldt et al. 2002)	10			*				
Pennati,G. et al.(Pennati et al. 1997)	23			*				
Migliavacca, F. et al(Migliavacca et al. 2001)	10			*				*
Zacek, M. et al.(Zacek & Krause 1996)	15			*				*
Beyar, R. et al.(Beyar et al. 1987)	12		*	*		*		*

After reviewing these models, a number of questions have been identified that need to be addressed when developing a cardiovascular model:

i. How many vascular elements should be used in the model to represent the total system including the heart chambers?
ii. Is it necessary to take into account the nonlinearity of the P-V relationship in the arteries?
iii. Does the model need to consider venous collapse, venous valves and external vascular pressure?

iv. Does the model need to take into account the autoregulation of flow in the vascular beds?

It should be borne in mind that the purpose of the research reported in this thesis is to integrate the cardiovascular and respiratory models with potential for further development and application. For this, the models should be able to represent essential features of the system while being as simple as possible in structure and function.

2.2 Mathematical model of the cardiovascular system

The new mathematical model of cardiovascular system developed in this research uses the Bath*fp* dynamic simulation package developed at the University of Bath (Tomlinson et al. 1993). Figure 2-8 shows the Bath*fp* simulation circuit developed for the cardiovascular hydraulic system. The model consists of 13 segments including

- the pulmonary capillaries (the lung),
- pulmonary arteries and veins,
- left and right heart,
- aorta,
- systemic arteries and veins,
- vena cava,
- systemic capillaries (the body),
- intrathoracic compartment,
- pericardium
- interventricular septum

Nonlinearity aspects in the arteries are incorporated into the model to produce realistic arterial pressure and volume waveforms. The discontinuity of vein compliance due to venous collapse is not considered. Intrathoracic pressure is included because it is important to represent the interaction of the respiratory and cardiovascular systems. Autoregulation will be included and discussed in Chapter 6. The characteristics of the model are described as follow:

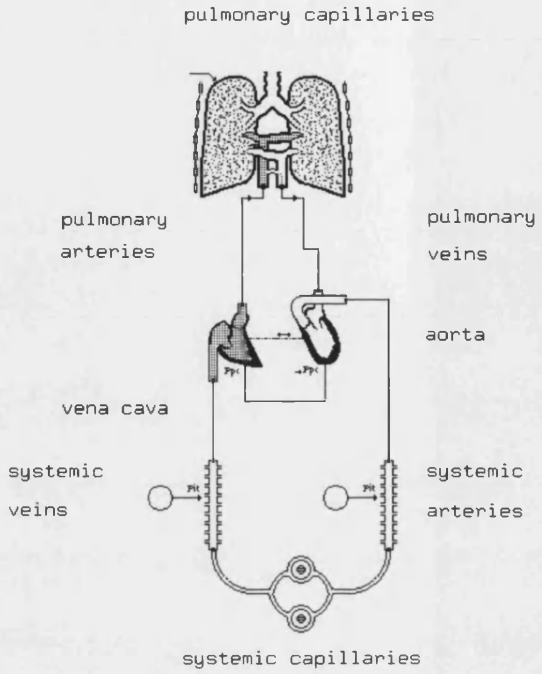

Figure 2-8 Cardiovascular Model circuit in Bathfp package; P_{pc}: pericardium pressure; P_{it}: intrathrocic pressure

2.2.1 Heart chamber

The heart is represented by a four-chamber model. The ventricles and atria are modelled as a time-varying elastance model (Suga 1971). The elastance term is assumed to vary over the cardiac cycle according to an exponential charge-discharge waveform and is characterised by a baseline and an amplitude component. The equations for the ventricles are given by

$$p_v = e_v V_v \tag{2-1}$$

$$e_v = \begin{cases} E_{va}\left[1 - e^{-t/\tau_{lc}}\right] + E_b & 0 \le t \le t_{ee} \\ (e_v|_{t_{ee}} - E_b)e^{-(t-t_{ee})/\tau_{lr}} + E_b & t_{ee} < t < t_r \end{cases} \tag{2-2}$$

And the equations for the atria are represented in a similar form:

$$P_a = e_a V_a \tag{2-3}$$

$$e_a = \begin{cases} E_{aa}\left[1 - e^{-(t-t_{ac})/\tau_{ac}}\right] + E_{ab} & t_{ac} \le t \le t_{ar} \\ (e_a|_{t_{ar}} - E_{ab})e^{-(t-t_{ar})/\tau_{ar}} + E_{ab} & t_{ar} < t < t_r + t_{ac} \end{cases} \quad (2\text{-}4)$$

2.2.2 Heart valves

Bernoulli's equation was used to model heart valve dynamics. This implies that the pressure drop caused by flow separations at the exit of the valve is proportional to the square of flow. The inertial term is related to the acceleration and deceleration of flow. The viscous resistance is also included. The pressure-flow relation for a valve is given by

$$\frac{dQ_{vlv}}{dt} = \begin{cases} \dfrac{P_a - P_v - b_v Q_{vlv}|Q_{vlv}| - R_{vlv}Q_{vlv} + \Omega_a P_a \dot{V}_a - \Omega_v P_v \dot{V}_v}{L_{vlv}} & P_a > P_v \\ 0 & otherwise \end{cases} \quad (2\text{-}5)$$

where

$$b_v = \rho / (2 \times 1333 A_{vlv}^2) \quad (2\text{-}6)$$

The constant term 1333 is the conversion factor when using pressure in mmHg. P_a is the pressure of the atrium and P_v is the ventricular pressure. A_{vlv} is the valve area. ρ is the blood density.

2.2.3 Interaction between left and right heart

Interactions between the left and right heart include:

- pressure coupling through the interventricular septum
- volume coupling among the chambers in the pericardium
- hemodynamic coupling via the pulmonary circulation

The shift of the septum is represented by an elastic compartment using the approach described by Maughan et al. (1987). Under this assumption, the left ventricular (LV)

pressure is the sum of the effective LV elastance times volume and the "cross-talk" pressure from the right ventricle (RV) and is given by

$$P_{lv} = \hat{e}_{lv} V_{lv} + k_{rl} p_{rv} \tag{2-7}$$

where $k_{rl} = e_{lv} / (E_s + e_{lv})$ and $\hat{e}_{lv} = E_s k_{rl}$.

Similarly, the RV pressure is given by

$$P_{rv} = \hat{e}_{rv} V_{rv} + k_{lr} p_{lv} \tag{2-8}$$

where $k_{lr} = e_{rv} / (E_s + e_{rv})$, $\hat{e}_{rv} = E_s k_{lr}$ and E_s = 45.9mmHg/ml, adopted from Maughan's experimental data (Maughan 1987).

In addition to the pressure coupling between the ventricles, the volume coupling is included in all chambers in the pericardium. In Sun's model, this is represented by a pericardial compartment with an exponential pressure-volume relationship. The pressure-volume relationship in the pericardium is given by

$$P_{pc} = K_{pc} e^{(V_{pc} - V_{pc0}) / \Phi_{pc}} \tag{2-9}$$

ϕ_{pc} is the volume constant while V_{pc0} is the volume offset and K_{pc} is set to unity according to Sun's model. V_{pc} is the sum of heart and pericardial fluid volumes and is set to be 30 ml under normal circumstances.

2.2.4 Arteries

Arteries are represented by a capacitance, a resistance and an inertance term. Viscoelastance is also included though it has less effect on the flow dynamics than the other three terms. Nonlinearity is introduced to the capacitance using an exponential pressure-volume relationship. For example, the pressure-volume relationship for aorta can be given by Sun et al. (1997)

$$\frac{dQ_{aa}}{dt} = \left[(P_{aa} - P_{sa}) - R_{aa}Q_{aa} + \Omega_{aa}\frac{dV_{aa}}{dt} - \Omega_{sa}\frac{dV_{sa}}{dt} \right] / L_{aa} \qquad (2\text{-}10)$$

$$P_{aa} = E_{aa}\Phi_{aa} \qquad (2\text{-}11)$$

$$E_{aa} = E_0 e^{V_{aa}/\Phi_{aa}} \qquad (2\text{-}12)$$

2.2.5 Veins

Although the physiological characteristics of the veins are different from arteries as described in Chapter 2, equations (2-10) and (2-11) can be used to describe both with some adjustment. A higher value is assigned to the volume constant Φ for the veins as the capacitance is relatively constant and veins are more compliant than arteries.

2.2.6 Capillaries

Nutrients and waste products exchange between blood and tissue in the capillaries, and for this reason, models of the capillaries must be included in the model to form an overall circulatory model. Pulmonary capillaries share the same mathematical model as arteries and veins. This approach was used by Sun et al. (1997) and good agreement with clinical data was obtained.

From a physiological point of view, the systemic capillaries have a huge cross-sectional area which slows down the blood flow so that chemical metabolic energy exchange can take place. The resistance of the systemic capillaries is determined by the resistance of the arterioles supplying the systemic capillaries and by the number of open precapillary sphincters. As a result, the resistance is expected to play a dominant role, rather than capacitance and inertance in the systemic capillary model.

2.2.7 Intrathoracic pressure

The most important interaction between the respiratory and cardiovascular systems is the gas exchange process. The effect of the intrathoracic pressure on blood flow is also of importance and the intrathoracic pressure is assumed to vary over time with an exponential charged-discharged waveform. On the basis of reported data, the intrathoracic pressure is assumed to vary from -3.7mmHg during expiration to -5.5 mmHg during inspiration as Figure 2-9 shows (Guyton 1991).

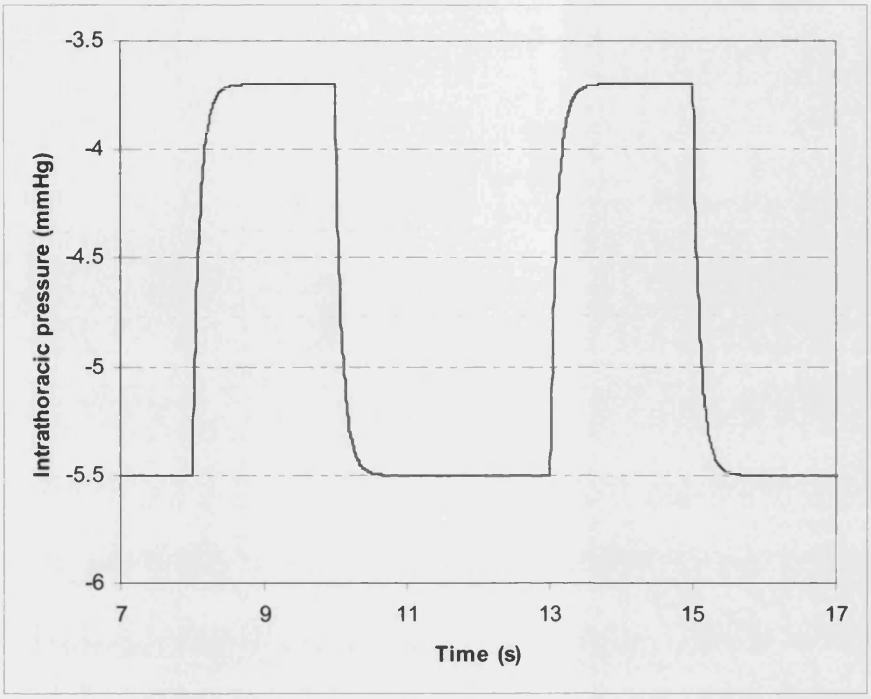

Figure 2-9 Intrathoracic pressure

2.3 Closure

A number of cardiovascular models varying in complexity have been developed (Lo 1995;Melchior et al. 1992;Pennati et al. 2004;Pennati et al. 1997;Sud et al. 1993;Sun et al. 1995). The most detailed includes a vascular model and some aspects relating to central nervous system control.

After reviewing the important features of the published cardiovascular models, a mathematical model of the cardiovascular system was developed including the necessary aspects to allow integration with a respiratory model. The model contains 13 segments including models of blood vessels and heart chambers. The heart serves as a hydraulic pump and the vessels are distensible pipes in a serial and parallel arrangement. Specifically, the heart was represented by a four-chamber model and the chambers, ventricles and atria, were modelled as a time-varying elastance model. Valves in the heart were modelled using Bernoulli's equation. The heart model also includes detailed interactions between left and right heart including the interventricular septum and the

pericardium. Blood vessels were represented by capacitance, resistance, viscoelastance and inertance terms. The capacitance is nonlinear and represented by an exponential pressure-volume relationship. The interaction between respiratory system and cardiovascular system was included by applying the intrathoracic pressure on the blood flow.

In the next chapter, realistic parameter values will be assigned to the model and the sensitivity test of the parameters will be described. Simulations will be compared with publish data in order to validate the model.

Chapter 3 Validation of the cardiovascular model

3.1 Introduction

Chapter 2 includes a description of the mathematical model developed for the cardiovascular system. In this chapter, the model will be validated using parametric data obtained from published literature. Tests were carried out to assess its suitability in predicting representative responses including sensitivity test of the parameters. This will allow the parameters that have an impact on the predicted response to be identified. Modelling of physiological and clinical phenomena will be described and compared to published data after the description of the parameter assignment and sensitivity test.

3.2 Parameter identification

All the parameters used in the model were obtained from physiological and/or clinical literature. The parameters that have been identified to define the hemodynamics in this study are given in Table 3-1.

The model parameters were firstly estimated in terms of the physiological range or the order of magnitude for the parameter value. The vascular resistances and inertances were calculated on the basis of fluid dynamic laws and the dimensions of the anatomic compartments that the individual sections of the model represent (Sun 1991). The heart valve parameters (inertance, resistance, and Bernoulli term for each valve) were obtained from a study using Doppler echocardiography data (Sun et al. 1995). The values for the parameters that could not be found from literature were fine tuned with their physiological ranges by trial and error by inspection of the predicted pressure and flow waveforms. A major determinant of the circulatory dynamics is the vascular elastance, which is nonlinear and specified by two parameters (E0 and Φ). For each elastance, these two parameters were iteratively adjusted until a reasonable representation for the hemodynamic waveforms and the average volume stored in the elastance was achieved. The volume constant Φ is generally of the same order of magnitude as the volume in the elastance. The baseline elastance for the contracting chambers were also determined on the basis of volume distribution in the heart.

Table 3-1 Parameter definition; See Notation for definition of abbreviations

	Pulmonary arteries	Pulmonary capillaries	Pulmonary veins	Aorta	Systemic arteries	Systemic capillaries	Systemic veins	Vena cava
R (mmHg · s2/ml)	0.01	0.04	0.005	0.04	0.8	0.2	0.005	0.005
L (mmHg · s2/ml)	0.0005	0.0002	0.0005	0.0005	0.0005	0.0005	0.0005	0.0005
Ω (mmHg · s/ml)	0.01	0.01	0.01	0.01	0.01	0.01	0.01	0.01
E0 (mmHg/ ml)	0.001	0.08	0.01	1.5	0.04	0.005	0.001	0.05
Φ (ml)	20	100	270	20	550	100	3200	20

	Left ventricle	right ventricle	left atria	right atria
Ω (mmHg · s/ml)	0.0001	0.0001	0.0005	0.0005
Eb (mmHg/ ml)	0.07	0.05	0.09	0.06
Ea (mmHg/ ml)	6	0.7	0.07	0.04

Kpc (mmHg)	1		
Vpc0 (ml)	380		
Φ (ml)	40		
Vpe (ml)	30		

	Mitral valve	Aortic valve	Tricuspid valve	Pulmonary valve
R (mmHg · s2/ml)	0.001	0.001	0.001	0.01
L (mmHg · s2/ml)	0.0002	0.0005	0.0002	0.0005
A (cm2)	5	4	5	4

Pitb (mmHg)	-3.7		
Pita (mmHg)	-1.8		
Tit (s)	0.1		

	tr (s)	tee (s)	tar (s)	tac (s)	τ_{vc} (s)	τ_{vr} (s)	τ_a (s)
	0.855	0.3	0.9	0.695	0.4	0.02	0.05

3.3 Simulation studies

3.3.1 Model fit to experimental data

The primary cardiovascular model contains 13 components. Parameter values of the integrated model were tuned to give good agreement with experimental data so as to represent a realistic cardiovascular system. Two criteria were used to justify the results: an accurate representation of the baseline hemodynamics in various parts of the system and a good fit to published pressure and flow waveforms.

Figure 3-1 shows the predicted pressure waveforms which has good agreement with those of experimental data. The predicted heart valve flow rate decreases to zero abruptly due to the closure mechanism, which assumes that valve flow ceases when the pressure gradient becomes zero in the model (Figure 3-2). As the aortic valve closes and the aortic walls relax, a rebound pressure wave against the aortic valve occurs, this is known as the dicrotic notch. The shorter aortic valve opening period due to this closure mechanism results in a relatively less distinctive dicrotic notch in the aortic pressure.

Predicted aortic flow exhibits similar waveforms to experimental data due to the use of the nonlinear characteristics for the arteries in this model (Figure 3-3). The phenomena including reported backflow and noise during the pressure decreasing phase for the aortic and mitral valves are neglected since such detailed modelling of these effects is beyond the scope of the current work.

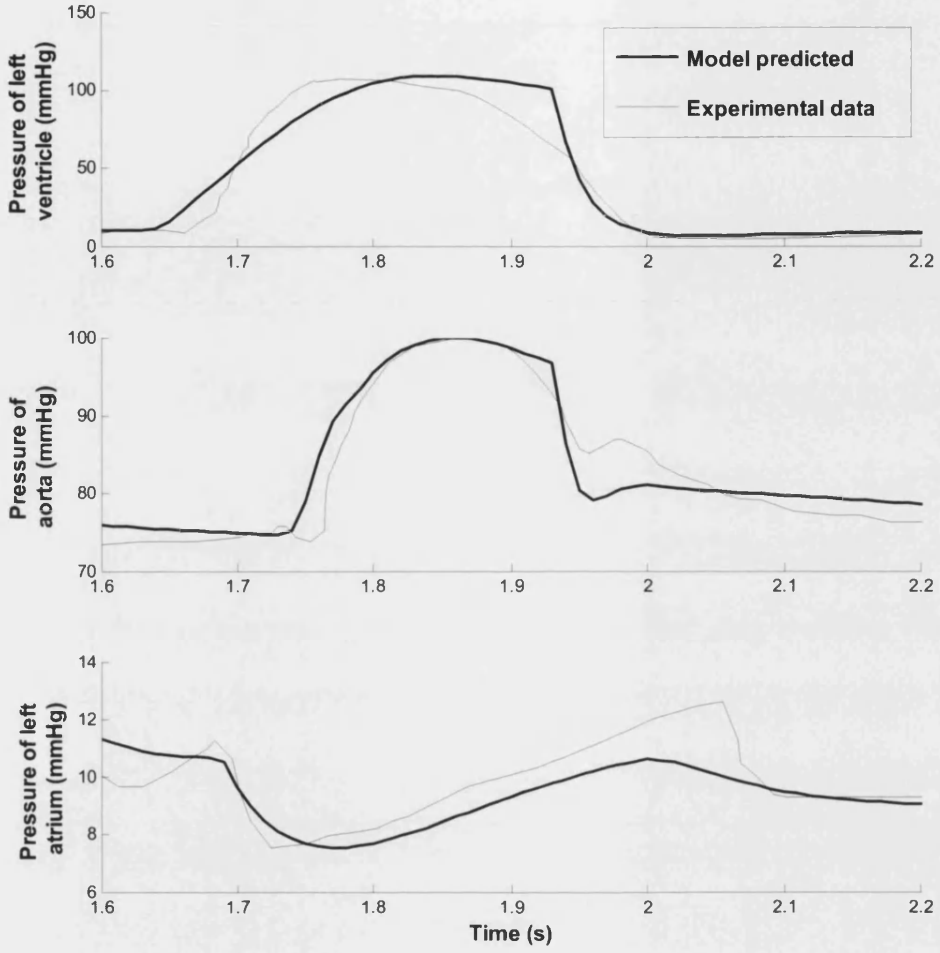

Figure 3-1 Model simulated pressure of left ventricle, aorta and left atrium (upper panel) and Experimental data from (Sugawara et al. 1989) (lower panel)

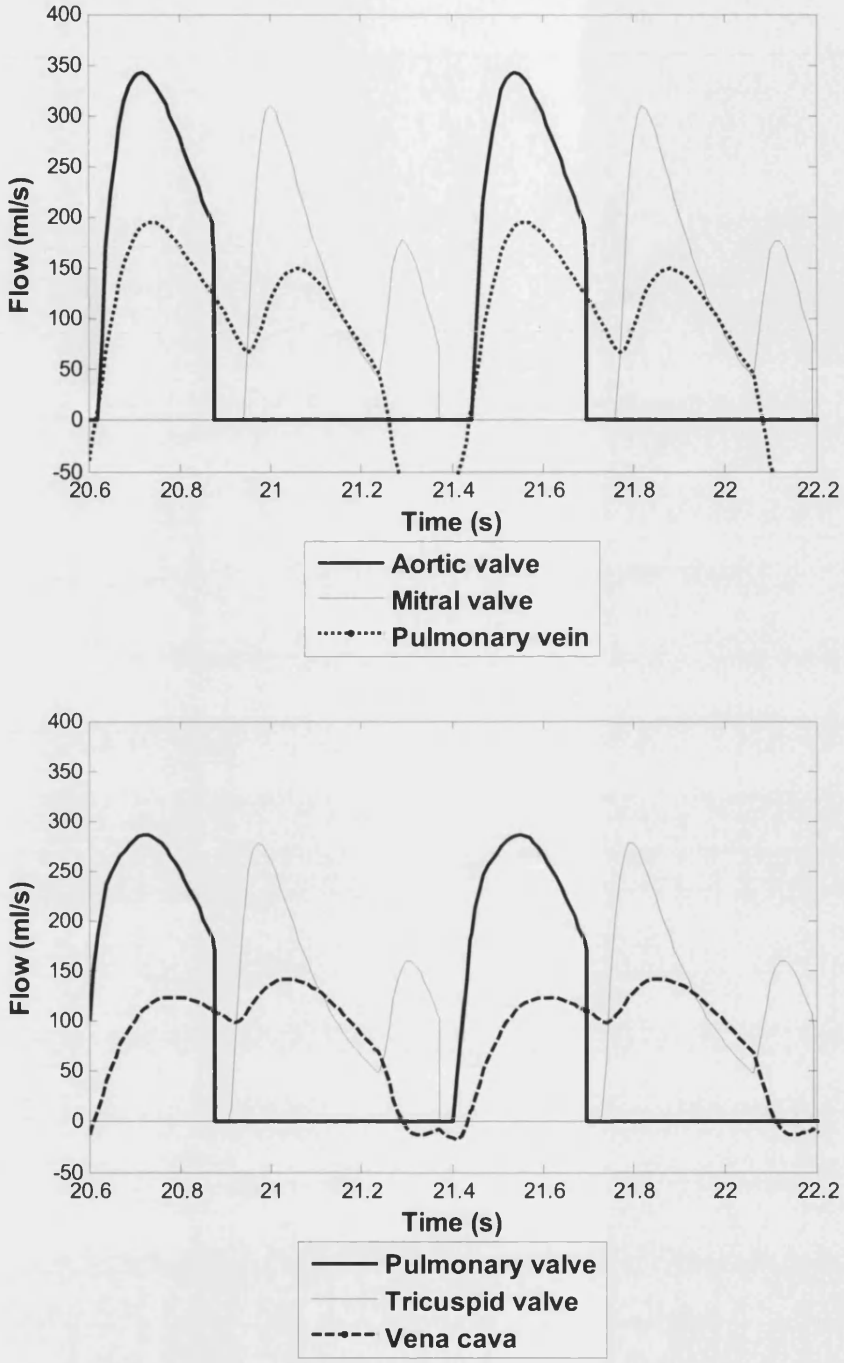

Figure 3-2 Heart valve flow and venous return for left and right heart

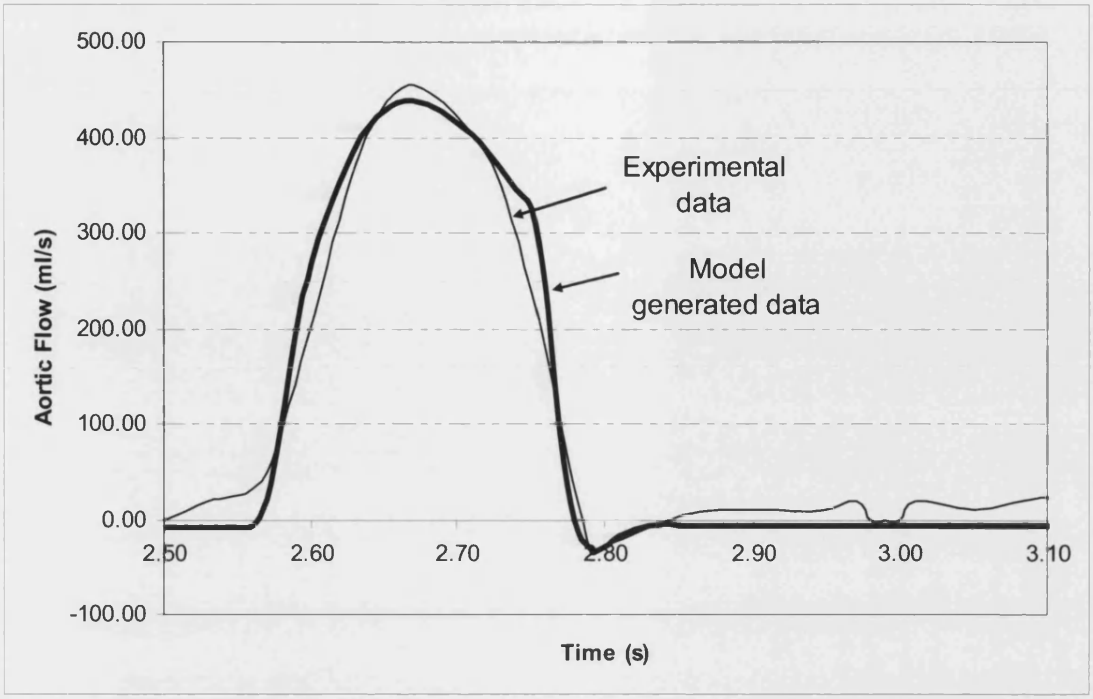

Figure 3-3 Aortic flows (Experimental data adapted from (Sugawara et al. 1989))

Simulated pressures and volumes are consistent with in vivo data (Table 3-2). The values fall into the correct range. The trend of decreasing pressure from the aorta to the veins agrees with normal physiological observation. Since the volume distribution provides crucial information for determining the elastance, it is necessary to look into the consistency of blood volume distribution between the model and the reported data. Table 3-3 shows that the volumes used for the major components are consistent with reported data.

*Table 3-2 Model representation of pressures and volumes at rest compared with in vivo data * assuming the body surface is 1.63 m^2. Body surface area is given approximately by (weight in kg + height in cm - 60)/100 m^2*

		Data from (Berne & Levy 1988;Fung 1984)	Model representation
Left atrial pressure (mean)		≦ 12 mmHg	8.00 mmHg
Left ventricular pressure	Peak systolic	100~150 mmHg	107.7 mmHg
	End - diastolic	≦ 12 mmHg	4.60 mmHg
Aortic pressure	Systolic	100~150 mmHg	99.90 mmHg
	Diastolic	60~100 mmHg	74.9 mmHg
Right atrial pressure (mean)		≦ 6 mmHg	5.95 mmHg
Right ventricular pressure	Peak systolic	15~30 mmHg	26.1 mmHg
	End - diastolic	≦ 6 mmHg	3.10 mmHg
Pulmonary arterial pressure	Systolic	15~30 mmHg	17.30 mmHg
	End - diastolic	4~12 mmHg	10.50 mmHg
Left ventricular end-diastolic volume at rest*		114~163 ml	120.0 ml
Left ventricular end-systolic volume at rest*		40~57 ml	49.7 ml
Stroke volume*		65~114 ml	70.4 ml
Pressure of pulmonary capillaries (mean)		10 mmHg	14.6 mmHg
Pressure of pulmonary veins (mean)		6 mmHg	8.87 mmHg
Systemic capillaries (mean)		20 mmHg	21.67 mmHg
Systemic veins (mean)		10 mmHg	7.21 mmHg

Table 3-3 Model representation of blood volume distribution in human circulatory system compared with in vivo data

	Blood volume distribution (%)(Guyton 1991)	Model prediction (ml (%))
Heart	7	330 (6.45%)
Pulmonary arteries	2.3	131 (2.56%)
Pulmonary capillaries	1.3	45 (0.88%)
Pulmonary veins	5.4	322 (6.29%)
Systemic arteries	13	920 (18.0%)
Systemic capillaries	7	376 (7.36%)
Systemic veins	64	2990 (58.45%)

3.3.2 Sensitivity test

A sensitivity test can provide a guide regarding the tuning of the parameter values to a certain physiological condition. The sensitivity is quantified by computing a gain factor as shown in following equation (Sun et al. 1997).

$$\text{sensitivity gain} = \frac{\%\ \text{change of affected (hemodynamic) index}}{\%\ \text{change of affected (model) parameter}} \qquad (3\text{-}1)$$

The hemodynamic indexes include cardiac output, systolic/diastolic aortic pressure, end-diastolic right and left ventricular, pulmonary arterial pressures, and right and left ventricular volumes; and mean right and left atria pressure; total pulmonary volume and total cardiac volume (heart volume); and systemic venous blood volumes. These were chosen because they are routinely measured to assess the physiological state of the cardiovascular system (Sun et al. 1997). Parameters include resistance, inertance, Bernoulli's resistance, parameters to define nonlinear elastance and time-varying elastance in all the components of the model. All of the results were obtained under steady state conditions (e.g. when initial transient had decayed).

The results of the sensitivity analysis are shown in Table 3-4. Only sensitive parameters are listed here which have a sensitivity gain larger than 0.1. The simulated hemodynamics is insensitive to most individual model parameters. Inertance (L), Capacitance (C), Resistance (R) and viscoelastance (Ω) are insensitive except for peripheral capillaries resistance. The systemic and pulmonary veins which account for the preload capacitances for the right heart and left heart are sensitive and they are a major determinant of cardiac output and aortic pressure. The pericardial volume offset (*Vpc0*) and intrathoracic pressure baseline (*Pitb*) were also found to be sensitive parameters.

Table 3-4 Sensitivity analysis results; Vsv: systemic venous blood volumes; Vhr: total cardiac volume; Vpul: total pulmonary volume

	cardiac output	systolic pao	diastolic pao	end-diastolic				mean			Vpul	Vhr	Vsv
				Prv	Plv	Ppua	Vrv	Vlv	Pra	Pla			
systemic veins													
E0	0.2	0.3	0.3	0.2	0.2	0.2	0.2	0.2	0.4	0.3	0.2	0.3	-0.1
phi	0.0	0.1	0.0	0.0	0.0	0.0	0.3	0.0	0.0	0.1	0.0	0.0	0.0
Right atrium													
Erab	0.0	0.1	0.1	0.1	0.1	0.1	0.1	0.1	0.2	0.1	0.1	-0.1	0.0
Eraa	0.0	0.1	0.0	0.1	0.1	0.0	0.1	0.1	0.0	0.1	0.1	0.0	0.0
right ventricle													
Ervb	-0.2	-0.2	-0.2	0.6	-0.2	-0.2	-0.3	-0.2	0.4	-0.2	-0.2	-0.1	0.1
Erva	0.2	0.2	0.2	-0.2	0.3	0.2	-0.2	0.3	-0.2	0.3	0.2	0.0	-0.1
pulmonary veins													
E0	0.2	0.3	0.3	0.0	0.0	0.0	0.0	0.0	0.4	0.3	0.2	0.3	-0.1
phi	0.0	0.0	0.0	0.0	0.0	0.0	0.0	0.0	0.0	0.0	0.1	0.0	0.0
left atrium													
Elab	0.1	0.1	0.1	0.1	0.1	0.1	0.1	0.1	0.1	0.2	0.2	-0.1	0.0
Elaa	0.0	0.0	0.0	0.0	0.0	0.0	0.0	0.0	0.0	0.0	0.0	0.0	0.0
left ventricle													
Elvb	-0.3	-0.3	-0.2	-0.1	0.7	0.4	-0.1	-0.3	-0.1	0.6	0.3	0.0	0.0
Elva	0.2	0.2	0.2	0.2	-0.2	-0.1	0.2	-0.2	0.1	-0.2	-0.1	-0.1	0.0
peripheral capillaries													
R	-0.2	0.5	0.7	-0.2	0.2	0.1	-0.2	0.2	-0.2	0.2	0.1	0.1	-0.1
E0	0.0	0.3	0.0	0.0	0.0	0.0	0.0	0.0	0.0	0.0	0.0	0.0	0.0
phi	0.0	0.0	0.0	0.0	0.0	0.0	0.0	0.0	-0.1	0.0	0.0	0.0	-0.1
Pericardium													
Vpc0	0.5	0.5	0.4	0.7	0.5	0.5	0.7	0.5	0.6	0.6	0.5	0.6	-0.2
Intrathoracic pressure													
Pitb	0.0	0.1	0.1	0.0	0.1	0.0	0.0	0.1	0.1	0.1	0.0	0.1	0.0

3.3.3 Atrial contraction

The atrial pressures show the characteristic shape of a wave (Figure 3-4). During the diastole period, the ventricular pressure drops below that of atrial pressure following the opening of the atrioventricular valves. The blood pressure which has slowly built up in the atrium during the ventricular contraction causes blood to flow quickly into the ventricle. The pressure builds up and release in the atrium during ventricular contraction can be seen as a wave and is called the *'v' atrial pressure wave*. The contraction of the atrium causes a rise in pressure in the atria, which is called the *'a' atrial pressure wave*; it pushes any blood left in the atria into the ventricles. During the ventricle systole period, the rapid closing of the atrioventricular valves causes a rise in pressure in the atria which is known as the *'c' atrial pressure wave*.

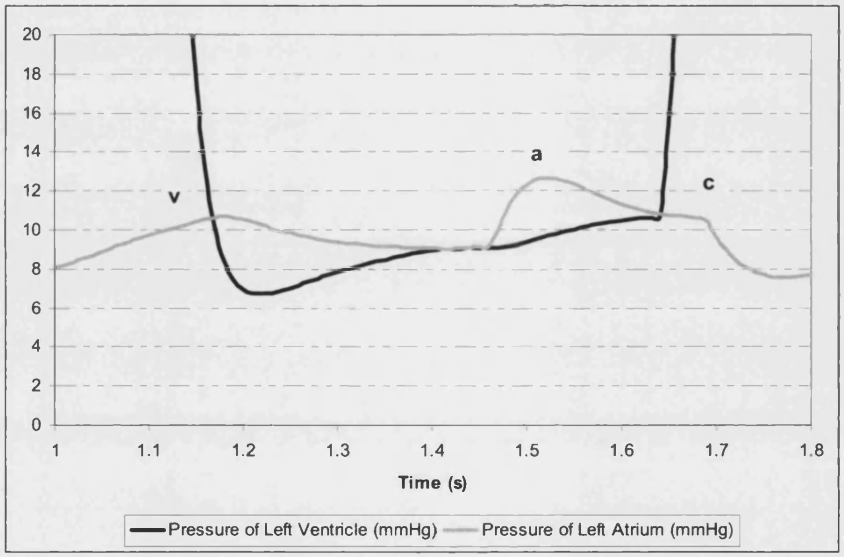

Figure 3-4 Pressures during ventrical filling. 'a' - atrial contraction; 'c'- bulging of tricuspid valve into atrium at start of ventricular contraction; 'v' - passive filling of right atrium and vena cava when tricuspid valve closes

The *'a' atrial pressure wave* re-establishes the pressure gradient and accelerated flow across the atrioventricular valves. The atrial contribution to filling can be defined as the flow without atrial contraction. The shaded areas in Figure 3-5 indicate the contribution due to the contraction of the atrium, which normally contributes around 15% of the ventricular filling and is relatively independent of heart rate in the resting state

(Sugawara et al. 1989). This activity becomes more important when the heart rate increases. However, an appropriately timed atrial contraction is not necessary for complete end-diastolic mitral valve closure. Clinical data shows that the mitral valve closes completely in the absence of an atrial contraction. Therefore, atrial contraction mainly contributes to ventricular filling and not to the valve closure.

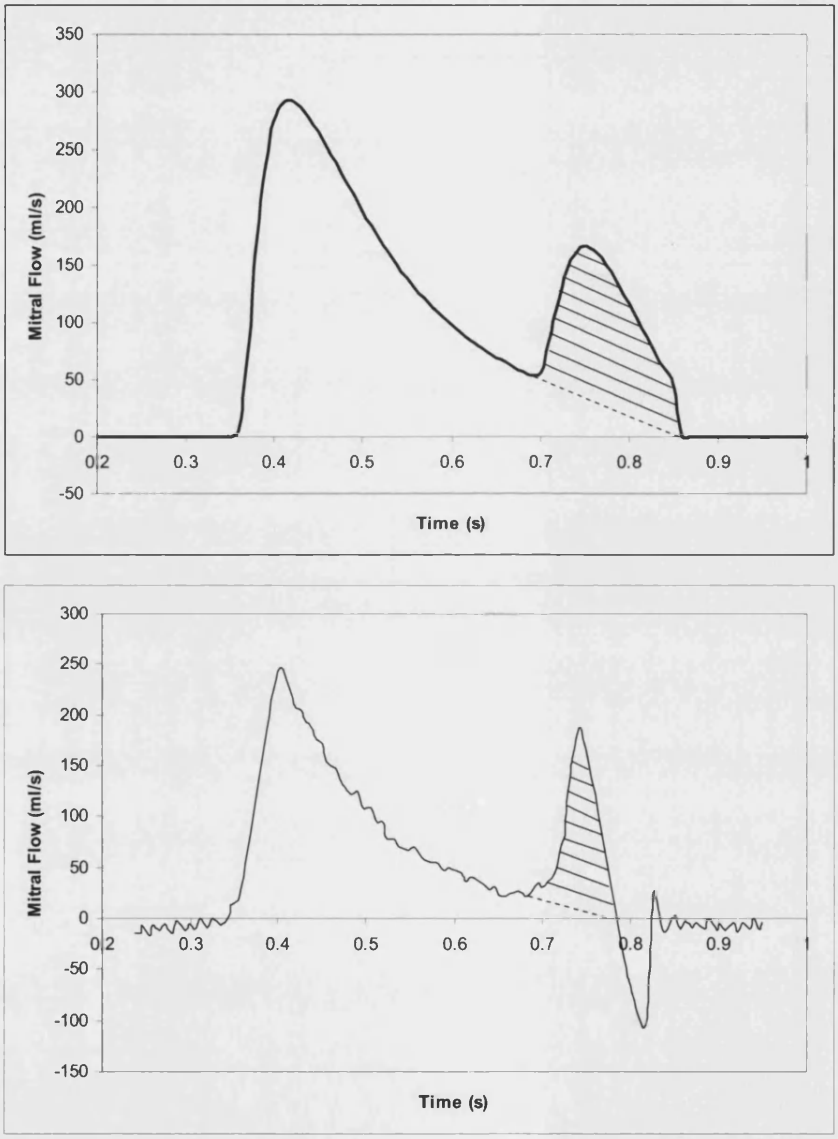

Figure 3-5 Mitral valve flow. Upper panel: model generated data; Lower panel: experimental data (Sugawara et al. 1989). Shaded area due to atrial contraction

3.3.4 Heart valves

The heart valve flow dynamics have been modelled using Bernoulli's equation. For the aortic valve flow, when the ventricular pressure exceeds the aortic pressure the opening of aortic valve is triggered. Blood passes into the aorta instantly which leads to the increase in aortic pressure. When the aortic pressure rises sufficiently, deceleration of the flow occurs and an adverse pressure gradient is produced which causes the valve to close.

Figure 3-6 shows three conditions with a varied inertial term that governs the deceleration and acceleration of flow. It can be seen that the higher the inertial term the faster the flow changes and the higher the maximum flow. Apart from the inertial term, introduction of the Bernoulli term as a function of the valve area enables the model to be tuned to model valvular stenosis (abnormal narrowing of a heart valve). Figure 3-7 shows the left ventricle and aortic pressure when changing the aortic valve area from 5 cm^2 to 1 cm^2. The pressure difference reflects mainly the conversion of some of the potential energy to kinetic energy. When there is an aortic valvular stenosis, the pressure difference is even more pronounced, because substantial energy is lost through friction due to blood passing rapidly through a narrow orifice.

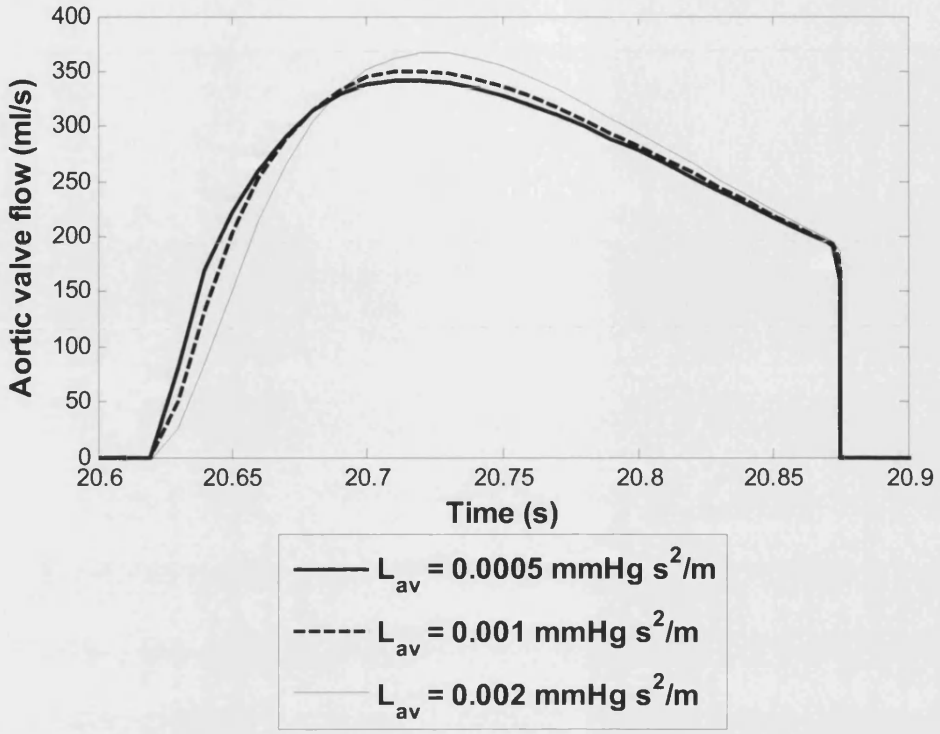

Figure 3-6 Aortic valve flow with different inertial terms

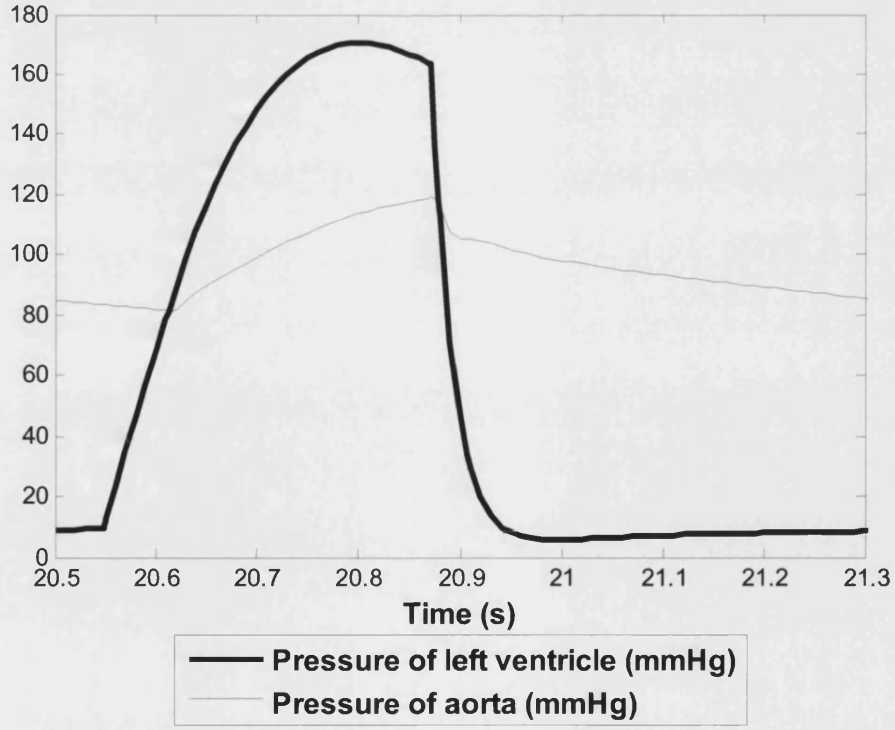

Figure 3-7 Pressure of left ventricle and aortic arteries

3.3.5 Capacitance non linear effect on arteries

The blood vessels are represented by capacitance, resistance, inertance and viscoelastance terms. Conventionally, the capacitance or compliance is represented using a linear function that depends on the volume and pressure of the vessels. However, experiments show that the arteries become stiffer in the high-pressure range (Melchior et al. 1992), indicating at the compliance of the arteries varies with pressure. An exponential pressure-volume equation included in the model effectively represents this behaviour without introducing a discontinuity into the model

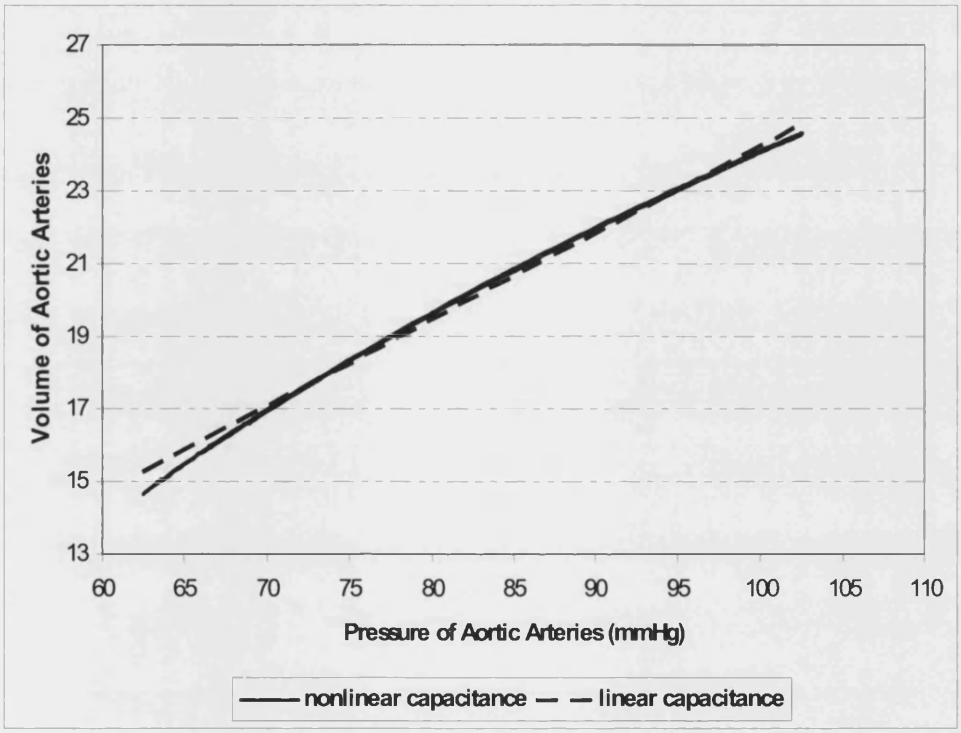

Figure 3-8 Volume – Pressure relationship of arteries

3.3.6 Interaction of ventricles

3.3.6.1 Volume coupling among the chambers in the pericardium

The pericardium is the fluid filled sac that surrounds the heart and the proximal ends of the aorta, vena cava and the pulmonary artery. The distensibility of the pericardium is small so it can prevent the heart from sudden overdistension. Removal of the

pericardium constraint effect should lead to a volume increase of each chamber. The phenomenon can be investigated by setting pericardial pressure coefficient K_{pc} to zero. Figure 3-9 shows the volume increase when removing the pericardium (thick line). Because of the volume increases, the pressure in each chamber also increases according to the pressure-volume relationship of ventricle (Figure 3-9). Although the changes of the end systolic pressure are significant, the end diastolic pressures remain roughly the same with differences of less than 1 mmHg.

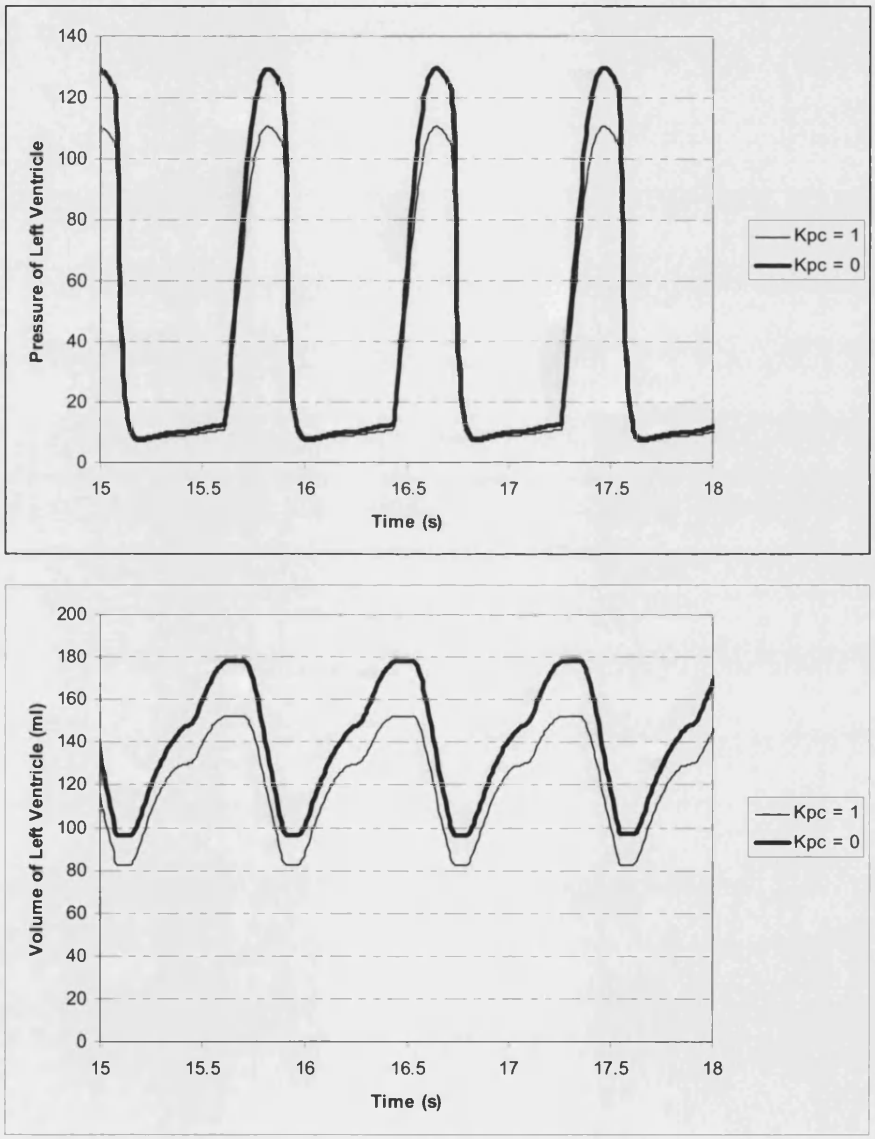

Figure 3-9 Effect of pericardium on pressure of ventricles

3.3.6.2 Pressure coupling through the interventricular septum

The intact pericardium imposes a mechanical constraint to the outward expansion so an increase in volume in one ventricle impairs the filling of the other ventricle. Normally, the greater LV pressures cause the septum to bulge toward the RV during both systole and diastole. Stiff and elastic interventricular septums were modelled by setting effective septal elastance (*Es*) to 1×10^6 and 46 respectively. When the septum becomes more elastic, the left ventricle tends to shift to the right ventricle which leads to a larger difference between their volumes.

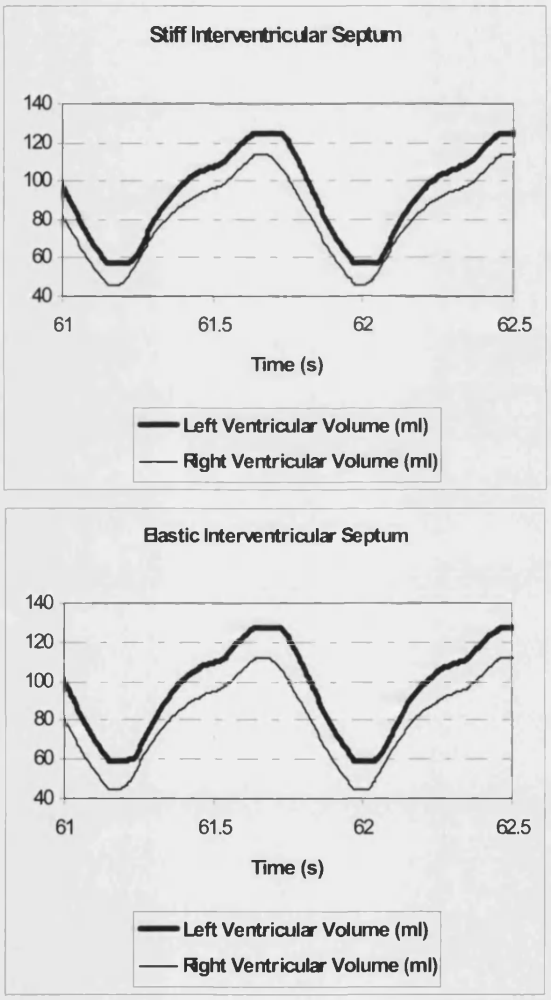

Figure 3-10 Effect of the interventricular septum on ventricular volume

3.3.7 Effect of Intrathoracic pressure on blood flow

The effect of intrathoracic pressure on blood flow needs to be considered in order to combine the respiratory system with the cardiovascular system. Figure 3-11 shows the simulation result of aortic pressure with consideration of respiratory effects during the normal resting condition. Aortic pressure appears to increase slightly during expiration and decrease during inspiration.

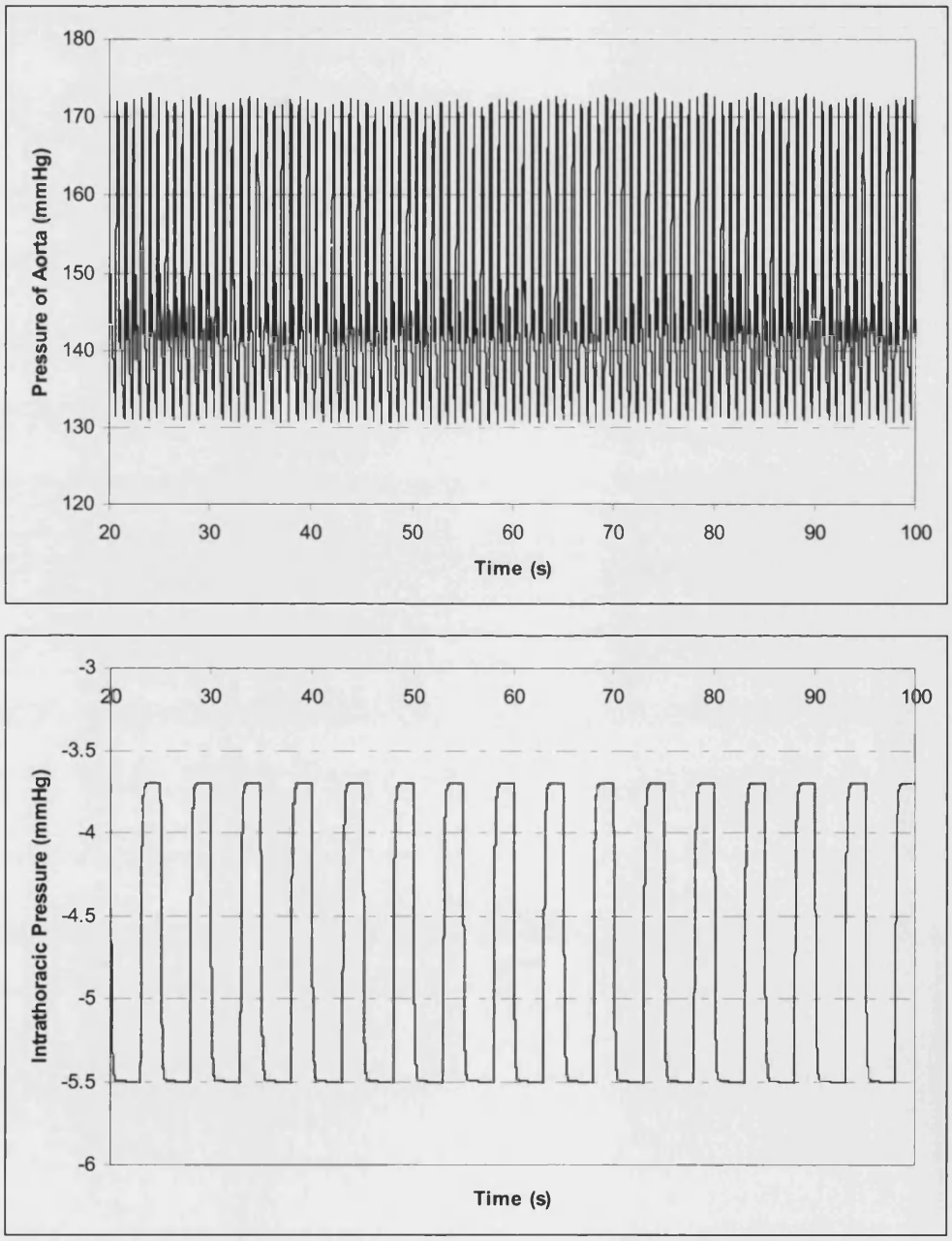

Figure 3-11 Simulation of respiratory effects on aortic pressure

3.4 Discussion

A primary cardiovascular model has been developed containing 13 components. The model consists of pulmonary circulation, systemic circulation and a four-chamber heart model. Parameter values for the integrated model were tuned so as to represent a realistic cardiovascular system. The results were justified by an accurate representation of the baseline hemodynamics in various parts of the system and a good fit to measured pressure and flow waveforms. The predicted waveforms of pressures and flows agree with measured pressure and flow waveforms (Figure 3-1). The aortic flow exhibits similar waveforms to the published experimental data (Figure 3-3) due to the use of the nonlinear characteristics for arteries in this model. Also the closure mechanism of heart valve produces the dicrotic notch in the aortic pressure. Important hemodynamic indexes such as cardiac output, end diastole and end systole pressures, mean volumes and flows are consistent with published data. The sensitivity analysis undertaken identifies parameters that are of primary importance to blood circulation. Sensitive parameters are listed in Table 3-4 which can give guidance for tuning the model. Pericardial volume offset is the most sensitive parameter mainly because the constraint effect of the pericardium is dominant; this is shown in the significant volume change of the heart due to the removal of the pericardium. The vascular resistance was also identified in the test to have a significant impact. This also indicates that the vascular resistance is a main control variable in the cardiovascular control system.

Further studies were focused on the improvement of the new mathematical model. Baseline hemodynamics generates characteristic shapes of atrial waves. A contraction of atrium normally contributes to around 15% of ventricular filling. This activity becomes more important when the heart rate increases. It will be shown that this activity is important when modelling diseases such mitral stenosis in Chapter 8.

However, an appropriately timed atrial contraction is not necessary for competent end-diastolic mitral valve closure. Clinical data shows that the mitral valve does close competently in the absence of an atrial contraction. Therefore, atrial contraction mainly contributes to ventricular filling and not to the valve closure. The model uses Bernoulli's equation to simulate heart valve dynamics. If the friction loss and the

Bernoulli term in the equation are neglected, it is clearly shown that deceleration flow is essential to the valve closure. For the mitral valve, the flow decelerates after blood injects into the ventricle. The deceleration causes the pressure to increase in the direction of flow. When the pressure acting on the ventricular side of mitral valve becomes higher than that on the other side, the net force acts to close the valve. The same principle applies to the aortic valve. Backward flow, or regurgitation only occurs in an abnormal heart as forward flow momentum prevents regurgitation at the time of final valve closure (Fung 1984). The Bernoulli term in the equation can be regarded as the dynamic pressure while the other pressure term is the static pressure. Hence, pressure gradients act as a driver force to the flow, which contribute to the acceleration/deceleration of the blood flow.

The blood vessels are represented by capacitance, resistance, inertance and viscoelastance terms. Improvements to the model concentrated on the nonlinearity of the blood vessels. Conventionally, the capacitance or compliance is a linear function depending on the volume and pressure of the vessels. An exponential pressure-volume equation represents this behaviour more accurately without introducing a discontinuity into the model. Venous compartments have different characteristics so it is improper to use the same mathematical model as the arteries. The compliance of the veins was suggested to be constant in literatures having a value of about 24 times higher than arteries, allowing the veins to store considerably more blood. These two characteristics were accomplished by assigning a high value of volume constant to the same mathematical model developed for the arteries. The capillaries resemble with a resistant vessel rather than an elastic vessel. Therefore, the resistant of the capillaries was set to be higher than other parts of the circulatory system. In some blood vessel models (Leaning et al. 1983;Ursino & Magosso 2003), viscoelastance was neglected as small contribution to hemodynamics. Actually, viscoelastance becomes more and more dominant as the blood flows towards the capillaries, where the walls become thinner and thinner. Fung (1984) suggested that viscous stresses play a dominant role in determining stability and turbulence in the arteries, and whether the streamline will separate from the wall of the vessel at branching points or at segments where a sudden change in cross section occurs such as in stenosis or aneurysm (an abnormal widening or ballooning of a portion of a blood vessel).

Interactions exist everywhere in a complex biological system such as the cardiovascular system. For example, interactions between ventricles including pressure and volume coupling may affect the performance of the heart significantly. The model of the interventricular septum enabled the volume of the left ventricle to shift to the right ventricle. The results are generally in accord with physiological principles. Pericardial coupling restrains the heart chamber from over distension (Figure 3-9). However, its insignificant difference between intact and removed septum suggests that such an interaction has minor effect on the global model and can therefore be ignored. Jackini and Weber (1980) suggested that the removal of the pericardium will increase end diastole pressure by 4.6 mmHg and a much larger increase of end systole pressure up to 17 mmHg. This phenomenon was assessed by setting K_{pc} to zero. The shift of pressure and volume agrees with their findings (Figure 3-9). This shows the pericardium plays a major role in the performance of the heart.

Respiratory effects on the cardiovascular system have also been considered. A simple model was attempted to demonstrate these effects. By applying intrathoracic pressure on both systemic arteries and veins, the pressures vary with expiration and inspiration. Further investigation will be described later in the thesis after incorporating the model with the respiratory model.

3.5 Closure

A 13-element mathematical model of cardiovascular system was developed and described in Chapter 2. In this Chapter, parameter values for the integrated model were tuned so as to represent a realistic cardiovascular system. The results were justified by an accurate representation of the baseline hemodynamics in various parts of the system and a good fit to measured pressure and flow waveforms. The sensitivity study undertaken provides a guide regarding the tuning of the parameter values to a certain physiological condition and identifies parameters which have impact on the cardiac performance.

The time-varying elastance model generated characteristic pressures and volumes waveforms of atria and ventricle. The exponential pressure-volume equation effectively represented the nonlinear property of the arteries. With the detailed features such as

interventricular septum, heart valves and pericardium, the model is capable of predicting a number of clinical or physiological phenomena. Valvular stenosis was modelled by changing the area of the valve. The shift of the ventricular pressure was demonstrated by changing the effective septal elastance. The constraint of the pericardium to the heart's sudden overdistension was investigated by altering the pericardial pressure coefficient to smaller value. Simulation also shows the effect of the intrathoracic pressure on the blood pressure.

Accurate simulations were demonstrated by the good fitting with published experimental data. The accurate representation of the hemodynamics in various parts of the system and the good fit to published pressure and flow waveforms provides confidence for the incorporation of the baroreflex control model and the respiratory model.

Chapter 4 Cardiovascular control system

4.1 Introduction

The cardiovascular control system has been investigated by both physiologists and engineers. This has resulted in the development of a range of different mathematical modelling approaches (Leaning et al. 1983;Levy & Zieske 1969;Ursino 2000;Warner & Cox 1962). Early researches (Levy & Zieske 1969;Warner & Cox 1962) concentrated on heart rate control due to its complexity and the interests of heart rate variability analysis. Levy and Zieske (1969) modelled the heart rate control in a quantitative way while Warner and Cox (1962) modelled it in a qualitative fashion. Warner's method has great influence on later models. Recent control system models (Leaning et al. 1983;Ursino 2000) included the control of other cardiac parameters such as cardiac contractility and blood vessel resistance in addition to the heart rate.

Figure 4-1 provides an overview of the cardiovascular reflex control system including inputs from the receptors, outputs to the effectors and the central nervous system. The arterial baroreceptors, which refer to aortic and carotid baroreceptors, and cardiopulmonary receptors are dominant sensors in the control system. Chemoreceptors, which sense the partial pressures of oxygen and carbon dioxide in the arterial blood and the brain, also have an influence on the cardiac responses.

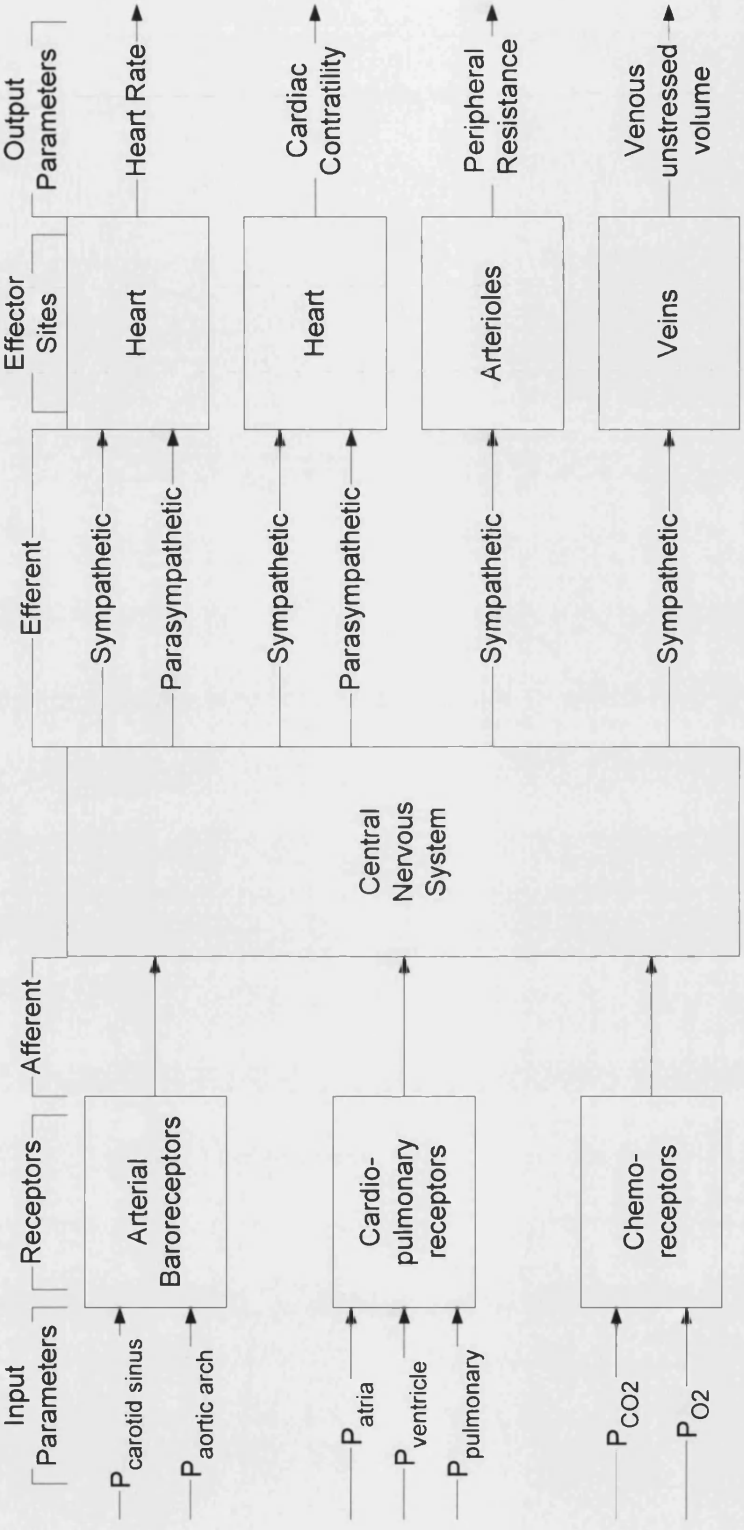

Figure 4-1 Cardiovascular reflex control system (adapted from (Melchior et al. 1992))

The baroreceptor reflex is the single most important mechanism for short-term control of arterial pressure. This reflex system consists of pressure receptors in the carotid arteries and aortic arch with afferent neurons running to the medulla in the central nervous system. The integration of inputs occurs in the medulla. The efferent pathways of the baroreceptor reflex involve the parasympathetic and sympathetic nervous systems.

Cardiopulmonary receptors respond to the absolute pressure in the atria and the pulmonary veins. Although they discharge at lower pressures than the arterial baroreceptors, on reaching the brain, the impulses initiate a similar response. Elevated cardiopulmonary pressure inhibits sympathetic output.

The primary purpose of the peripheral chemoreceptors, which are located in the carotid and aortic bodies, is to control respiration. Although the peripheral chemoreceptors respond to increased arterial P_{CO2}, increased H^+ concentration, and decreased arterial P_{O2}, the latter is most important physiologically. The increased discharge of these receptors, brought about by low arterial P_{O2}, stimulates increased activity of the cardiovascular centre, hence increasing vasoconstriction and blood pressure. When elevated arterial P_{O2} and low arterial P_{O2} occur simultaneously, the vasoconstrictor response is augmented, just as is the ventilatory response. The chemoreceptor responses can be overridden by the baroreceptor responses.

Researchers have mainly concentrated on the modelling of the baroreceptor because the baroreflex action is the most important short-term regulator for the arterial pressure and cardiovascular function (Lu et al. 2001;Ursino 2000;Ursino & Magosso 2003). This chapter will describe the development of an improved baroreceptor control model. The chemoreflex control will be described in Chapter 6.

4.2 Overview of the baroreceptor reflex models

The model of the baroreflex control system shown in Figure 4-2 includes the afferent activity coming from the baroreceptor (afferent compartment), the central neural level (central compartment), and the activity of the efferent (efferent compartment). The efferent sympathetic pathway (SNA) and parasympathetic pathway (PNA) run to their corresponding effector sites including the heart, capillaries and veins.

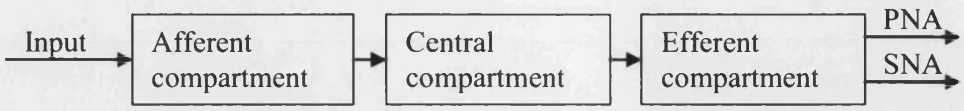

Figure 4-2 Simplified representation of the baroreflex model

One of the most detailed neural-controlled models was developed by Leaning which is largely based upon the works of Katona et al and Hyndman (Leaning et al. 1983). It includes models of the carotid sinus baroreceptor and the aortic arch baroreceptor. Outputs of these two receptors are fed into a two-region model of the controller, one for blood pressures above normal (region A in Figure 4-3) and the other for pressures below normal (region B in Figure 4-3) . The overall response of the controller is a linear combination of the outputs from the two regions. The model has four separate controllers for heart rate, myocardial contractility, vein tone and peripheral resistance. As it can be seen in Figure 4-3, it is difficult to assign physiological terms to the blocks or the parameters.

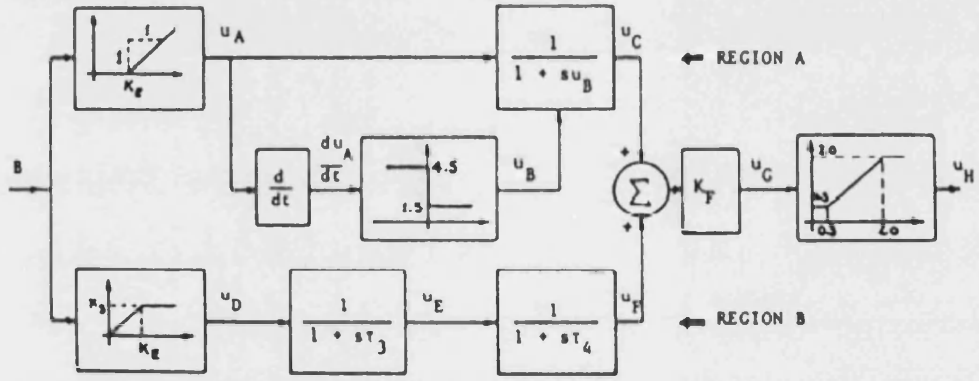

Figure 4-3 Block diagram of the two-region controller (here, controller of heart rate) (Leaning et al. 1983)

Recently, with better understanding of baroreflex, Ursino and other researchers (Lu et al. 2001;Ursino & Magosso 2003) developed baroreflex models that are divided into three compartments: afferent, central and efferent components. Aortic pressure is the input parameter to the afferent components (arterial baroreceptor). The baroreceptor sends firing pulses through the afferent components to the central compartment which

determines the demands of the body, forming the outflow of the efferent compartment. The efferent compartment consists of sympathetic and parasympathetic nerve divisions. The outputs from the central compartment pass along the efferent neural pathways and terminate at the effector sites and dendrites of the vagus (parasympathetic) neurons to the heart and the sympathetic neurons to the heart, arterioles, and veins.

4.2.1 Afferent compartment

In a baroreceptor reflex model, the major cardiovascular variable being regulated is the arterial pressure in the systemic circulation since it is the driving force for blood flow through all the organs except the lungs. The carotid pressure is usually used in the models because the carotid baroreceptor is the best understood among the receptors. The aortic pressure shows a similar range of pressure as the carotid pressure though it has little effect of pulse response.

Itani and Koushanpour (1989) reviewed the baroreceptor characteristics as follows:

- firing of the baroreceptors is directly proportional to the input pressure they sense
- the baroreceptors respond not only to the absolute pressure level but also the rate of change of pressure; moreover, they respond to positive rate of change differently to negative rates of change
- a minimum level of mean input pressure is required for the baroreceptors to start firing
- a delay occurs in the response of the baroreceptors to a transient pressure change
- the ratio of a change in output pressure to a change in arterial pressure varies with mean input pressure and peaks at some input pressure

Most models include one or more of the characteristics mentioned above. Ursino and other researchers (Lu et al. 2001;Ursino 2000) introduced a non-linearity into the afferent path or the effector sites. Recent research (Kawada et al. 2003), however, shows that the nonlinearity should dominate in the efferent pathway rather than at the baroreceptors.

4.2.2 Central compartment

The central nervous system is the integrating element of the overall control system. It gathers the input information coming from receptors through afferent nerves and sends out command information to the heart and blood vessels of the different parts of the circulation through efferent sympathetic and parasympathetic pathways. Many aspects of the system are not yet sufficiently understood and researchers usually assume it is a simple integrating element in the overall control process (Leaning et al. 1983;Ursino & Magosso 2003).

4.2.3 Efferent compartment

Kollai and Koizumi (1989) studied the effects of ascending stepwise pressure changes in the isolated carotid sinuses on cardiac vagal and sympathetic nerve activity and found the relationship between pressure and nerve activities can be represented as sigmoid functions. Sympathetic and parasympathetic activities are normalized to unity at the point of the highest value and plotted against arterial pressure as shown in Figure 4-4. Sympathetic activity has a negative slope at the normal arterial pressure while parasympathetic activity has a positive slope. The baroreceptor reflex gain was calculated as the amount of changes in autonomic nerve activity of blood pressure for each 20 mmHg step in the pressure rise. The maximum value of the baroreceptor reflex gain is defined as the baroreflex sensitivity. The point in the sigmoid function where this maximum value occurs is the operating point of the arterial baroreceptor.

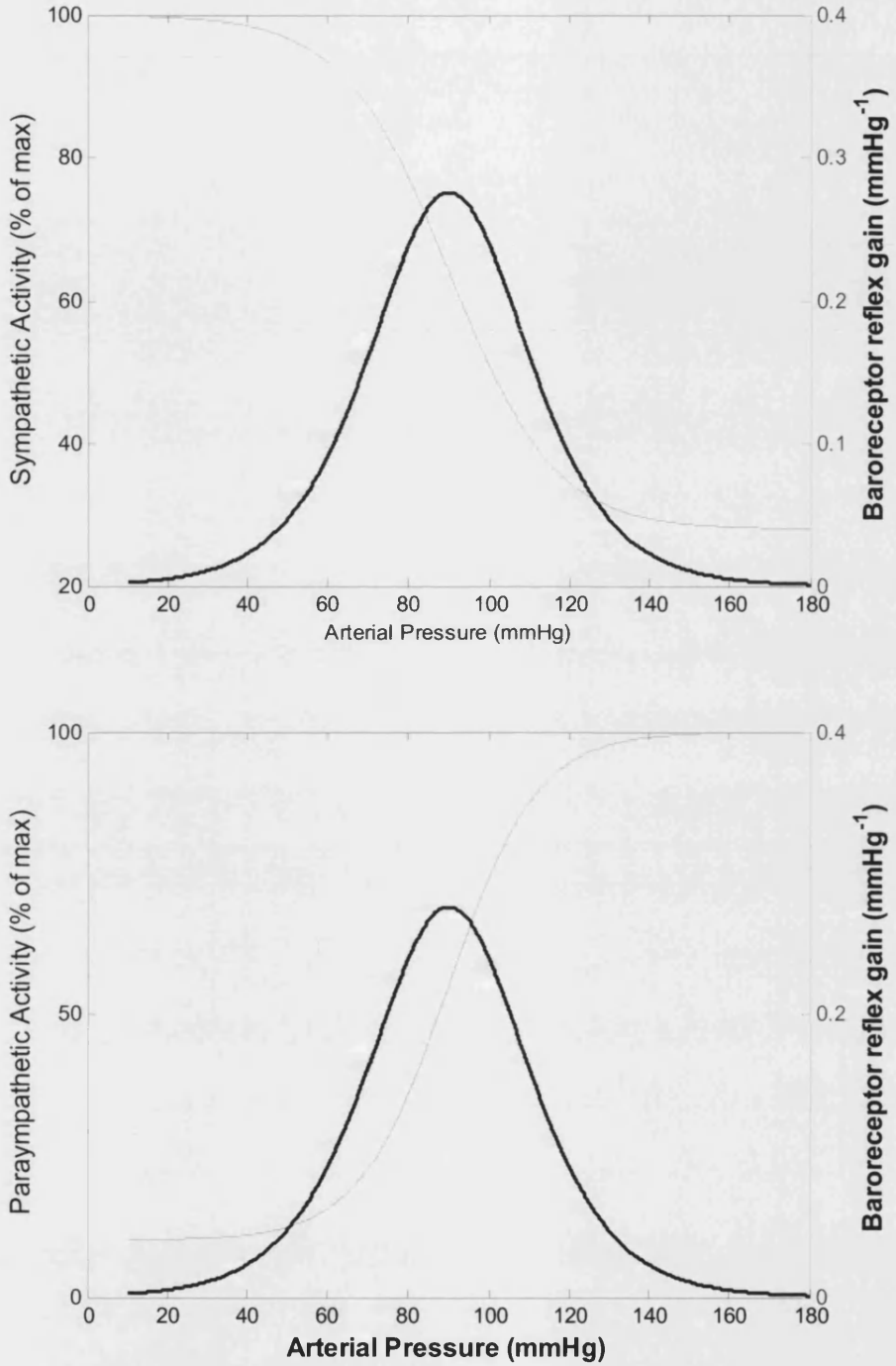

Figure 4-4 Relationships between the arterial pressure and sympathetic and parasympathetic activities (adapted from (Kollai & Koizumi 1989))

In humans, anticipation of exercise weakens both HR and blood pressure responses to positive and negative neck pressure. Central command exerts its influence on SNA and vagal control of HR by resetting the arterial baroreflex. After a transient period of

adjustment, the relationship between blood pressure and carotid sinus transmural pressure shifted to the right, suggesting resetting.

Figure 4-5 shows the shifting of the response curve. On the top panel, the operating point is shifted to a higher blood pressure laterally by the central command via baroreceptor afferents. On the lower panel, Muscle chemoreflex shifts the baroreflex function curve vertically. These two combined effects cause the curve shift up and to the right as show in the figure.

Although the parasympathetic nerve activity has an impact on heart contractility, the sympathetic nerve activity plays a major role in its control. Therefore, both parasympathetic and sympathetic nerve activity control the heart rate, while other output parameters of the regulator such as heart contractility, venous compliance and peripheral resistance are determined solely by sympathetic nerve activity.

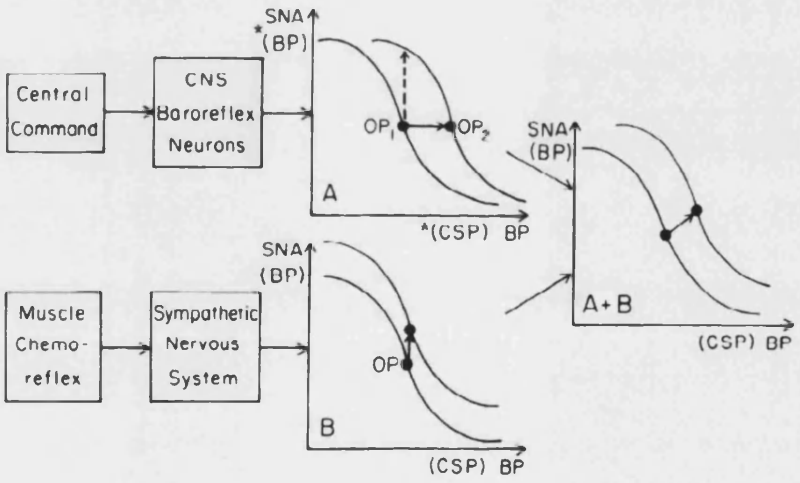

Figure 4-5 Resetting of operating point during exercise (Rowell & Oleary 1990)

4.2.4 Effector sites

The most detailed control system contains separate controls for the heart rate, cardiac contractility, arterial resistance and venous tone (Melchior et al. 1992). Each overall relationship between an input and output of the reflex system relies on experimental data correlations. The relationships combine serial and parallel linear and nonlinear functions.

Heart rate responds to both sympathetic and parasympathetic stimulation. More importantly, combined sympathetic and parasympathetic stimulations have a complicated interacted effect on heart rate change (Melchior et al. 1992). Warner and Russell (1969) investigated the effects of sympathetic and parasympathetic stimulation and the combined effect on the heart rate by stimulating both sympathetic and parasympathetic nerves to a particular frequency level. Three features were drawn from the experiments:

- the heart rate increases more rapidly than it decreases back to the control level
- the change in the heart rate due to sudden nerve stimulation is dependent on the frequency stimulated (this is more noticeable for sympathetic than parasympathetic nerve activity)
- the gain of the response is nonlinear

Interactions between the two nerve divisions on the control of the heart rate are taken into account. It is believed that the parasympathetic nerve is dominant over the resting period. Levy and Zieske (1969) interpret this interaction in the following form

$$\Delta HR = a_1 \cdot SNA + a_2 \cdot SNA^2 + a_3 \cdot PNA + a_4 \cdot PNA^2 + a_5 \cdot SNA \cdot PNA \tag{4-1}$$

where a_1 to a_5 are coefficients obtained from experimental data fitting.
The other interpretation is from Warner (Warner & Russell 1969)

$$HR_{sv} = HR_v + (HR_s - HR_0)\frac{(HR_v - HR_{min})}{(HR_0 - HR_{min})} \tag{4-2}$$

It is broadly accepted that a sympathetic stimulation causes changes in the cardiac contractility, venous compliance and peripheral resistance while parasympathetic stimulation has little effect on these effector sites.

4.2.5 System overall response to arterial pressure change

Figure 4-6 shows the interaction between key elements in the control system which affect overall response to arterial pressure change. If the arterial pressure decreases, for example during a hemorrhage, this causes the discharge rate of the arterial baroreceptors to decrease. Fewer impulses travel up the afferent nerves to the medullary cardiovascular centre, and this induces:

- increased heart rate due to the increased sympathetic activity to the heart and decreased parasympathetic activity
- increased ventricular contractility due to the increase in sympathetic activity to the ventricular myocardium
- arteriolar constriction due to the increase in sympathetic activity to the arterioles
- increased venous constriction due to increased sympathetic activity to the veins, this effectively decreases the venous unstressed volume

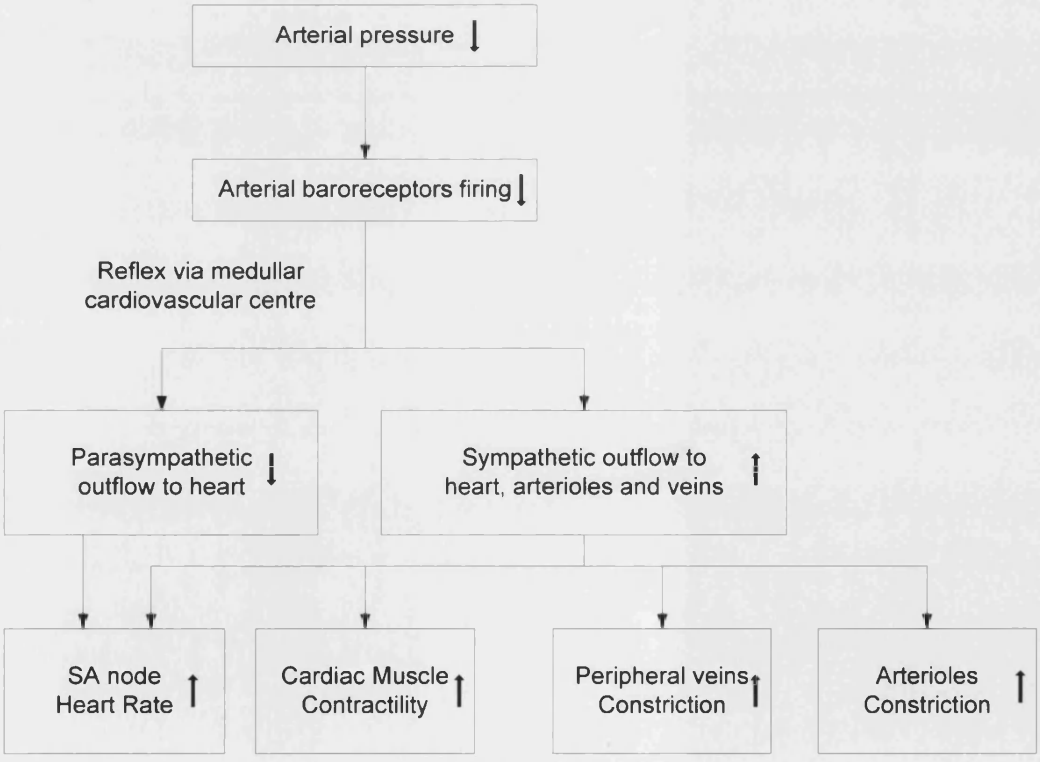

Figure 4-6 System overall response to arterial pressure change (Vander et al. 2001) (↑ represents increase, ↓ represents decrease)

4.2.6 Pulse generation

The controlled output variables feed into the cardiovascular system hydraulic model at the beginning of every heart beat using a generated pulsed signal. There are two ways to generate the signal, one of which is Integral Pulse Frequency Modulator (IPFM) (TenVoorde B.J. & Kingma R. 2000). IPFM works such that a pulse is output only when it reaches a certain threshold. A high pass filter is sometimes used to derive the mean value of arterial pressure over the period of a heart beat so that a pulse output can be generated (Ursino 2000).

4.2.7 Mathematical modelling of overall control system

Table 4-1 provides a comparison of the control elements and their characteristics in published models. The chemoreceptor is not listed and this effect will be covered in the Chapter 6. Control of venous tone and peripheral resistance are not listed because most of the models include these effects. From the table, it can conclude that aortic and aortic baroreceptor models are well developed while cardiopulmonary has received less attention due to its lower importance in cardiovascular system control. The control of heart rate and cardiac contractility are considered to be the most important control parameters in the models. Therefore, the baroreceptor will be modelled in this study. As the postural effect on the cardiovascular system is ignored in this study, carotid and arterial baroreceptors are simplified to be baroreceptor because carotid arterial pressure is the same as the arterial pressure in the supine position. Effector sites such as heart, veins and arterioles will be included.

Table 4-1Comparison of the reflex control system portion of overall cardiovascular system models (included in the model)*

Investigators	Receptors			Heart Rate and Cardiac Contractility		
	Carotid baroreceptor	Aortic baroreceptor	Cardio-pulmonary	Heart rate control	Heart rate control time lag	Control of cardiac contractility
Beneken and DeWit (Beneken & DeWit 1967)	*	*	*	*	*	*
Snyder and Rideout (Snyder & Rideout 1969)	*			*		
Boyers et al. (Boyers et al. 1972)	*		*	*	*	*
Hyndman Croston et al (Hyndman 1972)	*			*		*
Green and Miller (Green & Miller 1973)	*					
Avula and Oestreicher (Avula & Oestreicher 1978)	*					
Leaning et al. (Leaning et al. 1983)	*	*	*	*	*	*
Jaron et al. (Jaron et al. 1984)	*			*	*	
Ursino et al (Ursino & Magosso 2003)		*		*	*	*
Lu et al (Lu et al. 2001)		*		*	*	*
Sun, Y. et al (Sun et al. 1997)		*		*		

4.3 Mathematical model of the baroreceptor reflex

A baroreceptor reflex control model (Figure 4-7) has been developed in this research. The controlled/input parameter is the mean aortic pressure. The activity of sympathetic and parasympathetic nerves runs to the effector sites including the heart, veins and arterioles. The four main parameters involved in the regulation are the heart rate, the cardiac contractility, venous compliance and peripheral resistance. These parameters are fed into the hydraulic cardiovascular model and the resulting aortic pressure is fed back to the controller. The structure of the mathematical models for each compartment is described in the following sections.

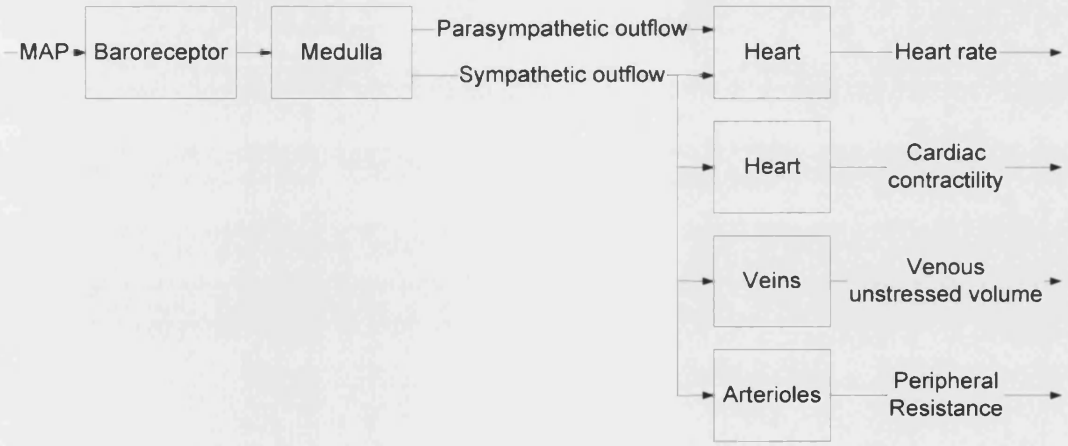

Figure 4-7: Baroreceptor reflex control flow chart

4.3.1 Afferent compartment

Mean arterial pressure (MAP) is used as the input to the afferent compartment. Carotid pressure is not used because this pressure is the same as the arterial pressure in the supine position. Since the mean aortic pressure is used as input; the baroreceptor response to the change of pressure can be ignored. However, features such as pressure threshold and time delay are still included in the model.

As mentioned above, the baroreceptor action potential frequency has a linear relationship with the mean arterial pressure within a pressure threshold. At a particular

steady pressure, there is a certain rate of discharge by the neurons in the baroreceptors. This rate increases when the arterial pressure rises and decreases when the pressure falls. A first order filter is used to represent the delay response to the pressure change and a gain element is used to represent the rate of discharge using:

$$P_{aff} = G_{aff} \frac{MAP}{1 + \tau_{aff} s} \tag{4-3}$$

4.3.2 Central compartment

The primary integrating centre for the baroreceptor reflexes is a diffuse network of highly interconnected neurons called the medullary cardiovascular centre, located in the brainstem medulla oblongata. The central compartment compares the mean arterial pressure and the demanding arterial pressure, and gives out the difference between the demanding and actual arterial pressure:

$$P_{error} = P_{aff} - \frac{P_{demand}}{1 + \tau_c s} \tag{4-4}$$

Note that the P_{demand} is the arterial pressure at the baroreflex operating point.

4.3.3 Efferent compartment

The efferent compartment comprises parasympathetic (PNA) and sympathetic (SNA) divisions which exhibit a sigmoid shape between the pressure and the nerve activities (Figure 4-4) (Kollai & Koizumi 1989). The two sigmoid functions in the two divisions of the efferent nerve outflow are given by:

$$SNA = \frac{SNA_{max} + SNA_{min} e^{Perror / ks}}{1 + e^{Perror / ks}} \tag{4-5}$$

where

$$k_s = (SNA_{max} - SNA_{min}) / (4 * S_s) \tag{4-6}$$

$$PNA = \frac{PNA_{min} + PNA_{max} e^{Perror / kv}}{1 + e^{Perror / kv}} \tag{4-7}$$

where

$$k_v = (PNA_{max} - PNA_{min})/(4 * S_v) \quad (4\text{-}8)$$

S_s and S_p are the slopes at the operating point of the sigmoid function.

4.3.4 Control of heart rate

Figure 4-8 shows the overall control scheme for the heart rate. A variable time constant first order transfer function is included in the path of both nerve divisions at the effector sites to represent the different heart rate response to increment and decrement of the nerve frequency. An exponential relationship with the input nerve frequency is used for the sympathetic branch time constant. A second order polynomial function is used to represent the nonlinear steady state gain (Levy & Zieske 1969). However, the steady state gain is only valid when the stimulated frequency is less than 8 Hz. According to experimental data of Levy and Zieske (1969) and Warner and Russell (1969), an exponential function is used to limit the gain. Warner also discovered a certain time delay for both nerve divisions. Therefore, a pure time delay is included in both divisions.

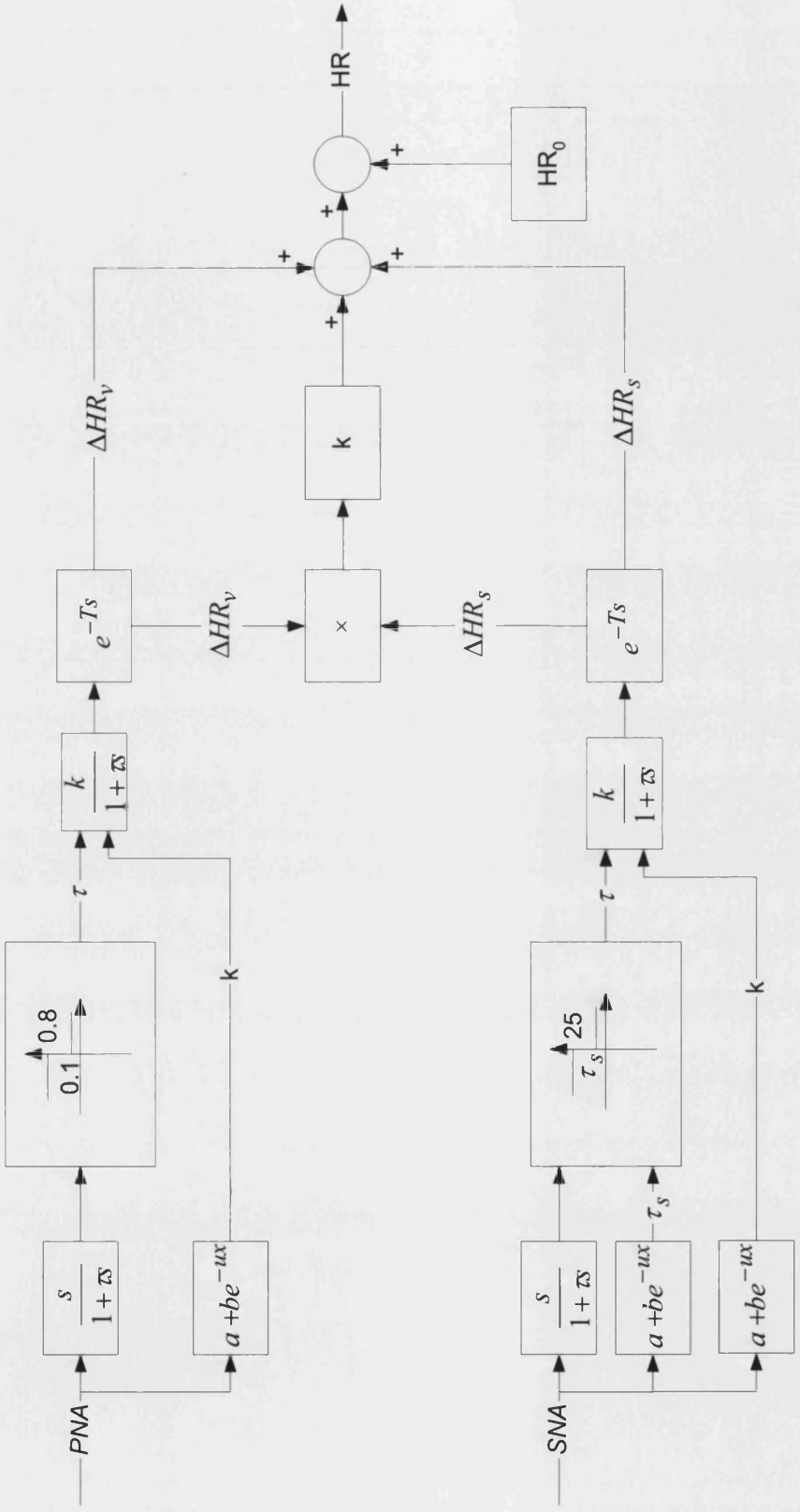

Figure 4-8 Block diagram of heart rate control scheme

The interactions between the two nerve divisions on the control of the heart rate are very complicated. Levy et al and Warner's methods have been simplified, and combined to provide a more comprehensive form as follows:

$$HR = HR_0 + \Delta HR \tag{4-9}$$

$$\Delta HR = \Delta HR_s + \Delta HR_v + c \cdot \Delta HR_s \cdot \Delta HR_v \tag{4-10}$$

$$\Delta HR_s = G_s \frac{f_s \cdot e^{-T_s s}}{1 + \tau_s s} \tag{4-11}$$

where

$$G_s = G_{s0}^k (1 - e^{-ks \cdot fs}) \tag{4-12}$$

$$k_s = G_{s0}^k / k_{s0}^k \tag{4-13}$$

$$\tau_s = \begin{cases} G_{s0}^\tau \cdot e^{-k_s^\tau \cdot fs} & when \quad fs \quad increases \\ 25 & when \quad fs \quad decreases \end{cases} \tag{4-14}$$

$$k_s^\tau = G_{s0}^\tau / k_{s0}^\tau \tag{4-15}$$

$$\Delta HR_v = G_v \frac{f_v \cdot e^{-T_v s}}{1 + \tau_v s} \tag{4-16}$$

where

$$G_v = G_{v0} (1 - e^{-kv \cdot fv}) \tag{4-17}$$

$$k_v = G_{v0} / k_{v0} \tag{4-18}$$

$$\tau_v = \begin{cases} 0.1 & when \quad fv \quad increases \\ 0.8 & when \quad fv \quad decreases \end{cases} \tag{4-19}$$

The cardiac timing events are described by linear approximations obtained by Beneken and De Wit (1967):

$$tr = 60 / HR \tag{4-20}$$

$$tee = 0.16 + 0.2 \times tr \tag{4-21}$$

$$tac = 0.91 \times tr - 0.06 \tag{4-22}$$

$$tar = tr + 0.04 \tag{4-23}$$

These timing values are then fed into the heart model to generate the cardiac activation functions.

4.3.5 Other effector sites

Other effector sites including arterioles and veins share similar characteristics. Sympathetic nerve outflow sends a signal to the effector sites which include a static gain, a first order filter and a pure time delay as shown in equation (4-24).

The first order filter and the pure time delay represent the main aspects of the response time pattern. It is worth noting that the gain for venous compliance is negative while the others are positive.

$$\sigma = G_{eff} \frac{SNA \cdot e^{-\tau_\sigma s}}{1 + \tau_\sigma s} \tag{4-24}$$

4.4 Closure

The cardiovascular regulation system is very complex. Many models have been developed by researchers in order to understand the whole picture of the cardiovascular regulation system. Researches have mainly concentrated on modelling the baroreceptor because the baroreflex action is the most important short-term regulator for the arterial pressure and cardiovascular function.

With a better understanding of the baroreflex, a more explicit baroreceptor reflex model has been developed in this research as a three-compartment model - afferent compartment, central compartment and efferent compartment. Significant improvements have been made in the presentation of the afferent compartment and the efferent compartment. Recent research (Kawada et al. 2003) indicates that the non-

linearity is dominant in the efferent pathway. Therefore, a sigmoid function has been introduced into the efferent compartment to produce sympathetic and parasympathetic nerve outflow to the effector sites. The effector model for the heart rate was enhanced by including the interaction between two autonomic nerve divisions.

It is anticipated that the improved model developed in this research will give most of the parameters physiological explanations and provide a clearer picture of how the baroreflex system works. The model inevitably uses equations containing parameters that need to be fitted to experimental data.

Chapter 5 Validation of the baroreflex control model

5.1 Introduction

This chapter describes the validation of the baroreflex control system model developed in Chapter 4. Because of the lack of published data relating to humans, some experimental data has been used from experiments undertaken on animals including dogs and monkeys.

Both open loop and closed loop simulations were used to compare the predicted responses to the published experimental data.

5.2 Parameter identification

The values of the parameters used to define the baroreflex control mechanism are shown in Table 5-1 parameter definition for baroreflex control model. All the parameters have been assigned on the basis of the clinical and/or the physiological literature. Specifically, the time delay and the time constant for the first order filter are reported by Ursino and Magosso (2003). Parameters regarding the efferent compartment and heart rate control were obtained from experimental data reported by Warner and Russell (1969).

Table 5-1 parameter definition for baroreflex control model

Afferent compartment			τ_{aff} =0.001 s G_{aff} = 1
Central Compartment			P_{demand} = 90 mmHg
Efferent compartment		Parasympathetic division	S_p = 0.0205 PNA_{max} = 6 Hz PNA_{min} = 0.6 Hz
		Sympathetic division	S_s = -0.0138 SNA_{max} = 4 Hz SNA_{min} =1.12 Hz
Effector sites	Heart rate	Sympathetic division	G_{s0}^{k} = 90 beats/min /Hz G_{s0}^{τ} = 10 beats/min /Hz k_{s0}^{k} = 0.28 k_{s0}^{τ} = 0.2
		Parasympathetic division	G_{v0} = 60 beats/min /Hz k_{v0} = 0.4 τ_v = 0.1s / 0.8s T_s = 3s T_v = 0.5
		interaction between two divisions	c = 0.017 HR_0 = 109 beats/min
	Myocardial constriction	left heart	$\tau_{\sigma,lv}$ = 1.5 s $T_{e,lv}$ = 2 s $G_{eff,lv}$ = 0.45 mmHg/ml/Hz E_{lv0} = 3 mmHg/ml
		right heart	E_{rv0} = 0.1 mmHg/ml $\tau_{\sigma,rv}$ = 1.5 s $T_{e,rv}$ = 2 s $G_{eff,rv}$ = 0.282 mmHg/ml/Hz
	Veins		$\tau_{\sigma,V}$ = 10 s $T_{e,V}$ = 5 s $G_{eff,V}$ = -275 ml/Hz V_0 = 3200 ml
	Arterioles		$\tau_{\sigma,R}$ = 1.5 s $T_{e,R}$ = 3 s $G_{eff,R}$ = 0.2 mmHg/(ml/s)/Hz R_0 = 0.3 mmHg/(ml/s)

5.3 Simulation studies

5.3.1 Model fit to heart rate

Warner and Cox (1962) investigated the effects of sympathetic and parasympathetic stimulation and the combined effect on the heart rate of dogs by stimulating both sympathetic and parasympathetic nerves to a particular frequency level. They stimulated the sympathetic nerve to four frequency levels and recorded the response of the heart rate as shown in Figure 5-1. The same procedure was also applied to the parasympathetic nerve as indicated by the results presented in Figure 5-2. The predicted response of the heart rate obtained from the model agrees well with the experimental data. The intrinsic heart rate was set to be 142 beats/min for dogs, compared with 109 beats/min for humans.

Using the variable-time-constant first order transfer function and the nonlinear gain, the model produced results in very good agreement with the experimental results. As Figures 5-1 and 5-2 show, the change of the heart rate with the frequency is not linear. Instead, the responses of the heart rate to the nerve stimulations saturate at higher frequencies. This justified the use of the exponential gain for the nerve activity models. The heart rate decreases much slower after the cessation of stimulation, in contrast to the abrupt termination of the response after parasympathetic activity. In the model, this was achieved by adjusting the values of the time constants in the first order filters in the sympathetic and parasympathetic control models. The values used were 0.8 seconds for the parasympathetic model and 25 seconds for the sympathetic model. As no other information was available, these values were also used to predict human responses.

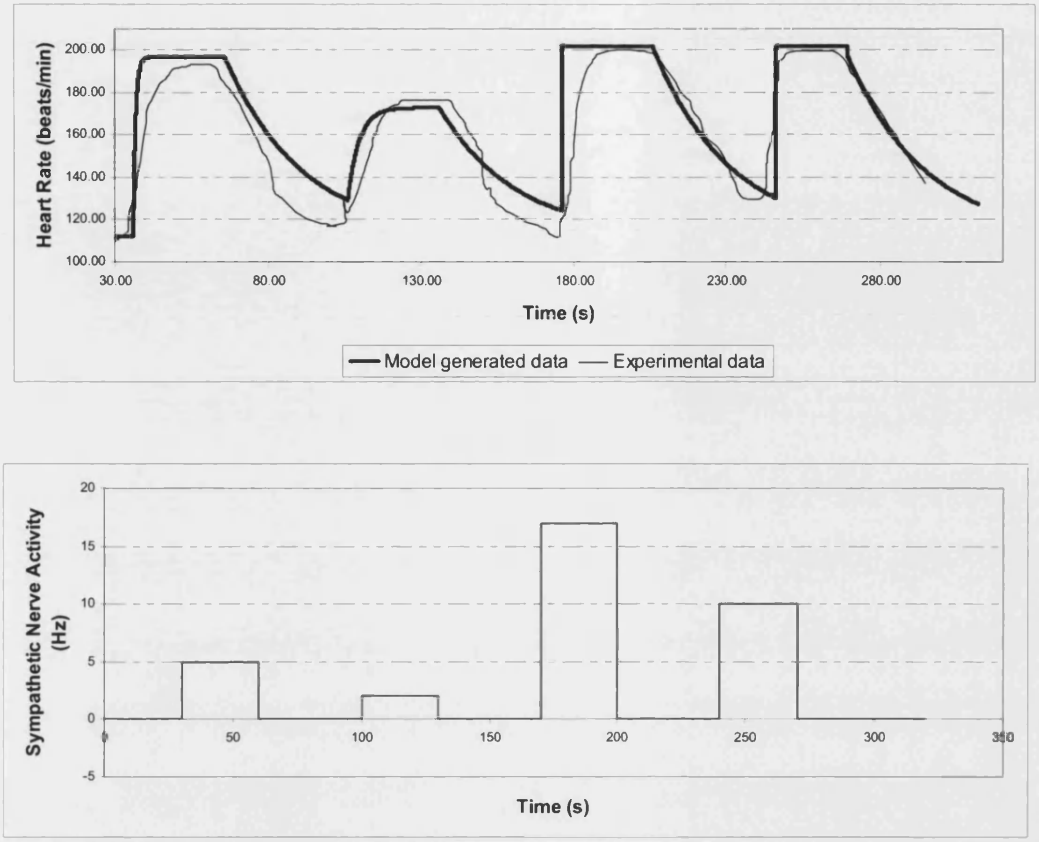

Figure 5-1Heart rate response to the sympathetic nerve stimulations. Canine experimental data adapted from (Warner & Cox 1962)

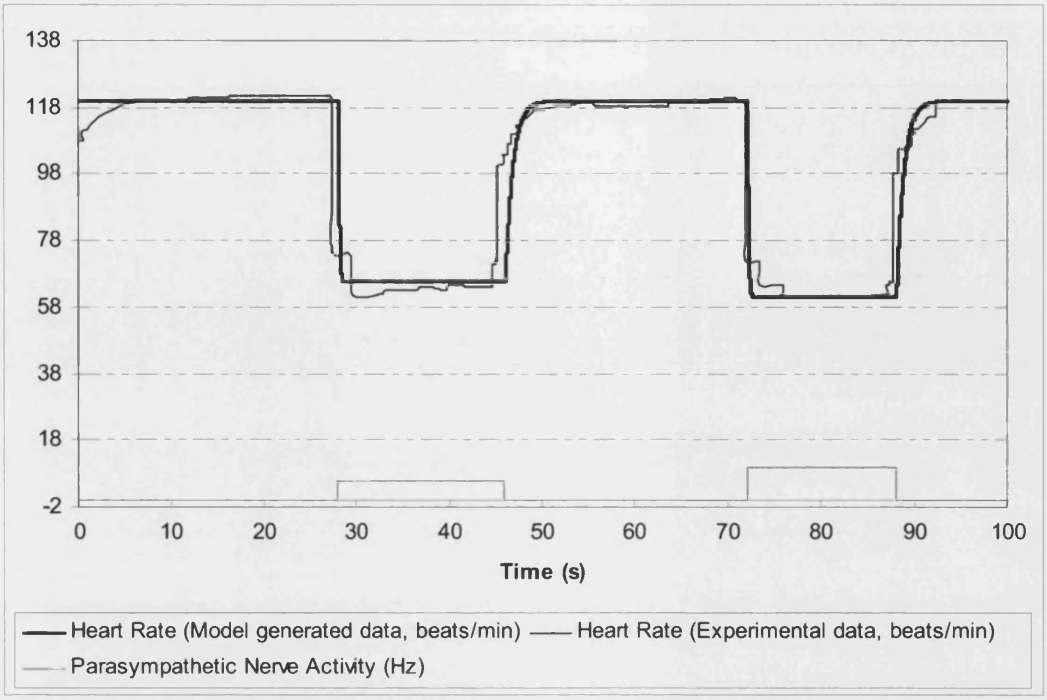

Figure 5-2 Heart rate response to parasympathetic nerve stimulations. Canine experimental data adapted from (Warner & Cox 1962)

5.3.2 Artificial heart pacing

In order to simulate the effect of artificial heart pacing on cardiac output, the feedback loop relating mean arterial pressure to heart was disconnected, and the heart rate was considered to be an external input signal. The heart rate was given different values ranging between 30 and 190 beats/min, and the corresponding steady state values of cardiac output and stroke volume were determined.

Figure 5-3 shows that the cardiac output increases with heart rate at the lower heart rate levels, but then reaches a plateau and decreases at higher frequencies. The reason why the cardiac output (CO) fails to increase further at high values of heart rate is due to a decline in ventricular filling and hence the stroke volume (SV) shows the same trend as CO (Figure 5-4).

Melbin and co-workers (Melbin et al. 1982) suggested that the circulatory response to increasing heart rate (HR) can be characterized by the slope of the SV-HR curve (dSV/dHR). Figure 5-5 compares the dSV/dHR versus HR relationship (normalized at

80 beats/min) obtained from the model with that reported in Melbin et al (1982). The agreement between the model and the experiment is considered to be acceptable.

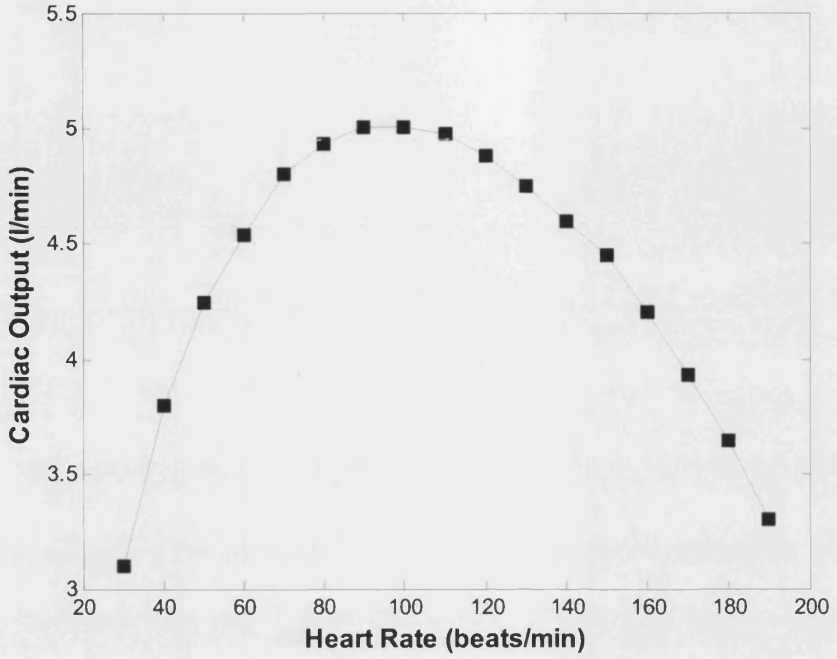

Figure 5-3 Effect of heart pacing on cardiac output

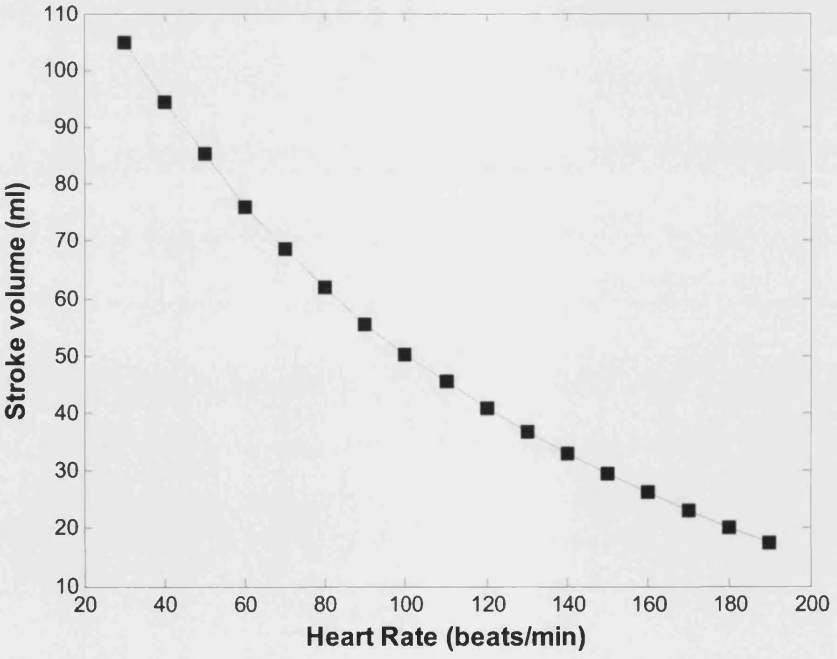

Figure 5-4 Effect of heart pacing on stroke volume

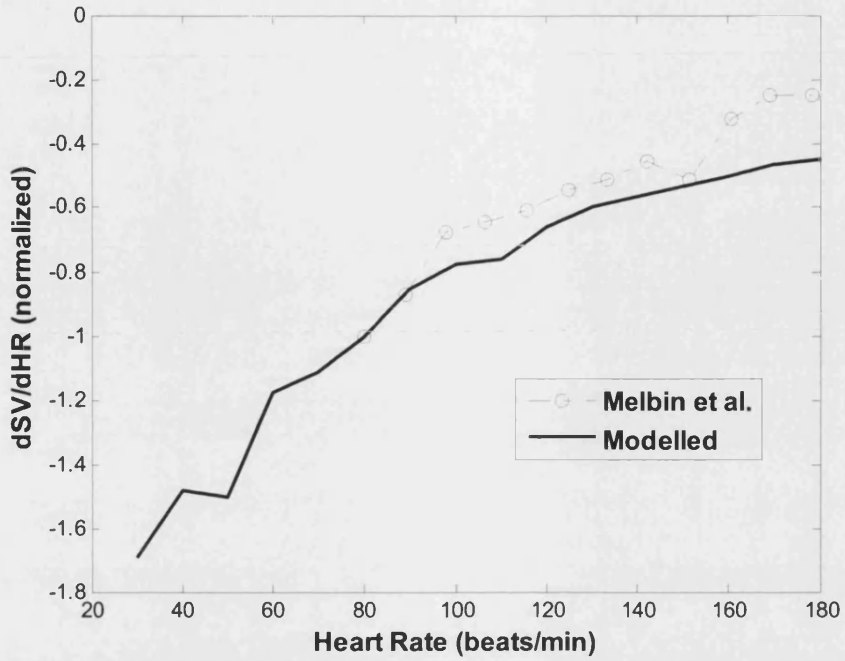

Figure 5-5 dSV/dHR versus heart rate. Experimental data from (Melbin et al. 1982)

5.3.3 Model fit to sigmoid function

In order to model the drug controlled carotid sinus pressure in the experiment performed by Cornish et al. (1989), the feedback loop was disconnected and a step input pressure from 60 to 220 mmHg was fed into the control loop. Figure 5-6 shows good agreement between the model generated steady state values normalized at 85 mmHg and the experimental data (Cornish et al. 1989).

Heart rate is regulated by the baroreceptor reflex. Acute changes in arterial blood pressure elicit inverse changes in heart rate via the baroreceptor reflex (Berne & Levy 1988). The inverse relation between heart rate and arterial blood pressure is usually most pronounced over an intermediate range of arterial blood pressures. In an experiment conducted on conscious, chronically instrumented monkeys, this range varies between about 70 and 160 mmHg. When the normalized carotid pressure is less than 0.5, the normalized heart rate tends to a constant value of 1.58 while at pressures greater than 1.5 the heart rate tends to a constant value of 0.65.

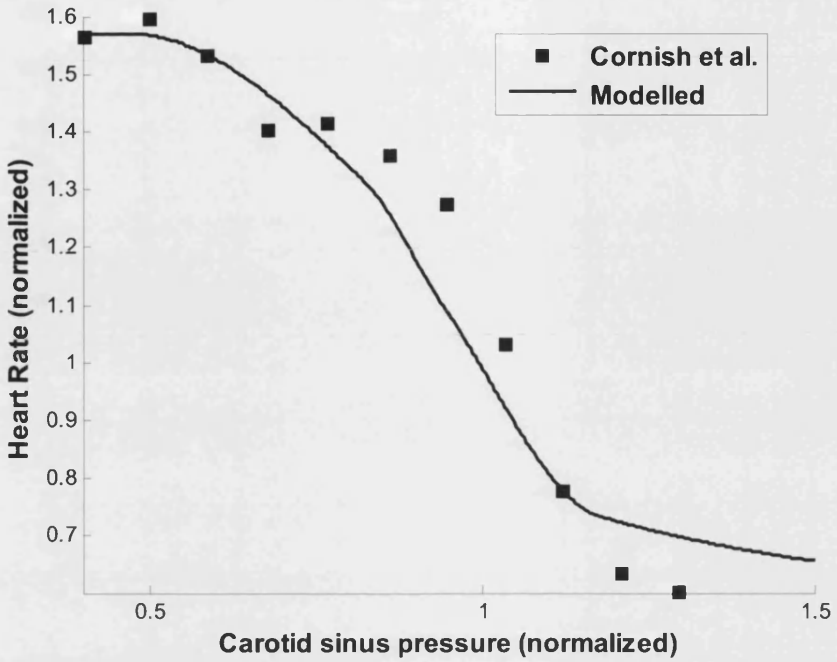

Figure 5-6 Heart Rate as a function of mean arterial pressure

5.3.4 Exercise

The baroreflex is generally considered not to be an important controller of the circulation during exercise as the chronic denervation of the baroreceptors does not produce an obvious deficit in blood pressure stability or level once the response to moderate-to-heavy exercise had stabilized (Rowell & Oleary 1990). However a sudden transient drop in blood pressure was observed at the onset of exercise after baroreceptor denervation. This is evidence that the baroreceptor reflex remained sensitive at the onset of exercise. Melcher and Donald (1981) also provided clear evidence of maintained baroreflex sensitivity during exercise.

The effect of baroreflex on the cardiovascular system at the onset of exercise was simulated by shifting the operating point of the central compartment and locally induced vasodilatation in the exercising muscles. Toska and Eriksen (1994) recorded the responses of 10 healthy men at the onset of moderate, dynamic exercise while supine. The data used here is the average of the 10 responses. The shift of the operating point was estimated to be 7% by Elstad et al. (2002). Note that this shift is directly proportional to the intensity of exercise (Walgenbach & Donald 1983). The

vasodilatation can be modelled by decreasing the peripheral resistance using a time constant of 5.5 seconds (Elstad et al. 2002). This value is estimated to be 0.18 mmHg s/ml according to Toska and Eriksen's experiment.

Figure 5-7 shows the predicted cardiovascular responses at the onset of exercise. These show the same trend as the experimental results in Figure 5-8. After the onset of exercise, the heart rate increased rapidly to reach a short-lived plateau. Thereafter, it decreased slightly to a steady level above the resting level. A transient decrease in stroke volume at the onset of exercise delayed the increase in cardiac output by a few seconds. The stroke volume returned to its resting level and the cardiac output increased with heart rate. The mean arterial pressure increased during the first few seconds after the onset of exercise and then showed a transient decrease to a minimum level slightly above the resting value after the onset of exercise, followed by a rapid increase to just above the resting value. Total peripheral conductance, which is calculated by dividing cardiac output by mean arterial pressure, decreased rapidly to a minimum and then increased to a stable level for the rest of the exercise period.

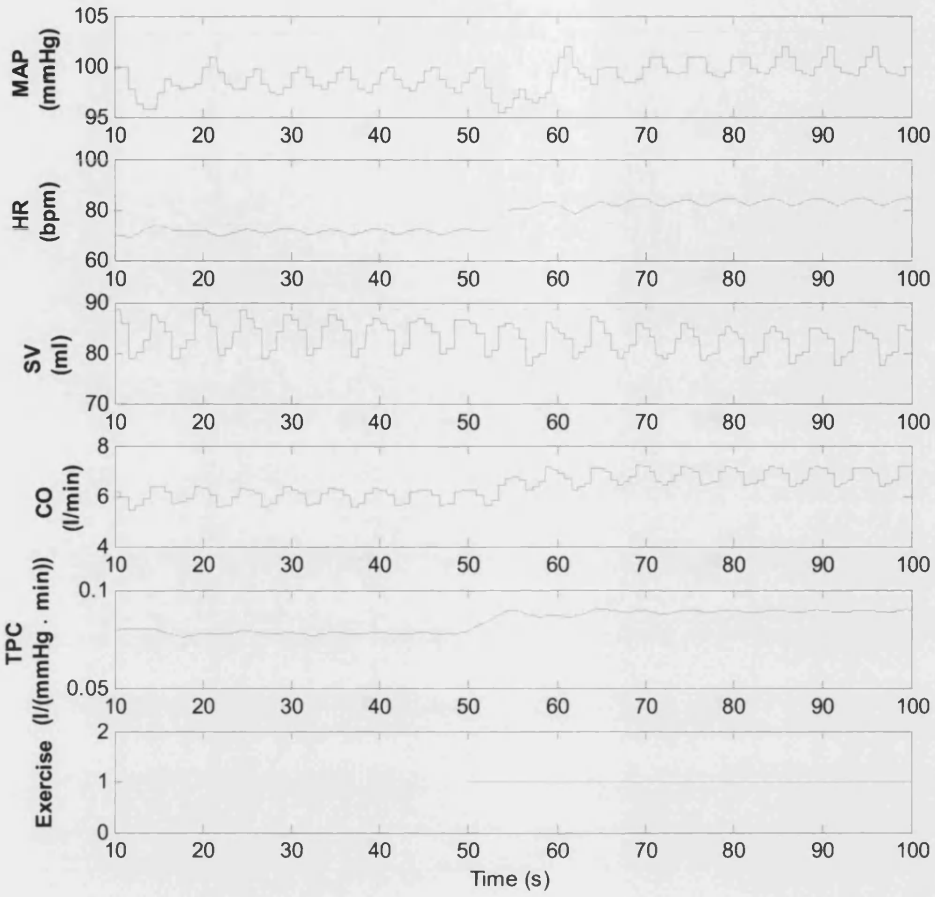

Figure 5-7 Cardiovascular response predicted by the model. MAP, mean arterial pressure; HR, heart rate; bpm, beats/min; SV, stroke volume; CO, cardiac output; TPC, total peripheral conductance

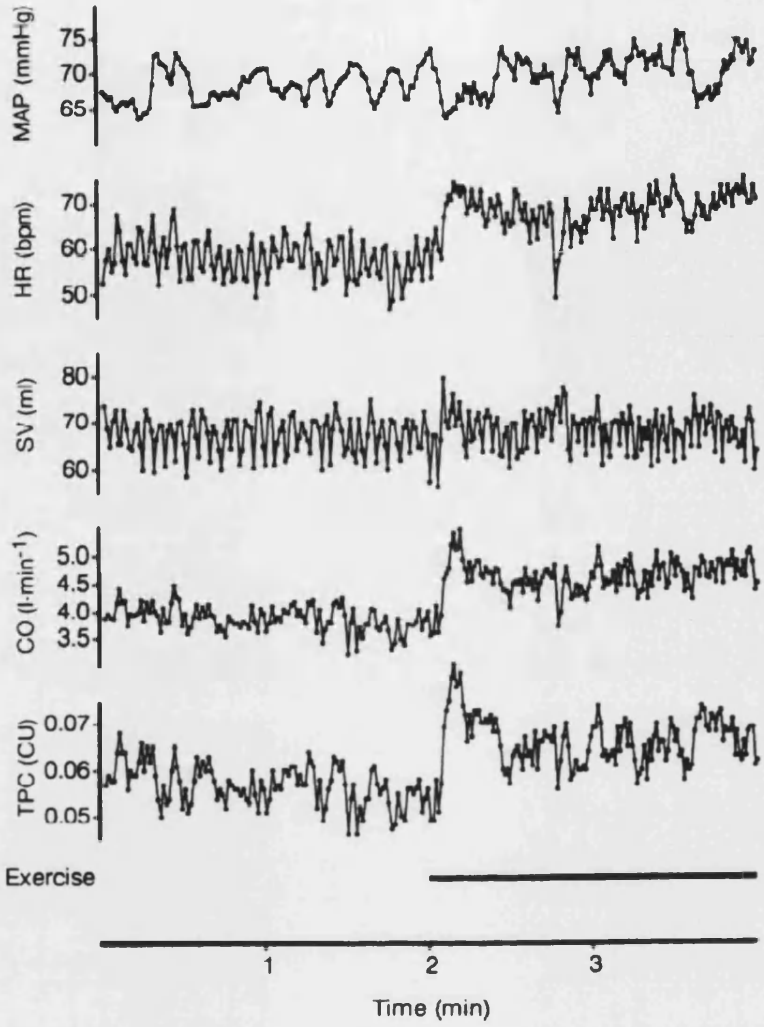

Figure 5-8 Primary recording of cardiovascular variables from 1 typical experiment. MAP, mean arterial pressure; HR, heart rate; bpm,beats/min; SV, stroke volume; CO, cardiac output; TPC, total peripheral conductance (calculated by dividing CO by MAP, unit: $l \cdot min^{-1} \cdot mmHg^{-1}$) (Toska & Eriksen 1994)

5.3.5 Respiratory effects on the cardiovascular system

Respiratory effects on the cardiovascular system have also been considered in order to integrate the cardiovascular model with the respiratory model. The Valsalva manoeuvre is a useful bedside test of autonomic function. It is a technique for increasing the intrathoracic pressure by trying to breathe out forcibly (using the diaphragm and abdominal muscles) when the glottis (the opening between the vocal cords) is closed.

Simulation of the Valsalva manoeuvre was accomplished by increasing the intrathoracic pressure to 40 mmHg during a prolonged expiration period of 10s (Figure 5-9).

During expiration, the intrathoracic pressure is elevated. This leads to the holding back of the venous return and the pulmonary reservoir is gradually depleted. Therefore, the arterial pressure can decrease below the normal level. Without autonomic control, the blood pressure falls and remains low until the intrathoracic pressure is released. For this condition, the heart rate remains constant at 70 beats/min as shown in Figure 5-10. If the baroreceptor reflex is activated, it would cause vasoconstriction and a tachycardia (rapid heart rate), trying to raise blood pressure. This is shown in Figure 5-9 when the heart rate increases to over 100 beats/min. For inspiration, the arterial pressure increases to the normal level as a result of the retained venous return. The restoration of venous return causes an overshoot of the blood pressure, which leads to a baroreceptor mediated bradycardia (slow heart beat) when the baroreceptor reflex is activated (Figure 5-9). The overshoot is absent without autonomic control (Figure 5-10).

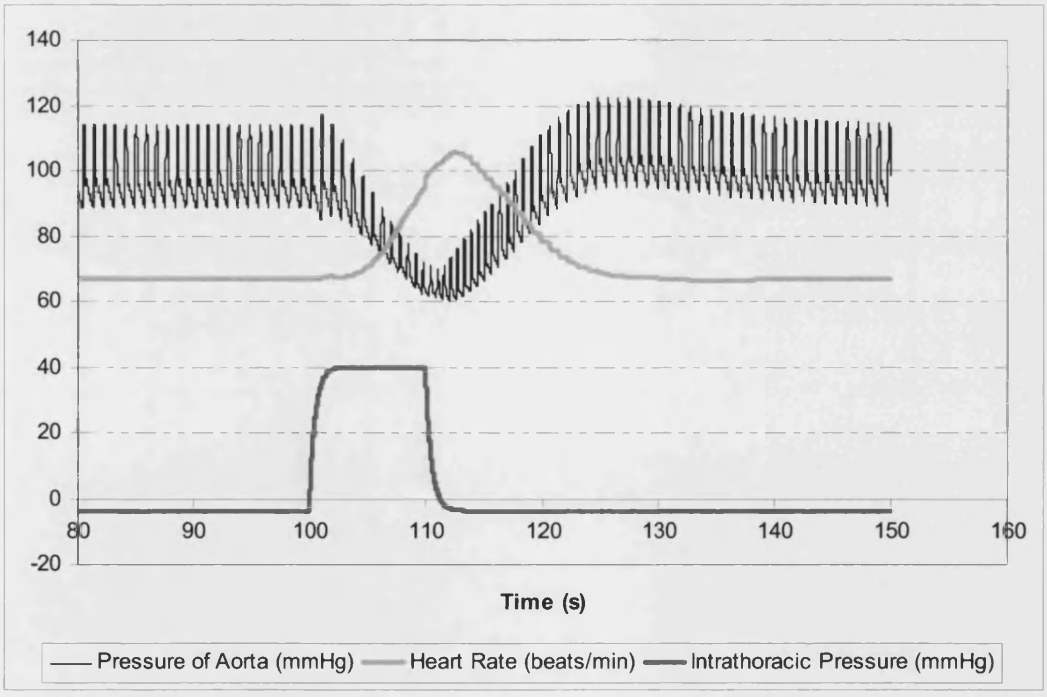

Figure 5-9 Valsalva manoeuvre with baroreceptor reflex

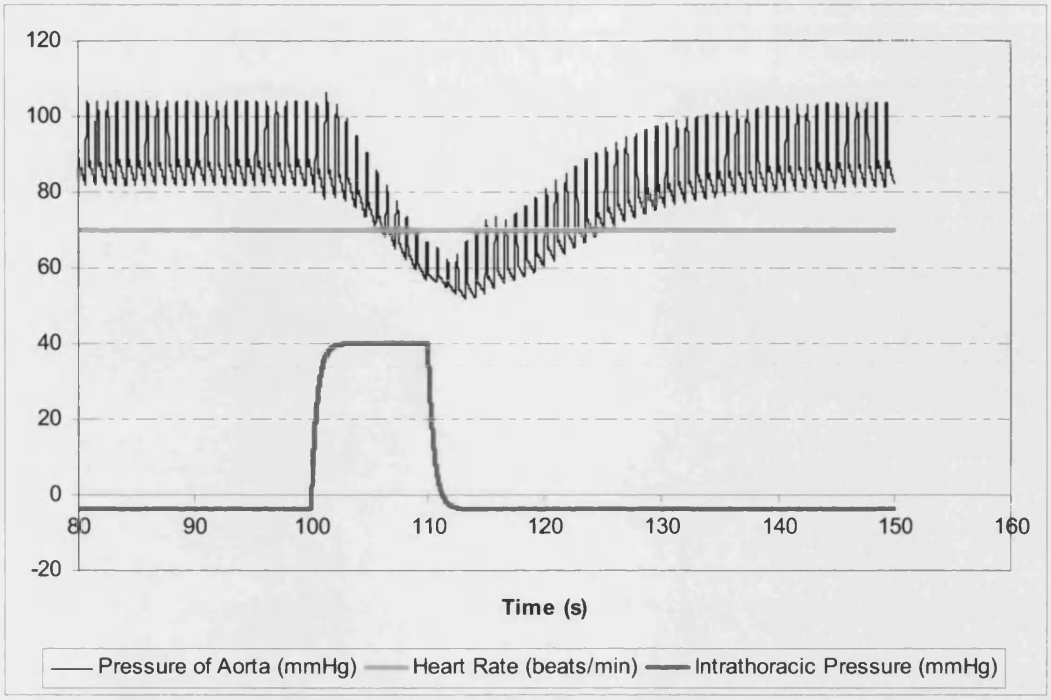

Figure 5-10 Valsalva manoeuvre without baroreceptor reflex (Heart Rate = 70 beats/min)

5.3.6 Power spectral density

Power spectral analysis is often used to investigate the baroreflex control system performance in the frequency domain. A typical power spectrum for the heart rate contains two major components (Figure 5-11):

1. a high frequency (0.18-0.4 Hz) component, which is synchronous with respiration;
2. a low frequency (0.04 to 0.15 Hz) component that is mediated by both the parasympathetic and cardiac sympathetic nerves.

The power spectral density (PSD) of the predicted heart rate was estimated using Welch's method (built-in function Pwelch in Matlab® 7.0, Hanning window, length of the Fast Fourier Transform (FFT) is 2^{12}, 50% overlap). Figure 5-12 shows two peaks: one at around 0.07 Hz which is the low frequency component, the other one at around 0.2 which is the high frequency.

As a measure of vagal activity, spectral analysis of the high-frequency component probably offers no additional information over time-domain measures of respiratory sinus arrhythmia. On the other hand, the low frequency component deserves further investigation. The low frequency derives from both the parasympathetic and sympathetic activities and has been hypothesized to reflect the delay in the baroreceptor loop. Figure 5-13 to Figure 5-16 show the change in PSD when the gain of vagal and sympathetic gains were increased and reduced by 20%. The power spectrum was more sensitive to changes in the sympathetic gain than the parasympathetic gain. This indicates that the model is more sensitive to the change of the sympathetic outflow than the parasympathetic outflow.

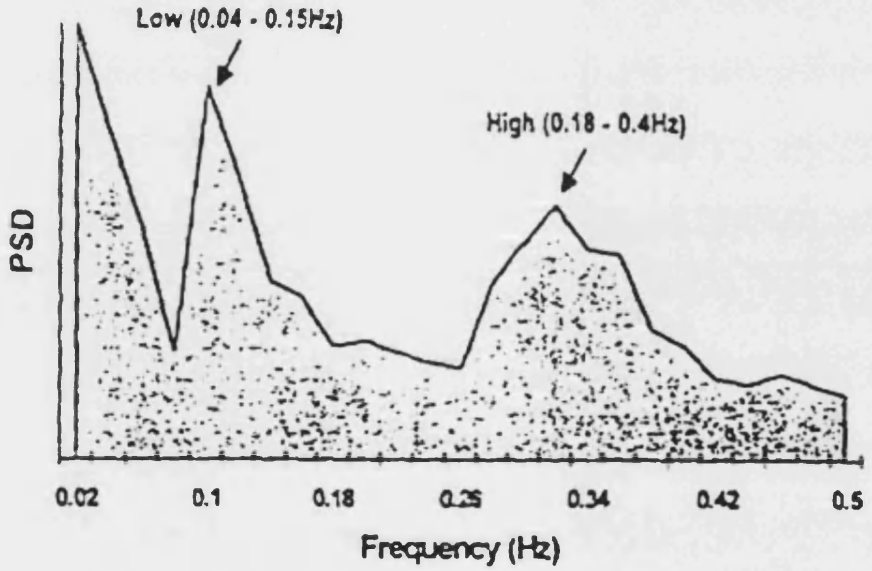

Figure 5-11 Power spectrum of Heart Rate (PSD = power spectral density) (John & MacArthur 1997)

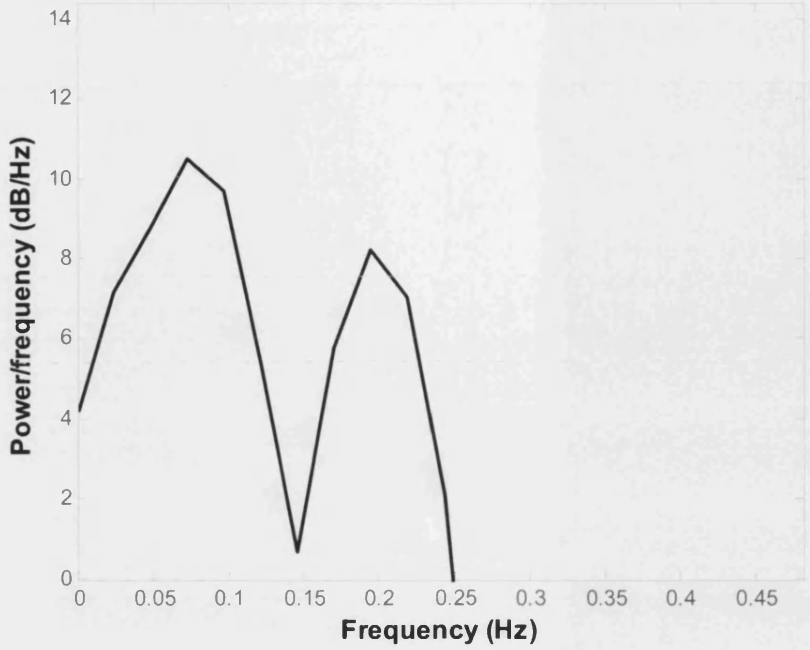

Figure 5-12 Power spectrum of Heart Rate generated from model

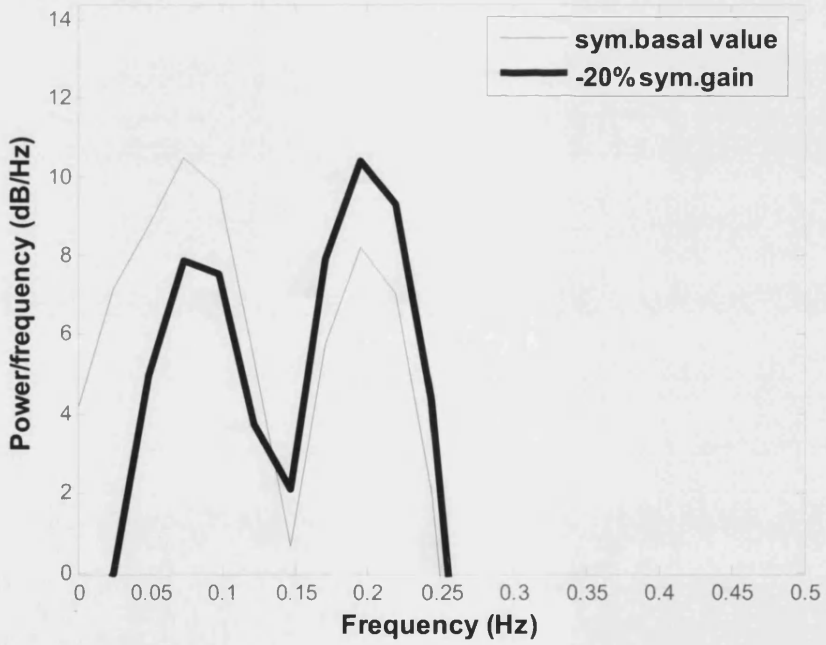

Figure 5-13 Comparison of power spectrum of Heart Rate between sympathetic gain at basal value and sympathetic gain decreased by 20%

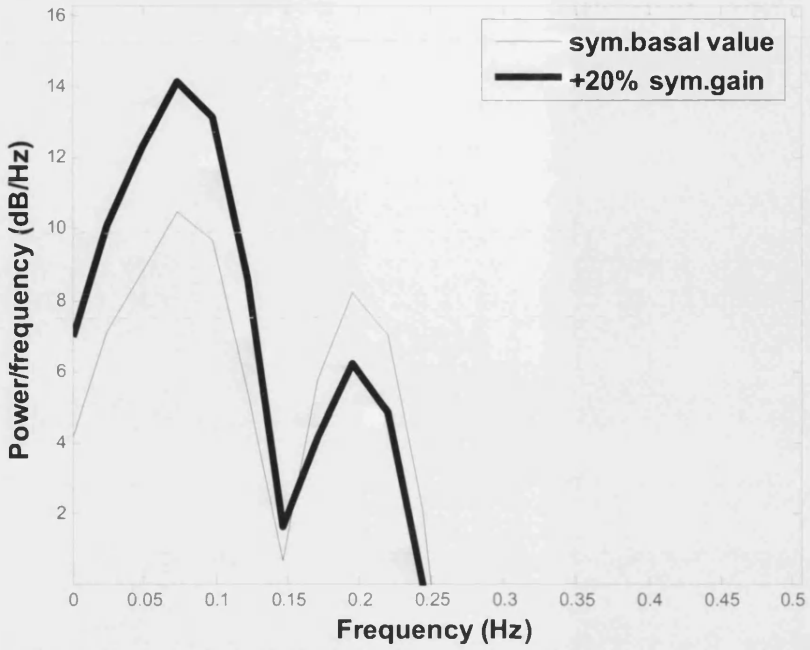

Figure 5-14 Comparison of power spectrum of Heart Rate between sympathetic gain at basal value and sympathetic gain increased by 20%

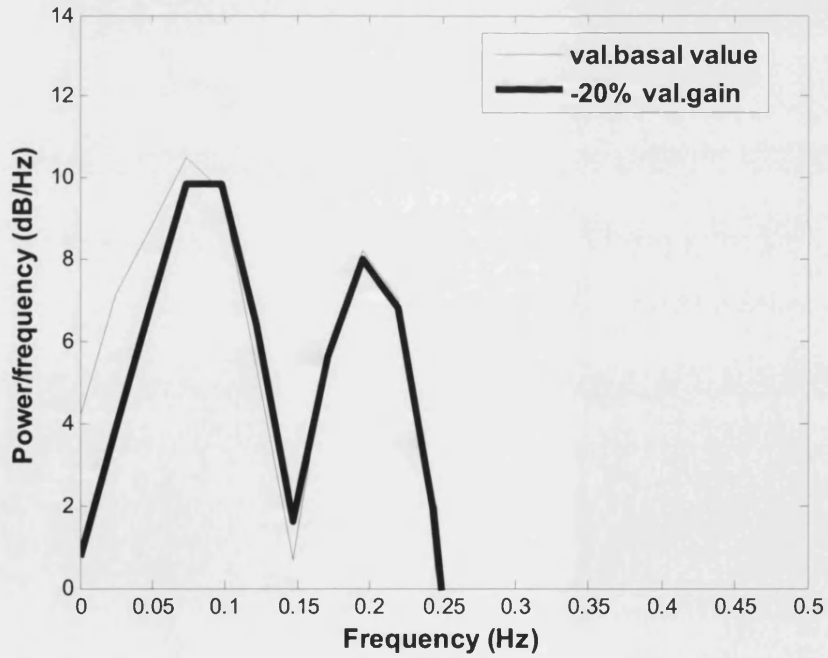

Figure 5-15 Comparison of power spectrum of Heart Rate between vagal gain at basal value and vagal gain decreased by 20%

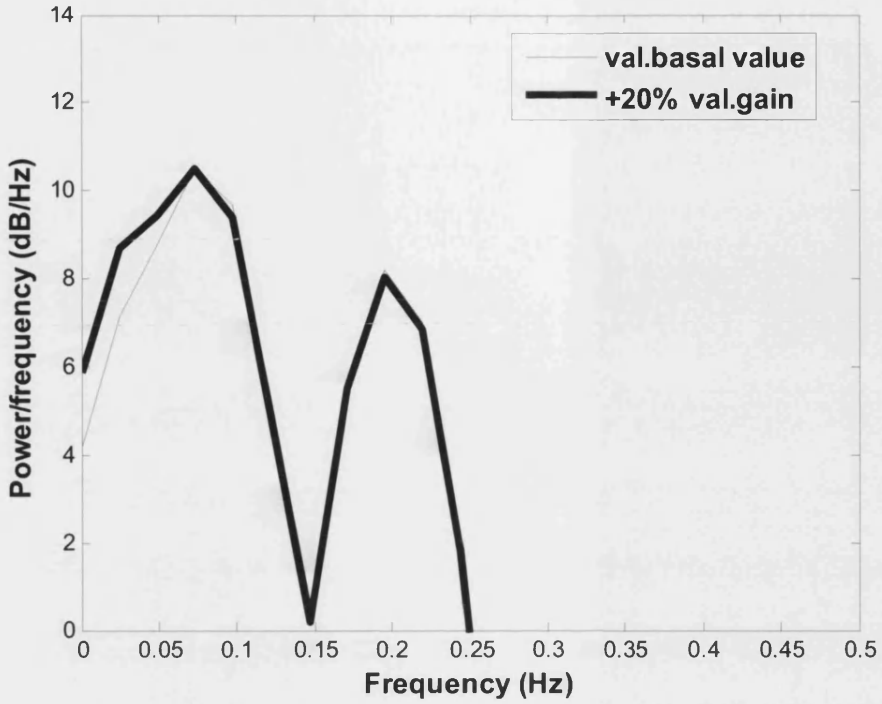

Figure 5-16 Comparison of power spectrum of Heart Rate between vagal gain at basal value and vagal gain increased by 20%

5.4 Discussion

This chapter describes the validation of the model described in Chapter 4. Two open loop tests were performed to assess the static response of the baroreflex control model. They are artificial heart pacing and drug induced blood pressure change.

To assess the cardiac output responses, artificial heart pacing was modelled by an external input to the heart rate. The resulting cardiac output and stroke volume show good agreement with experimental data. Cardiac output is the product of stroke volume and heart rate. Stroke volume is determined by three factors: preload, afterload and contractility.

- Preload is the ventricular volume at the end of diastole. An increased preload leads to an increased stroke volume.

- Afterload is the resistance to ventricular ejection. This is caused by the resistance to flow in the systemic circulation and is the systemic vascular resistance.
- Contractility accounts for the ability of the myocardium to contract in the absence of any changes in preload or afterload. Increased contractility leads to an increase in stroke volume.

All these factors were included in the model (see Chapter 4). An increase in heart rate decreases the duration of diastole. Hence ventricular filling is diminished, that is, the preload reduces, hence the stroke volume decreases. The afterload increases due to an increased heart rate. The rise in heart rate also enhances myocardial contractility which leads to a rise in stroke volume. Stroke volume decreases due to the predominant decreased preload. Therefore, the biphasic change in cardiac output induced by a change in heart rate was influenced markedly by the actual level of the heart rate. Over the lower frequency range, the reduction in stroke volume was proportionately less than the increase in heart rate, causing the cardiac output to increase. At the high pacing frequency, the increments in heart rate reduce the cardiac output. This indicates the decrement in stroke volume has exceeded the increment in heart rate over this high range of pacing frequencies.

Arterial pressure can change when certain drugs are infused into the blood stream. This was modelled by applying a step input pressure to the control system rather than the feedback from the cardiovascular system. The response of the heart rate plotted against the pressure in Figure 5-6 shows a sigmoid shape. Over an intermediate range of arterial pressures, the alterations in heart rate were achieved by the changes in vagal and sympathetic neural activity. Below this range, there is the intense sympathetic activity and the virtual absence of the vagal activity. Above this range, the low heart rate is the contribution of intense vagal activity and a constant low level of sympathetic activity. This physiologic phenomenon was successfully modelled by the inclusion of the two sigmoid shaped functions into the sympathetic and vagal nerve divisions.

Closed loop control tests were also performed to assess the model's transient characteristics. Power spectrum analysis of heart rate variability is a popular method for the study of physiologic mechanisms and disease. Clinical applications include

predicting the risk of arrhythmic events or sudden cardiac death after heart attack and the diabetic neuropathy (a complication of diabetes causing damage to the nerves). Recently, its role in the evaluation and management of heart failure has also been recognized (Stys & Stys 1998). Two peaks were found in the power spectrum of the predicted heart rate. The low frequency is the combined effect of vagal and sympathetic nerve activity while the high frequency is caused by the influence of the respiration on the cardiovascular system. The high frequency is mainly determined by the change of systemic arterial pressure. The intrathoracic pressure causes the fluctuation of systemic arterial pressure. The fluctuation stimulates the baroreflex control system at the respiratory period. At this frequency, the baroreflex works entirely through the fast vagal control component while the sympathetic control component is nearly damped out because of its low-pass filtering dynamics. Therefore, the high frequency peak found in the spectrum analysis of the heart rate is often used as an index of the vagal activity. However, the sensitivity test of the two autonomic divisions shows that the high frequency peak is more sensitive to the sympathetic gain change. This is because the sympathetic outflow has a large influence on the vascular resistance which has a significant effect on the mean arterial pressure. The low frequency peak is usually used as a reflection of the sympathetic activity (Ursino & Magosso 2003). This was clearly shown in the simulation where a 20% change of the sympathetic gain leads to a significant change in the PSD amplitude as shown in Figures 5-13 and 5-14.

The hemodynamic responses at the onset of exercise were also modelled. This was implemented by shifting the operating point of the central compartment and decreasing the total peripheral resistance. The initial decrease of the peripheral resistance is caused by the immediate vasodilatation in the exercising muscles. Its increase afterward reflects vasoconstriction in the non-exercising tissues caused by the regulation of the baroreflex. The increase of heart rate was caused by the dip in mean arterial pressure and mediated by fast vagal baroreflex regulation. After a decrease in mean arterial pressure during the first few seconds of exercise, the mean arterial pressure returned to its resting level because the operating point for arterial pressure control was increased.

Another interesting investigation is the Valsalva manoeuvre. It is a useful bedside test of an autonomic function. By applying an intrathoracic pressure difference between the

systemic and pulmonary circulation, the simulation of the manoeuvre was accomplished. The baroreceptor regulation provides a demonstration of a realistic arterial waveform.

5.5 Closure

A description of the validation of the model of the baroreflex control system described in Chapter 4 has been given in this chapter.

Two open loop tests, artificial heart pacing and drug induced blood pressure change, were performed to assess the response of the baroreflex control model. Artificial heart pacing was modelled by applying an external input to the heart rate. The predicted cardiac output and stroke volume show good agreement with published data. The biphasic changes of the cardiac output with heart rate were also demonstrated by the artificial heart pacing. Over the lower frequency range, the reduction in stroke volume is proportionately less than the increase in heart rate, therefore, the cardiac output increases. At the high pacing frequency, the increments in heart rate decrease the cardiac output because the decrement in stroke volume have exceeded the increment in heart rate over this high range of pacing frequencies. Drug induced blood pressure change was used to assess the nonlinearity of heart rate response due to the baroreceptor regulation. The relationship between the predicted heart rate and mean arterial pressure was a sigmoid shape which is in line with experiment data.

Tests were also performed to assess the model's transient response. In the power spectrum of the heart rate generated by the model, two peaks were found at 0.07 Hz and 0.2 Hz which both fall into the frequency range observed in experiments. The low frequency value was the combined effect of vagal and sympathetic nerve activity while the high frequency value indicates the influence of respiration on the cardiovascular system. The change in the peaks is useful in the evaluation of the parasympathetic and sympathetic activities. This was demonstrated by varying the gain of the two autonomic divisions. The high and low peak of the heart rate spectrum were both more sensitive to the change of the sympathetic gain although parasympathetic outflow has a dominant effect on the heart rate control. This is because the sympathetic outflow has a significant influence on the vascular resistance which adjusts the baroreflex input - mean arterial pressure. The influence of the respiration on the cardiovascular system was also

demonstrated by simulating a Valsalva manoeuvre. The baroreceptor regulation enables demonstration of a realistic arterial waveform due to the Valsalva manoeuvre. Hemodynamic responses at the onset of exercise were also modelled. The predicted result obtained from the model shows the same trend as the experimental results and also successfully demonstrates the contribution of the baroreceptor regulation during exercise. Both open loop and closed loop tests show the ability of the model to predict the static and dynamic hemodynamic responses due to environmental disturbances.

Chapter 6 Cardiopulmonary model

6.1 Introduction

One of the main functions of the cardiovascular system is to deliver oxygen to the cells and remove carbon dioxide from them. Oxygen is passed from the respiratory system into the cardiovascular system and carbon dioxide is passed from the cardiovascular system to the respiratory system. Hence it was necessary to create a respiratory model that integrated with the cardiovascular model to form a detailed model of the cardiopulmonary system. In this way, the mutual interactions occurring between the two systems can be investigated.

Integrating the respiratory model with cardiovascular model allows the modelling of chemoreceptors to become feasible. However, the way in which the chemoreceptors work with the baroreceptors is an important issue. Although no final conclusions have been drawn regarding the interaction between the two systems, a considerable amount of research (Bellville et al. 1979;Cooper et al. 2005;Daly & Scott 1958;Dalymde et al. 1965;Downing & Siegel 1963;Du & Chen 2007;Karim et al. 1980;Korner 1971;Potter 1981;Rowell & Oleary 1990;Somers et al. 1991;Ursino et al. 2001a;Ursino et al. 2001b) has thrown some light on how these two receptors interact and their influence on the cardiac response.

A review of the modelling approaches used to represent the respiratory system will be described. The findings obtained were used to first develop an enhanced model of the human respiratory system which was then allow the cardiopulmonary system to be simulated.

6.2 Review of the respiratory models

The primary function of the respiratory system is to supply blood with oxygen (O_2) in order for the blood to deliver O_2 to all parts of the body. Respiration is achieved by breathing. Inspired gas passes through the mouth, nose, trachea and the lungs before being exchanged in alveolus. Oxygen in the inspired gas passes into blood while carbon

dioxide (CO_2) carried in the blood passes into the alveolus. Carbon dioxide is expired from the lungs following the opposite route as the oxygen supply.

Numerous models have been developed to represent the respiratory system. The complexity of the models extends from single to multi-compartments depending on computer performance and particular applications. In 1954, Grodins et al (1954) described a simple respiratory model that included a realistic control system. Since Grodins' model, several other models of the respiratory system have been developed. Recent models include specific aspects of the respiratory control in humans, such as CO_2 homeostasis or ventilatory response to isocapnic hypoxia. A simulation model of the respiratory system needs to include the mechanics of breathing, the gas exchange process and the regulation processes that control breathing. This section reviews the main features of the respiratory models found in literature.

6.2.1 Mathematical models of human lung mechanics of breathing

Two types of lung model can be used to model the mechanics of breathing including the volume change of the lung and the effect of the chest wall. One is represented as a mechanical device and the other is based on a Windkessel model.

6.2.1.1 Mechanical model

Mechanistic components are used to represent the lungs, trachea and other components of the respiratory system in a mechanical model. The lung and pleural compartment are usually represented as a linear actuator with spring and viscous resistance effects (Figure 6-1) (Tomlinson et al. 1994a); the intrathoracic extrapulmonary zone of the tracheobronchial tree is considered as a passageway acting as a mass-spring damper system (Figure 6-2).

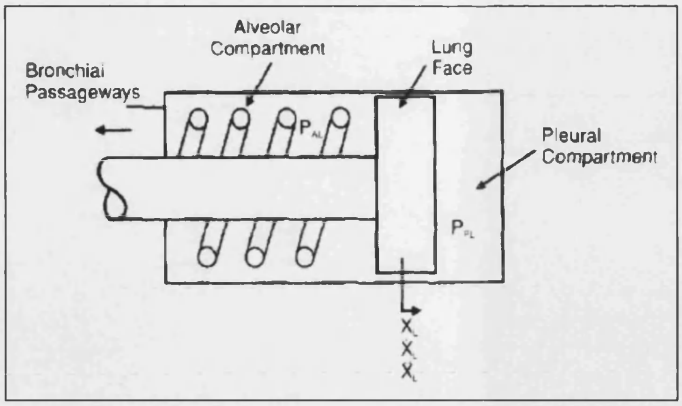

Figure 6-1 Lung model (Tomlinson et al. 1994a)

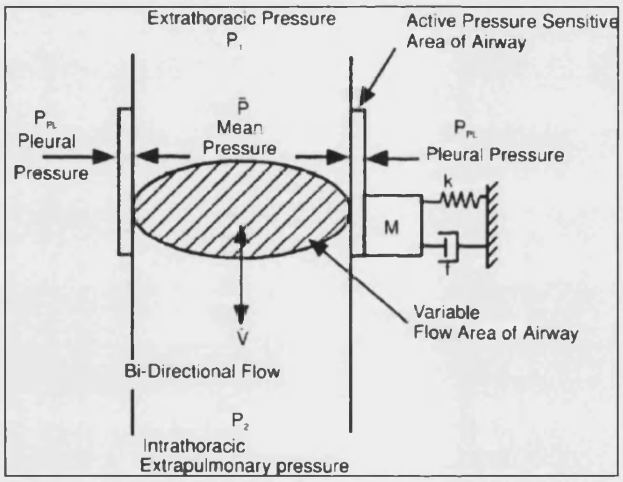

Figure 6-2 Tracheobronchial tree model (Tomlinson et al. 1994a)

Motion of the lung wall, which includes lung stiffness ($k(x_l-x_0)$), a viscous force ($f\frac{dx_l}{dt}$) and a Coulomb resistance force (F_c) is given by

$$M\frac{d^2x_l}{dt^2} = (P_{lung} - P_{pl})A_l - f\frac{dx_l}{dt} - k(x_l - x_0) - F_c \qquad (6\text{-}1)$$

The pressure in the lung is given by

$$\frac{dP_{lung}}{dt} = \frac{nRT}{V_l}(Q_l - \dot{V}_l) \qquad (6\text{-}2)$$

A similar equation to that outlined for the lung motion can also be used for the pleural compartment. In this case, the equation for the pleural compartment is

$$M_{pl}\frac{d^2x_{pl}}{dt^2} = F_{th} + (P_{pl} - P_{at})A_{pl} - f_{pl}\frac{dx_{pl}}{dt} - k_{pl}x_{pl} - F_c \qquad (6\text{-}3)$$

Using this approach, parameters such as stiffness (k), viscous friction (f) and piston/lung area (A) are required. However, such parameters are impossible to measure directly from humans and have no physiological meaning to clinicians and medical staff.

6.2.1.2 Windkessel model

The Windkessel theory first arose from the analogy of early fire engines where the repeated strokes of the water pump were smoothed out to provide a nearly continuous flow by an air compression chamber. In physiological modelling, the Windkessel model was first applied to a cardiovascular system to model the blood vessels as elastic storage vessels. In the lung, each alveolus also acts like an elastic chamber, allowing the lung to be idealised as a one-elastic-chamber model whose volume and pressure are the average of all the alveoli.

The storage capacity of the elastic lung can be determined from its dispensability D_i, such that

$$D_i = \frac{dV}{dP} \qquad (6\text{-}4)$$

where V is the volume and P is the internal gas pressure.

The bulk modulus, or the modulus of volume elasticity, k is related to the dispensability by the relationship,

$$k = \frac{VdP}{dV} = \frac{V}{D_i} \qquad (6\text{-}5)$$

The rate of change of the volume in the elastic chamber $\frac{dV}{dt}$ can be written as:

$$\frac{dV}{dt} = \left(\frac{dV}{dP}\right)\frac{dP}{dt} \qquad (6\text{-}6)$$

or

$$\frac{dV}{dt} = D_i \frac{dP}{dt} \tag{6-7}$$

The mass balance can be written for the gas in the elastic chamber as

$$\text{Inflow - Outflow = Rate of storage} \tag{6-8}$$

$$Q_{in} - Q_{out} = D_i \frac{dP}{dt} \tag{6-9}$$

Flow is bidirectional in the lung, so the above equation above can be simplified as follows

$$Q(t) = D_i \frac{dP}{dt} \tag{6-10}$$

Therefore, the lung can be modelled as a Windkessel elastic chamber whose change of volume is proportional to the internal gas pressure.

6.2.2 Mathematical models of the gas exchange process

The gas exchange process in the lungs has been modelled and studied in the past from different perspectives and at different levels of detail. The simplest models for gas exchange assume that the diffusive and chemical processes involved in oxygen uptake and carbon dioxide release are in equilibrium as soon as the blood leaves the pulmonary capillaries. The ventilation and cardiac output are based on the average values of each cardiac cycle. Detailed studies also considered the chemical and diffusive processes in blood plasma and the red blood cells. These studies do not assume equilibrium of the diffusive and chemical processes that involve carbon dioxide, but the alveolar gas concentration is assumed to be constant since they do not take into account the mechanics of ventilation (Ben-Tal 2006).

6.2.2.1 Gas exchange model for a healthy lung

The gas exchange process in a healthy lung is modelled by calculating the partial pressure gradient between the alveolar and the blood. The partial pressure of oxygen (P_{O2}) and carbon dioxide (P_{CO2}) that diffuse between the pulmonary capillaries and the alveoli can be determined by Dalton's Law where:

$$P_{o2} = f_{O2} \cdot P_{alv} \tag{6-11}$$

$$P_{co2} = f_{CO2} \cdot P_{alv} \tag{6-12}$$

and f_{O2} and f_{CO2} are the concentrations of oxygen and carbon dioxide. The flux of oxygen and carbon dioxide can be estimated from

$$D_{O2}(P_{O2,puc} - P_{O2,alv}) \tag{6-13}$$

$$D_{CO2}(P_{CO2,puc} - P_{CO2,alv}) \tag{6-14}$$

where D_{O2} and D_{CO2} are the diffusion capacities of oxygen and carbon dioxide respectively and $P_{O2,puc}$ and $P_{CO2,puc}$ are the blood partial pressures of oxygen and carbon dioxide. From these two expressions, it can be seen that the direction of the flux depends on the partial pressure difference between the alveoli and the blood. The higher partial pressure in the alveoli leads to gas diffusion from alveoli to the blood and vice versa. Therefore the total net flux of gas into the alveoli is given by (Ben-Tal 2006)

$$Q_{alv} = Q + D_{CO2}(P_{CO2,puc} - P_{CO2,alv}) + D_{O2}(P_{O2,puc} - P_{O2,alv}) \tag{6-15}$$

where Q is the gas flow to the lung.

The total net flux of gas into the blood is given by

$$Q_{alv} = Q_{puc} - D_{CO2}(P_{CO2,puc} - P_{CO2,alv}) - D_{O2}(P_{O2,puc} - P_{O2,alv}) \tag{6-16}$$

The rate of change of f_{O2} and f_{CO2} can be expressed as (Ben-Tal 2006)

$$\frac{df_{O2}}{dt} = \frac{1}{V_{alv}}\begin{bmatrix} D_{O2}(P_{O2,puc} - P_{O2,alv}) + (f_{O2i} - f_{O2})Q_i \\ -f_{O2}(D_{CO2}(P_{CO2,puc} - P_{CO2,alv}) + D_{O2}(P_{O2,puc} - P_{O2,alv})) \end{bmatrix} \tag{6-17}$$

$$\frac{df_{CO2}}{dt} = \frac{1}{V_{alv}}\begin{bmatrix} D_{CO2}(P_{CO2,puc} - P_{CO2,alv}) + (f_{CO2i} - f_{CO2})Q_i \\ -f_{CO2}(D_{O2}(P_{O2,puc} - P_{O2,alv}) + D_{CO2}(P_{CO2,puc} - P_{CO2,alv})) \end{bmatrix} \tag{6-18}$$

where Q_i is the inspired gas flow and f_{oi} and f_{ci} are the inspired concentration of oxygen and carbon dioxide, respectively.

6.2.2.2 Gas exchange model for a diseased lung

The gas exchange model described above is suitable for a single-compartment lung model. However, it would be unrealistic to use this approach to model a diseased lung because of the localised damage to the alveoli. For this reason, Tilley et al (Tilley et al. 2006) introduced a multi-compartment lung model which can effectively model a damaged lung. For a healthy lung, it is expected that the ventilation to perfusion ratio $\dot{V}/Q$ are log-normally distributed with an average value for $\dot{V}/Q$ ratio of 1 (Figure 6-3) whereas a lower average $\dot{V}/Q$ ratio for lungs damaged by disease display a bimodal distribution (Figure 6-4). Oleic acid injection (induced pulmonary edema) (Figure 6-4 B) and repeated lung lavage (washing out of the lungs) (Figure 6-4 C) has a bimodal distribution of blood flow with one value at a normal $\dot{V}/Q$ ratio and the other value representing the low $\dot{V}/Q$ region of the damage lung. Figure 6-5 (West & Wagner 1977) shows the partial pressure of the alveolar carbon dioxide and $\dot{V}/Q$ ratio varying with the corresponding partial pressure of oxygen. Knowing this relationship, the exchange of oxygen and carbon dioxide in each lung unit can be determined by matching the $\dot{V}/Q$ ratio for each lung compartment. Simple mixing theory then determines the total partial pressure of oxygen and carbon dioxide in the lung.

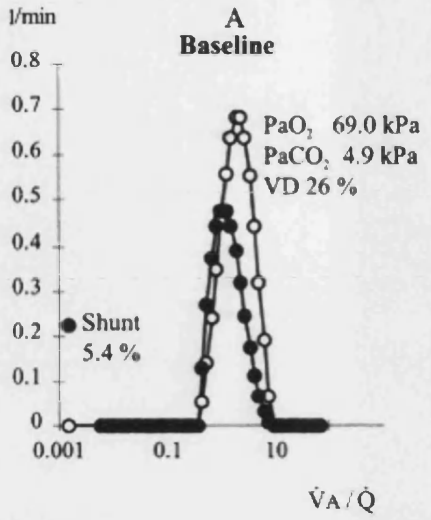

Figure 6-3 $\dot{V}$ / Q ratio distribution before induction of lung injury; y-axis: ventilation (○) and perfusion (●) in L/min; x-axis: $\dot{V}$ / Q ratio; VD: Dead space ventilation (Neumann & Hedenstierna 2001)

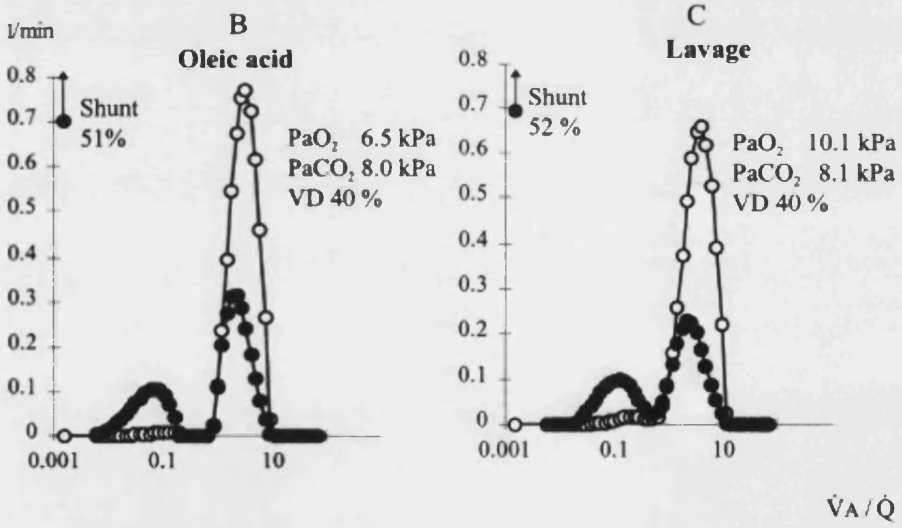

Figure 6-4 $\dot{V}$ / Q ratio distribution after induction of lung injury; y-axis: ventilation (○) and perfusion (●) in L/min; x-axis: $\dot{V}$ / Q ratio; VD: Dead space ventilation (Neumann & Hedenstierna 2001)

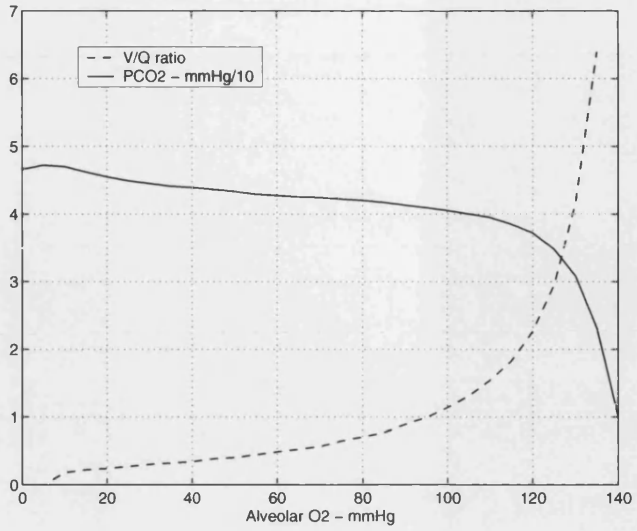

Figure 6-5 $\dot{V}/Q$ ratio and P_{CO2} varying with P_{O2} (West & Wagner 1977)

6.2.3 Carriage of constituent gases by blood

Oxygen is primarily transported in the arterial blood by binding to deoxygenated haemoglobin. The amount of oxygen present depends on the haemoglobin content of the blood, the saturation level of the haemoglobin and the mixed venous partial pressure of oxygen (Lo 1995). The oxygen content is usually determined according to the dissociation curve of oxygen. As Figure 6-6 shows, the relationship between P_{O2} and the oxygen concentration is sigmoid in shape.

The majority of carbon dioxide is carried in the blood by being physically dissolved and bound to proteins as carbamino compounds, and as carbonic acid. The carbon dioxide content is also determined by the dissociation curve of carbon dioxide. In addition, the relationship between P_{CO2} and CO_2 content is nonlinear. The degree of oxygenated blood affects the CO_2 dissociation curve. In Figure 6-6, CO_2 dissociation curves at 97.5% and 70% HbO_2 are shown. The greater the saturation of haemoglobin with O_2, the less will be the CO_2 content for a given P_{CO2}.

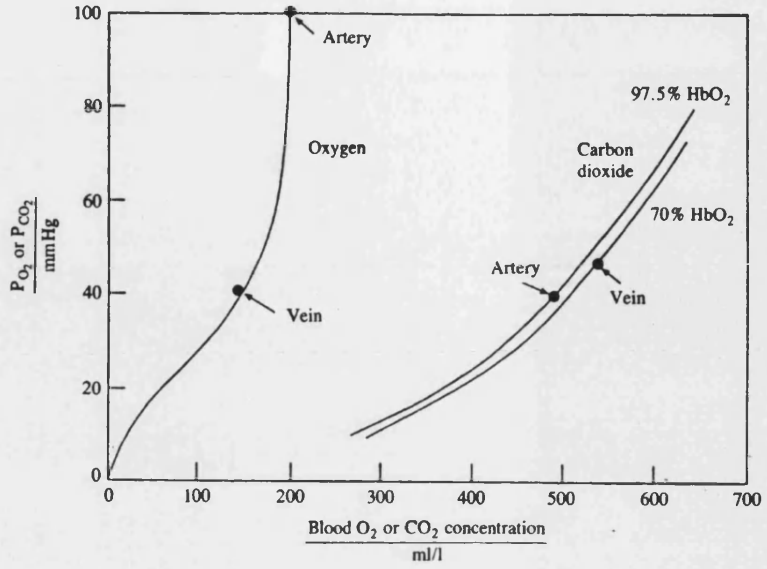

Figure 6-6 O_2 and CO_2 dissociation curve (Tomlinson et al. 1994a)

The concentration of each gas constituent in each cardiovascular compartment can be determined by the mass balance equation as follow (Lu et al. 2001;Tomlinson et al. 1994b)}

$$\frac{dC_i}{dt} = \frac{Q_{in}C_{in,i} - Q_{out}C_i}{V} \tag{6-19}$$

where V is the blood volume in each compartment.

6.2.4 Mathematical models of respiratory regulation

Figure 6-7 summarizes the regulation mechanism of the respiratory system. The respiratory regulation includes receptor elements which are sensitive to the change of the partial pressures, lung volume and temperature, central nervous system which transmits efferent signals to the effector sites to control the respiratory frequency and thoracic force. The breathing is continuously monitored by chemoreceptors, which detect changes in the partial pressure of oxygen (P_{O2}) and carbon dioxide (P_{CO2}), and by mechanoreceptors, which survey changes in thoracic mechanics. Other receptors such as the thermal receptor and the vascular baroreceptors and mechanoreceptors monitor the vascular pressures and the temperature at different sites in the body. The activity of

these receptors allows ventilation to be adjusted automatically so that the arterial blood gases are kept within acceptable limits despite changing internal and external conditions.

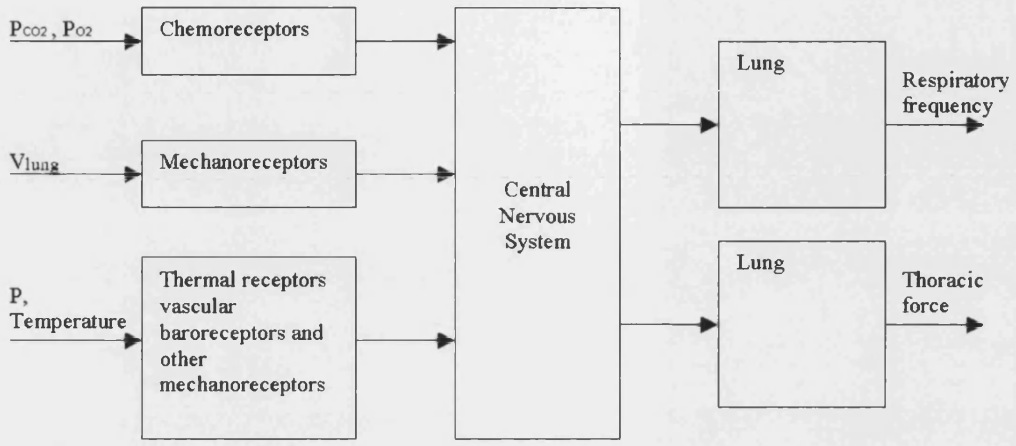

Figure 6-7 Regulation of respiratory system

The major receptors in the control of respiration are the peripheral chemoreceptors and central chemoreceptors. Peripheral chemoreceptors respond to changes in the arterial blood including arterial P_{O2} and arterial hydrogen-ion concentration. The central chemoreceptors respond to changes in the brain extracellular fluid which are stimulated by changes of arterial P_{CO2}. As Figure 6-8 shows, the decrease of arterial P_{O2} and increase of arterial P_{CO2} induce the firing of peripheral chemoreceptors. The increased arterial P_{CO2} also increase the firing of the central chemoreceptors. The elevation of the firing of both chemoreceptors stimulates the medullary inspiratory neurons to increase ventilation.

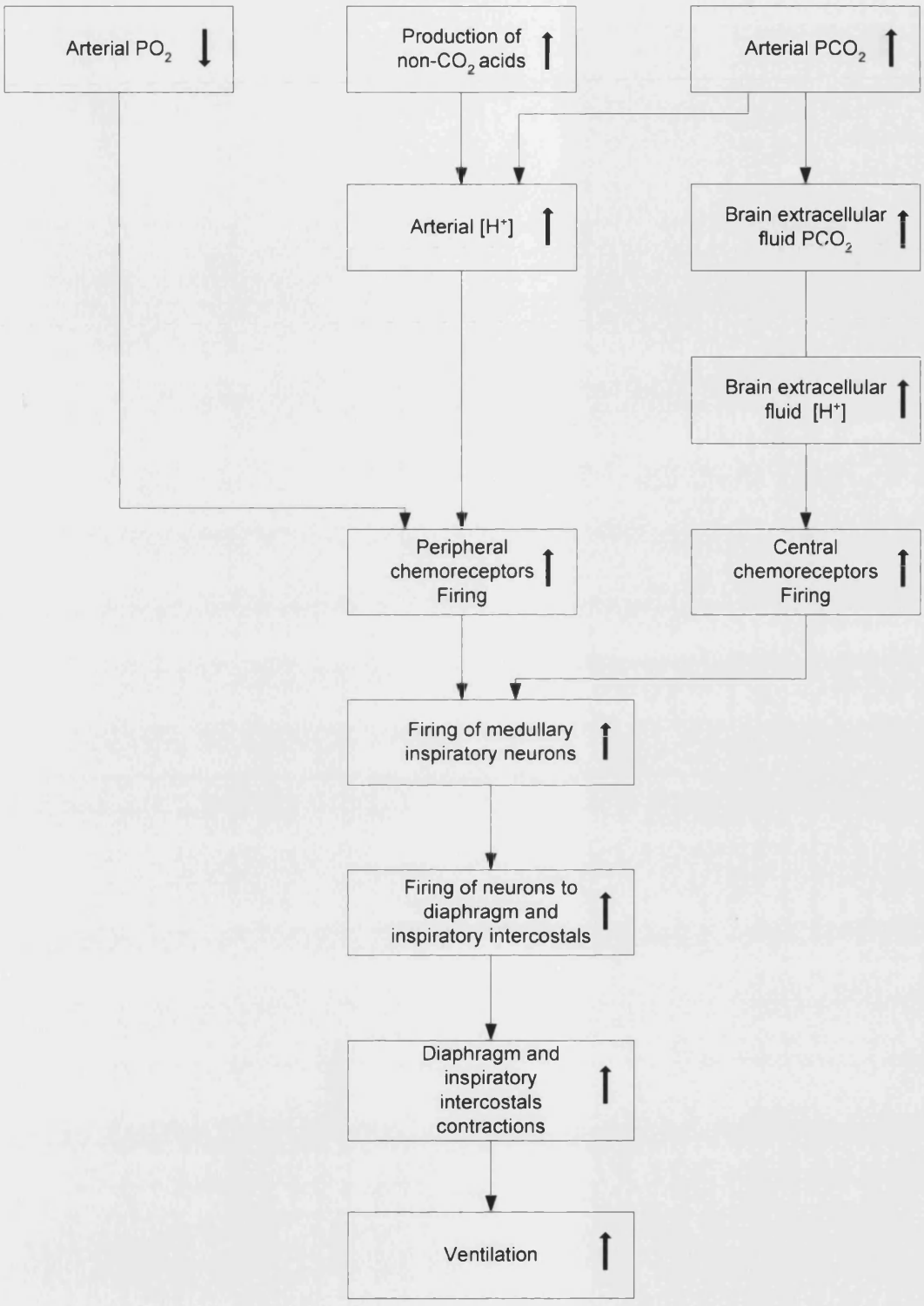

Figure 6-8 Flow chart of chemoreceptor control on ventilation (↑: increase; ↓: decrease) (Vander et al. 2001)

There are various mechanoreceptors in the lung that modify breathing. In the elastic tissues of the lung and the chest wall are lung stretch receptors. The exact function of these receptors is not fully understood but animal tests have shown that they are responsible for various reflexes. Stretch responses occur when the lung and chest wall are distended that inhibit further inspiration. This is a safety mechanism to avoid over-distension. Conversely, opposite responses occur when the lung volume is low. A small increase in lung size may stimulate the stretch receptors to cause further inspiration. The information from these receptors in the lung is carried to the respiratory centre along the vagus nerve.

Both the central and peripheral chemoreceptors have been studied extensively due to their importance in respiratory control. However the study of the mechanoreceptors has received relatively less attention as it is a secondary control mechanism compared to the chemoreceptors. This receptor is an important control feature during exercise.

Several mathematical models of the respiratory control system have been proposed in order to gain a deeper understanding of the system in humans. These can be divided into two groups: 'minimal' models and 'physiological' models (Ursino et al. 2001a).

6.2.4.1 Minimal model

'Minimal' models use simple differential equations to link ventilation to CO_2 and O_2 partial pressures without considering the feedback signals from the rest of the human body. They have been used extensively for the estimation of the main parameters of the controllers, the examination of the possible site of action of the hypoxic ventilatory decline and the analysis of the stability margins of the ventilatory control system. The main advantage of these models is that they can be easily solved with little computation time, hence they are particularly suitable to fit real clinical curves through parameter estimation procedures. A typical model was developed by Bellville et al. (Bellville et al. 1979). It is a two-compartment model to link end tidal partial pressure of CO_2, $P_{ET,CO2}$ stimulus to ventilation response as follows:

$$x_1(t) = g_1[P_{ET,CO2}(t - T_1) - k]/(1 + \tau_2 s) \qquad (6\text{-}20)$$

$$x_2(t) = g_2[P_{ET,CO2}(t - T_2) - k]/(1 + \tau_2 s) \quad (6\text{-}21)$$

$$y(t) = x_1(t) + x_2(t) \quad (6\text{-}22)$$

$x_1(t)$ represents the effect of the central chemoreflex on the ventilation while $x_2(t)$ represents the effect of peripheral chemoreflex on the ventilation. Their combining effect results in the ventilation response y(t). It can be seen that these two compartments contains a time constant, time delay and gain. The number of estimated parameters is reduced to a minimum, which is necessary for a tractable model and to attain the maximum confidence in the estimated parameter values. Although the two-compartment model is simple, it incorporates the essential physiological elements of the central and peripheral chemoreceptors.

6.2.4.2 Physiological model

Complete 'Physiological' models have been developed in order to overcome the shortcomings of the 'minimal' models. They require heavy computation but permit the ventilatory response to be studied in its actual environment. Earlier models such as Grodins's model (Grodins et al. 1967) includes chemical details on O_2 and CO_2 transport, acid-base buffering, blood flow regulation and a simplified ventilation controller to regulate the O_2 and CO_2 partial blood pressures. This is achieved using the chemical concentrations at receptor sites as the inputs and ventilation as the outputs to the respiratory model. In recent chemoreflex models (Ben-Tal 2006;Hsing-Hua & Khoo 2002;Lo 1995;Ursino et al. 2001a), the controlled variables are P_{CO2} and P_{O2} in the brain and P_{CO2} in the tissue arterial blood, and the outputs to the respiratory model are tidal volume and breathing duration. As shown in Figure 6-9, the ventilation increases as the P_{O2} reduces at a given P_{CO2}. In order to increase ventilation, the tidal volume V_T is increased and the breath duration is decreased. The duration time is dominant in shortening the expiratory time while the inspiratory time has little effect on ventilation.

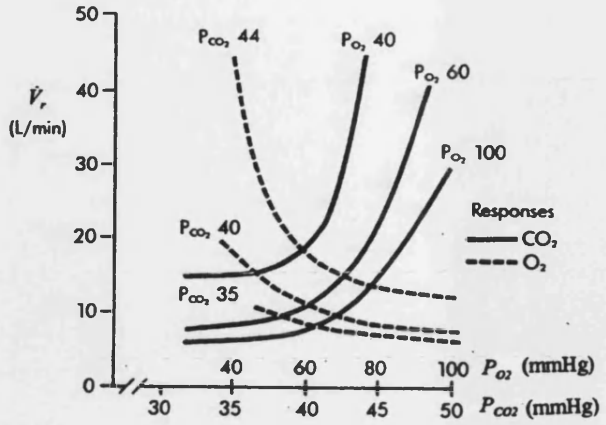

Figure 6-9 Ventilatory responses to the arterial PCO_2 and PO_2 (Lo 1995)

Recently Ursino et al. (Ursino et al. 2001a) updated Bellville's model by introducing a nonlinear gain and varied pure delay for the peripheral chemoreceptor model. The nonlinear gain has a sigmoid shape while the pure delay is inversely proportional to cardiac output because the time for the gas to transport from the lungs to the chemoreceptor sites increases if the blood flow decreases.

In addition to the delays in the response of the respiratory pattern generator to changes in ventilatory demand, there are dynamic shifts in the operational points of the system depending on the metabolic rate. For example, the operating point during sleep shifts to a higher CO_2 level. During exercise, the operating point shifts to higher ventilation but, in this case, the CO_2 level is not affected. From an engineering perspective, these shifts and the subsequent behaviour are similar to 'integral plus proportional' control, which minimizes errors to set-point changes during sleep or exercise. Models of the ventilatory response during exercise have been developed using the mathematics of integral control (Yamamoto 1980;Yamamoto 1978). During exercise, the alveolar ventilation can increase by as much as twenty fold (Vander et al. 2001). In Lo's model (Lo 1995), the controller output is adjusted according to the overall O_2 consumption. The gain and the threshold are changed such that both are proportional to the level of overall O_2 consumption. In addition, Lo (Lo 1995) used the combination of proportional and integral control actions to define the required thoracic force for the lung expansion. This allowed the shift of the ventilation during exercise to be modelled.

6.2.5 Comparison of respiratory models

Table 6-1 summarizes the features included in the published respiratory models. Most lung models are based on a one-compartment model with the multi-compartment lung model being used for a diseased lung. Airway mechanisms play an important role in the respiratory model for both healthy and diseased lungs. In patients, the airway mechanism is more complicated due to the obstructive airway caused by diseases such as chronic obstructive pulmonary disease. The breathing mechanism is conventionally modelled as a mechanical model and this is sufficient to model a healthy person. The Windkessel model is a new approach for the breathing mechanism which was originally developed for blood vessels. Only a few authors have modelled the gas transport in the blood and the respiratory regulation.

The main purpose of the respiratory model developed here is to model a healthy lung for integration with the cardiovascular model. Therefore, features associated with the cardiovascular system such as gas exchange process and gas transport must be included. Respiratory regulation will also be included in order to develop a comprehensive cardiopulmonary model. As to the lung model, the use of the Windkessel lung model was investigated as a possible approach for modelling a healthy lung in a more physiological manner. A single compartment lung was chosen because this is considered to be sufficient to model a healthy lung. Airway mechanics were included as well since this is a very important site where acute and chronic diseases can develop.

*Table 6-1 Comparison of lung model; ME: mechanical model; WI: Windkessel model (*included in the model)*

Investigators	lung model		Airway mechanism	lung mechanism		Gas exchange process	Gas trans-port	Regulation receptors	
	One-compart-ment	Multi-compart-ment		ME	WI			Chemo-	Lung stretch
(Tomlinson et al. 1994a)	*		*	*		*			
(Tilley et al. 2006)		*	*		*	*	*	*	
(Lo 1995)	*		*	*		*	*	*	*
(Lu et al. 2001)	*		*	*		*			
(Liu et al. 1998)	*		*	*		*			
(Ben-Tal 2006)	*			*		*	*		
(Ursino et al. 2001a;Ursino et al. 2001b)	*			*		*	*	*	*
(Grodins et al. 1967)	*			*		*	*	*	
(Tang et al. 2005)		*	*	*		*	*		

6.3 Development of the respiratory model

6.3.1 Air passageways

The air passageways were modelled using the method of Tomlinson et al. (Tomlinson et al. 1994b) because it is the most complete model available. In this model, the passageway is divided into three zones:

1. extra-thoracic zone,
2. intra-thoracic extra-pulmonary zone,
3. and intra-thoracic intra-pulmonary zone.

The extra-thoracic zone includes the downstream side of the nasal passageways, leading to the trachea. The intra-thoracic extra-pulmonary zone is the bronchial passageways. The intra-thoracic intra-pulmonary zone is the distal airway close to the alveoli.

6.3.1.1 Extra-thoracic zone

The extra-thoracic zone includes two compartments, the nose and mouth. The nose and the mouth are largely responsible for filtering, warming and humidifying the inspired gas. The resistance of the nasal passages accounts for up to 50% of the total airway resistance while the mouth accounts for about 25% during quiet breathing. The nonlinear relationships between the pressure drop and flow rate for the mouth and nose were correlated with the experimental data and the following relationships were found for the nose and mouth respectively:

$$\Delta P_n = 0.025 \rho v_n^2 \cdot \left[1 + \left(1000 + \frac{10^6}{\mathrm{Re}_n}\right)\right] \qquad (6\text{-}23)$$

$$\Delta P_m = 0.005 \rho v_m^2 \cdot \left[1 + \left(1000 + \frac{10^6}{\mathrm{Re}_m}\right)\right] \qquad (6\text{-}24)$$

where $\mathrm{Re}_n = \rho v_n \tilde{d} / \mu$ and $\mathrm{Re}_m = \rho v_m \tilde{d} / \mu$.

6.3.1.2 Intra-thoracic extra-pulmonary and intra-pulmonary zone

The flow in this region is laminar and the openings of the air passageway are directly influenced by the degree of inflation of the lung. The elastic wall of the trachea and the bronchial passageways is idealised as a mass-spring-damper system and the force acting on the wall of a single airway is given by

$$M\frac{d^2x_{aw}}{dt^2} = (P_{aw} - P_{pl})A_{aw} - f\frac{dx_{aw}}{dt} - k(x_{aw} - x_{0,aw}) \tag{6-25}$$

where x is the displacement of the elastic wall. The effective flow area of the airways is thus determined by the number of extra-pulmonary airways n_e and the elastic wall displacement x.

$$A_e = n_e\pi \cdot x_{aw}{}^2 \tag{6-26}$$

6.3.2 Human lung mechanics of breathing

The model for lung mechanics of breathing is usually modelled as a mechanical device. In order to develop a more physiological lung model, a Windkessel model for a healthy lung is developed below.

The lung is idealized as a balloon with the pleural pressure acting on its external surface rather than on a constant piston area in the mechanical model. Motion of the lung wall is given by

$$M\frac{d^2x_l}{dt^2} = (P_l - P_{pl})A_l - f\frac{dx_l}{dt} - k(x_l - x_{0,l}) \tag{6-27}$$

$$A_l = 4\pi \cdot x_l^2 \tag{6-28}$$

$$\frac{dV_l}{dt} = A_l \cdot \frac{dx_l}{dt} \tag{6-29}$$

The pressure of gas within the lung can be calculated as:

$$\frac{dP_l}{dt} = \frac{dV_l}{dt} / C_l \tag{6-30}$$

However, it was found difficult to simulate realistic lung movements using this approach (Figure 6-10). Firstly, instead of the constant lung compliance, the lung compliance derived from lung pressure-volume curves varies with lung volume and also changes in lung diseases (Berne & Levy 1988). Secondly, an accurate tidal volume is difficult to obtain using similar lung motion setting to those used in the mechanical model.

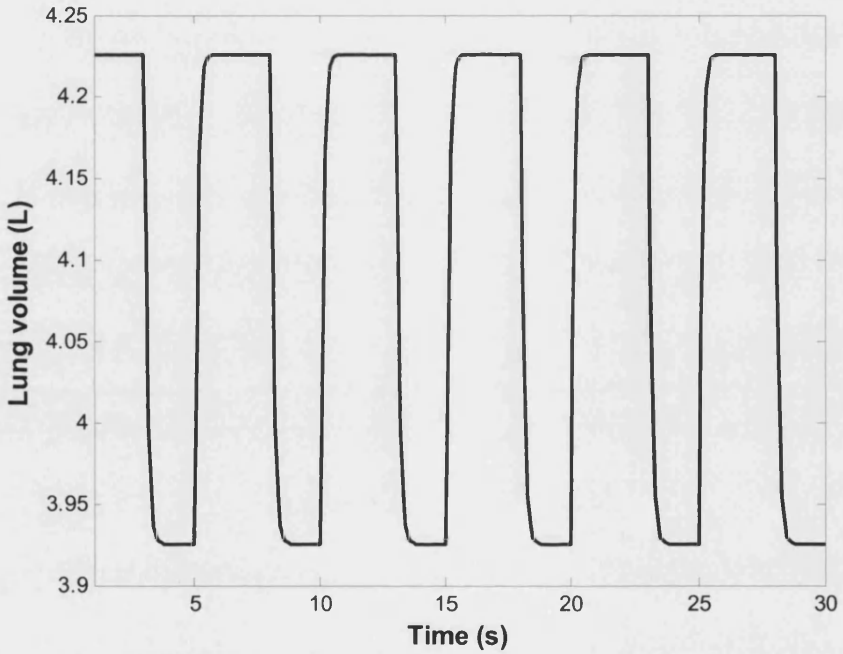

Figure 6-10 Lung volume generated by Windkessel model

The pressure-volume relationship described by the mechanical model is more realistic as shown in equation (6-2). The $\frac{nRT}{V_l}$ term in the equation is the inverse of lung compliance C_{lung} and takes account of the compliance changes due to lung volume and temperature.

The lung and the pleural compartments are modelled as two pistons acting together with spring and fiction resistance effects. The motion of the lung wall is determined using equation (6-1) presented earlier.

The conceptual lung area A_l mainly depends on the pressure difference between the alveoli and the pleural compartment. The stiffness, k, of the moving lung and chest wall system comprises two distinct effects: one due to the lung and surrounding tissue and the other due to the ribcage, diaphragm and pleural compartment. The large variation in these terms, over the working range of the lung, from residual volume to total lung capacity, have been assessed by numerous researchers (Lo 1995). The net force on the lung wall is zero at the functional residual capacity, when the lung wall displacement is x_0.

The pleural compartment was modelled in a similar manner to that of the lung except that the compartment is filled with liquid rather than gas. The face of the pleural compartment was also idealized as a piston which is driven by the action of forces generated by the ribcage and diaphragm, intrapleural pressure and atmospheric pressure. Intercostal and diaphragm thoracic forces due to neurogenic action also play a role in the motion of the pleural compartment. The equation of motion, including viscous and Coulomb friction forces is given by equation (6-3).

The pleural compartment is regarded as a closed control volume of trapped pleural fluid of volume V_{pl} which compresses during inhalation giving an increase in pleural pressure and expands during exhalation giving a decrease in pleural pressure. The rate of change of pleural pressure depends on the motion of the lung wall and pleural compartment wall and is given by

$$\frac{dP_{pl}}{dt} = \frac{B}{V_{pl}}\left(\frac{-A_{pl}dx_{pl}}{dt} + \frac{A_l dx_l}{dt}\right) \tag{6-31}$$

6.3.3 Gas exchange

The respiratory model developed here is intended to be integrated with the cardiovascular model which has a pulsatile blood flow. The pulsatile blood flow is not compatible with the multi-compartment lung model since average blood flow is required to calculate the $\dot{V}/Q$ ratio for each compartment. Although the average blood

flow can be calculated every cardiac cycle, this will weaken the advantage of the cardiovascular model.

Therefore, a single compartment gas exchange model is used. The diffusion in the lung is highly efficient as there is only a thin sheet of tissue separating the blood and the alveolar spaces. In a healthy person's lung, the partial pressure of the gases in the alveoli and in the blood reaches equilibrium within one cardiac cycle (Figure 6-11 when $D_{mO2} = 40$). However, in a low diffusion capacity lung, i.e. a diseased lung, it takes much longer to reach equilibrium (Figure 6-11 when $D_{mO2} < 10$). Therefore, for a healthy lung, it is assumed that the partial pressure of gases in the pulmonary capillaries is equal to that in the alveoli.

$$P_{blood,i} = P_{alv,i} \tag{6-32}$$

where *i* represents the gas constituents.

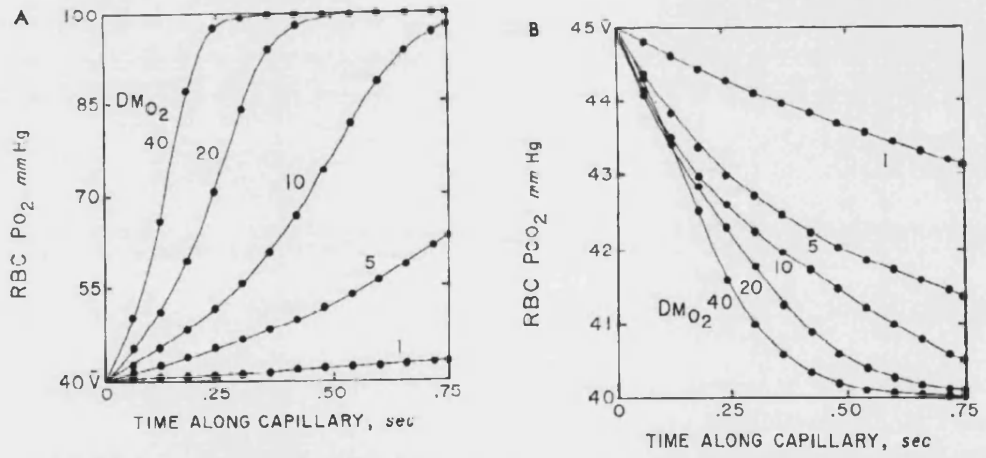

Figure 6-11 Time courses for blood P_{O2} (A) and P_{CO2} (B) at normal and reduced capillary diffusion capacity (D_{mO2}) ; Alveolar P_{O2} and P_{CO2} are kept at 100 and 40 mmHg; RBC (red blood cell) (Wagner & West 1972)

With the partial pressures of O_2 and CO_2 known, the gas concentrations in the blood can be determined by the equations used to represent the dissociation curves shown in Figure 6-6.

$$C_{co2} = 0.5384(1 - e^{-0.0289 P_{co2}}) + 0.1891 - (0.1891 - 0.125) C_{o2} / \hat{C}_{o2} \quad (6\text{-}33)$$

$$C_{o2} = \hat{C}_{o2}(1 - e^{-1.02 \eta \cdot P_{o2}})^2 \quad (6\text{-}34)$$

The variable η is given by

$$\eta = 0.44921 pH - 0.10098 pH^2 + 0.0066815 pH^3 - 0.454 \quad (6\text{-}35)$$

where

$$pH = 9 - \log_{10} C_H \quad (6\text{-}36)$$

$$C_H = 795 \left[\frac{0.51 P_{co2} / 760}{C - 0.51 P_{co2} / 760} \right] \quad (6\text{-}37)$$

The concentrations of the inert gases are simpler and can be calculated using Henry-Dalton law as follow:

$$C_i = S_i P_i \quad (6\text{-}38)$$

The gas exchange in the alveolar is assumed to take place at the end of the lung capillaries. Therefore, the diffusion rate of the gases is determined by the difference between the concentrations of gas from the capillaries blood and from the alveolar:

$$\dot{V}_i = Q_{alv}(C_{puc,i} - C_{al,i}) \quad (6\text{-}39)$$

where Q_{alv} is the blood flow through the alveolar.

A certain proportion of blood flowing from the pulmonary artery is shunted to the pulmonary vein without gas exchange taking place in the alveolar. Therefore, Q_{alv} is not equal to the flow through the pulmonary capillaries. Usually, 2% of the blood is shunted in a healthy lung, therefore

$$Q_{alv} = (1 - f_{sh})Q_{pua} \tag{6-40}$$

where $f_{sh} = 0.02$.

Taking into account the shunted gas concentration, the gas concentrations flowing into the pulmonary vein are

$$\frac{dC_{O2}}{dt} = \frac{Q_{in}C_{in,O2} - Q_{out}C_{O2} - \dot{V}_{CO2}C_{O2} + \dot{V}_{O2}}{V_{puc}} \tag{6-41}$$

$$\frac{dC_{CO2}}{dt} = \frac{Q_{in}C_{in,CO2} - Q_{out}C_{CO2} - \dot{V}_{CO2}C_{co2} - \dot{V}_{CO2}}{V_{puc}} \tag{6-42}$$

6.3.4 Gas transportation

The gas constituents passing from the mouth to the alveolar compartment and vice versa are defined by continuity of mass. The mass transfer rate of each constituent is given by the equation

$$\frac{dm_i}{dt} = \frac{m_{i1}}{\sum m_{i1}} q_1 + \frac{m_{i2}}{\sum m_{i2}} q_2 + \ldots \tag{6-43}$$

The model accounts for four gas constituents at present: oxygen, nitrogen, helium (for diving applications) and carbon dioxide.

The alveolar compartment consists of two zones: one allows gas diffusion and one, which is termed the alveolar dead zone, does not. It is necessary to separate these two zones so that the diffusion process is realistic. The gas constituents in the alveolar compartment is calculated by

$$\frac{dm_i}{dt} = \frac{f_{dv}m_i}{\sum m_i} q - \dot{U}_{o2} + \dot{U}_{co2} \tag{6-44}$$

and in the alveolar dead space by

$$\frac{dm_i}{dt} = \frac{(1-f_{dv})m_i}{\sum m_i} q \tag{6-45}$$

where $f_{dv} = \begin{cases} 0.2 - \dfrac{V_{Danat}}{V_T} & V_T \geq 0.875L \\ 0 & V_T < 0.875L \end{cases}$, V_{Danat} is the anatomical dead space comprising the volume of the respiratory passages, extending from the nostrils and mouth down to just before the alveoli. It has a volume of about 0.175 L in a healthy lung.

Individual gas partial pressures in the alveoli can be determined from the mass fraction and total pressure using the formula

$$P_{i,alv} = P\left(\frac{m_i}{m}\right)\left(\frac{R_0}{M_i R}\right) \tag{6-46}$$

The specific gas constant R in terms of the mass fractions of constituent gases is given by

$$R = \frac{R_0}{M} = R_0 \sum_{i=1}^{N}\left(\frac{m_i}{m}\right)\frac{1}{M_i} \tag{6-47}$$

The carriage of the constituent gases by blood is adapted from Tomlinson's method (described in section 6.2.3) to a dynamic process which takes into account the gas concentration change due to the blood volume change.

The concentration of each gas constituent can be determined by the mass balance equation as follow

$$\frac{dC_i}{dt} = \frac{Q_{in}C_{in,i} - Q_{out}C_i - \dot{V}C_i}{V} \tag{6-48}$$

where V is the blood volume in the blood vessel.

6.3.5 Metabolic process in the tissue compartment

The metabolic tissue process model generates an oxygen consumption rate and carbon dioxide production rate which vary for different work efforts. The O_2 consumption for a person at rest is around 0.265 L/min and increases as work load increases (Lo 1995). During light dynamic work, the O_2 uptake increases gradually to a steady state when the work commences and decreases slowly to the initial level after the work is completed. This phenomenon can be represented using a first order system response to determine the oxygen consumption rate in the tissue.

The production rate of CO_2 can be calculated from the respiratory quotient RQ which is the ratio between CO_2 production rate and O_2 consumption rate. The RQ is 1.0 in oxidation of glucose and other carbohydrates while for protein breakdown it is 0.8.

Knowing the production rate of CO_2 and the consumption rate of O_2, the rate of change of O_2 and CO_2 concentration in the tissue can be determined from:

$$\frac{dC_{o2}}{dt} = \frac{Q_{in}C_{in,o2} - Q_{out}C_{o2} - \dot{V}_c C_{o2} - \dot{V}_{o2}}{V_c} \tag{6-49}$$

$$\frac{dC_{co2}}{dt} = \frac{Q_{in}C_{in,co2} - Q_{out}C_{co2} - \dot{V}_c C_{co2} + \dot{V}_{co2}}{V_c} \tag{6-50}$$

$$\dot{V}_{co2} = RQ \cdot \dot{V}_{o2} \tag{6-51}$$

6.3.6 Respiratory regulation

6.3.6.1 Regulation of cerebral blood flow

The brain is the least tolerant of ischemia (lack of blood) of the various body tissues. Interruption of cerebral blood flow for as little as 5 seconds results in loss of consciousness, and ischemia lasting just a few minutes results in irreversible tissue damage (Berne & Levy 1988). Therefore, local regulation of the cerebral circulation is predominant over neural factors. Generally, the total cerebral blood flow is constant and shows excellent autoregulation between about 60 and 160 mmHg mean arterial pressure (Berne & Levy 1988).

The cerebral vessels are well known to be sensitive to P_{CO2} and brain O_2 supply. In addition, the flow is also influenced by metabolic factors. The following equations can be used to calculate the responses of the cerebral blood flow adopted from the literature (Patterson, Jr. et al. 1965):

$$\dot{Q}_b = (Q_{b,metabolic} + \Delta Q_{b,o2} + \Delta Q_{b,co2} - Q_b)/\tau_{Qb} \tag{6-52}$$

where

$$\Delta Q_{b,O2} = \begin{cases} 2.785 - 0.1323P_{b,O2} + 2.6032\times10^{-3}(P_{b,O2})^2 \\ -2.324\times10^{-5}(P_{b,O2})^3 + 7.6559\times10^{-8}(P_{b,O2})^4 & P_{b,O2} < 104mmHg \\ 0 & P_{b,O2} \geq 104mmHg \end{cases} \tag{6-53}$$

$$\Delta Q_{b,CO2} = \begin{cases} 2.323\times10^{-2} - 3.1073\times10^{-2}P_{b,CO2} \\ +8.0163\times10^{-4}(P_{b,CO2})^2 & P_{b,CO2} < 38mmHg \\ -15.58 + 0.76P_{b,CO2} - 1.295\times10^{-2}(P_{b,CO2})^2 \\ +9.39\times10^{-5}(P_{b,CO2})^3 - 2.1745\times10^{-7}(P_{b,CO2})^4 & P_{b,CO2} > 44mmHg \\ 0 & otherwise \end{cases} \tag{6-54}$$

6.3.6.2 Mechanoreceptors

Spontaneous respiration is produced by a rhythmic discharge of motor neurons that innervate in the respiratory muscles at the pleural compartment to generate a thoracic force. In addition, 'stretch receptors' in the lung parenchyma convert the stretching stimulus into a burst of nerve impulses, which provide a feedback signal to the respiratory centres.

Lo (Lo 1995) used a proportional and integral controller to control the thoracic force which drives the lung to demand volume. The equation of the controller is given by:

$$F_{th} = G_p(V_{l.dem} - V_l) + G_l \int_0^t (V_{l.dem} - V_l)dt + F_{th,exercise} \tag{6-55}$$

$$F_{th,exercise} = G_{exercise}(V_{l,dem,exercise} - V_l) \tag{6-56}$$

$F_{th,exercise}$ represents the set-point changes during exercise.

6.3.6.3 Chemical control of respiration

Chemical control of respiration is also included in the model. The controlled variables are the P_{CO2} and P_{O2} in the brain.

For $P_{a,co2} > 38$ mmHg, the inspiratory flow controller including the effect of exercise is (Lo 1995):

$$\frac{V_T}{t_{insp}} = 0.062\left(1 + \frac{23.2}{P_{b,O2} - 30}\right)\left[P_{b,CO2} - 35.2\frac{\left(3.5 - \dot{V}_{O2,to}\right)}{(3.5 - 0.265)}\right] \tag{6-57}$$

while for $P_{a,co2} \leq 38$ mmHg

$$\frac{V_T}{t_{insp}} = 0.062\left(1 + \frac{23.2}{P_{b,O2} - 30}\right)\left[38 - 35.2\frac{\left(3.5 - \dot{V}_{O2,to}\right)}{(3.5 - 0.265)}\right] \tag{6-58}$$

The equation for the inspiratory and expiratory time controller is given by

$$t_{insp} = \begin{cases} 1.5 - 0.0526V_T & V_T < 1.9L \\ \dfrac{0.49815}{V_T - 1.285} + 0.59 & V_T \geq 1.9L \end{cases} \tag{6-59}$$

$$t_{\exp} = 0.64 t_{insp} + \frac{11.1}{\left(\frac{0.4}{0.062}\right)\left(\frac{V_T}{t_{insp}}\right) + 2.73} \tag{6-60}$$

Hence, the respiratory period is:

$$t_{cy} = t_{insp} + t_{\exp} \tag{6-61}$$

and the tidal volume is evaluated from

$$V_T = \left(\frac{V_T}{t_{insp}}\right) t_{insp} \tag{6-62}$$

Thus, the demanded lung volume is determined from:

$$V_{l.dem} = \begin{cases} V_T + V_{frc} & \text{during inspiration} \\ V_{frc} & \text{during expiration} \end{cases} \tag{6-63}$$

where V_{frc} is the lung functional residual capacity. This value is normally assumed to be constant but it can vary during forced expiration.

6.3.6.4 Chemical control of cardiovascular system

It has been reported that there is a central antagonistic interaction between the peripheral chemoreflex and arterial baroreflex under normal and disease states (Du & Chen 2007). Baroreflex activation inhibits the sympathetic response to hypoxia (decreased P_{o2}), whilst the response to hypercapnia (increased P_{co2}) is preserved (Somers et al. 1991). It appears that this antagonistic interaction occurs for both conditions (Cooper et al. 2005).

The response of the cardiac activity is biphasic by the stimulation of both the chemoreceptors and baroreceptors. During modest hypoxia, cardiac contractility and heart rate are increased (Karim et al. 1980), as is the total peripheral resistance (Dalymde et al. 1965). Venoconstriction occurs which means the venous unstressed

volume decreases (Dalymde et al. 1965). The cardiac responses are depressed during severe hypoxia (Berne & Levy 1988).

Acute activation of the peripheral chemoreceptors with isocapnic hypoxia resets the baroreflex control of the sympathetic activity to higher pressures without changes in baroreflex sensitivity (Halliwill et al. 2003). This also explains the reduction of vagal activity in response to hypoxia (Cunningham et al. 1972). Therefore it is believed that the peripheral chemoreceptor sends signals to the medulla and 'resets' the baroreceptor by changing the demanded arterial pressure. This arterial pressure demand contributes to the resetting of the operating point of the baroreflex. The published experimental data varies in species and study preparation. Some experiments undertaken on animals indicated different results relating to the influence of the chemoreflex on the baroreflex sensitivity (Cooper et al. 2005). Since the purpose of this study is to model the human cardiopulmonary system, the model uses the conclusion drawn from human tests and the baroreflex sensitivity is considered to be constant without being influenced by the chemoreflex output.

The relationship between the mean arterial pressures and the gas content in the blood is given by (Rothe et al. 1990):

$$\Delta MAP = \begin{cases} k_1 + k_2 \cdot P_{b,CO2} + k_3 / P_{b,O2} & P_{b,co2} > 40mmHg \quad and \quad P_{b,O2} < 104mmHg \\ k_1 + k_2 \cdot 40 + k_3 / P_{b,O2} & P_{b,co2} \le 40mmHg \quad and \quad P_{b,O2} < 104mmHg \\ k_1 + k_2 \cdot P_{b,CO2} + k_3 / 104 & P_{b,co2} > 40mmHg \quad and \quad P_{b,O2} \ge 104mmHg \end{cases} \tag{6-64}$$

This value is the arterial pressure at the baroreflex operating point in the central compartment of baroreflex model described in Chapter 4. Thus the resetting of the baroreflex is linked to the peripheral chemoreceptor.

The central chemoreceptor, located in the ventrolateral medullary, monitors the carbon dioxide concentration in the cerebrospinal fluid. Simmons et al. (2007) demonstrated that mild central chemoreflex activation does not affect the operating point or gain of the baroreflex in humans. Somers et al. (1991) and Cooper et al. (2005) also observed that the baroreflex operating point during the activation of the chemoreceptor by

hypercapnia does not change significantly the sensitivity of the baroreflex. Pitsikoulis et al. (2007) suggested that the central chemoreceptors significantly contribute to the modulation of the sympathetic outflow independently from the baroreceptors and pulmonary receptors.

Oikawa et al. (2005)suggested that hypercapnia induces an increase in the mean arterial pressure due to an activation of the sympathetic nervous system via the central chemoreceptors and a decrease in the heart rate due to a secondary reflex activation of the parasympathetic nervous system, via arterial baroreceptors, in response to the rise in arterial pressure. The mechanism of the interaction between the central chemoreceptor and the baroreceptor established so far is very immature. Therefore, the model for the central chemoreceptor is based on the assumption made by Simmons et al. that the central chemoreceptor alters the gain of the sympathetic nerve activity and there is no influence on the parasympathetic nerve activity.

The relationship between the percentage change of the sympathetic nerve activity gain and the P_{CO2} is based on an experiment undertaken by Lioy and Trzebski (1984) in rats where the action of the baroreceptors, peripheral chemoreceptors, and lung-stretch receptors was excluded:

$$\Delta G_{SNA} = \begin{cases} k_4 \cdot P_{b,CO2} + k_5 & P_{b,CO2} > 40mmHg \\ k_4 \cdot 40 + k_5 & P_{b,CO2} \leq 40mmHg \end{cases} \quad (6\text{-}65)$$

6.4 Closure

This chapter contains a review of published respiratory models and describes development of a respiratory model for integration with the cardiovascular model.

The respiratory model includes the mechanics of breathing, gas exchange process and the regulation of the respiratory system. The gases passing from the nasal passageways through the trachea to the alveolar compartment are modelled using the mass conservation equation. The lung and the trachea tree are modelled as a mechanical device after comparing the results with a Windkessel lung model. The gas exchange in

the alveolar compartment is assumed to take place at the end of the lung capillaries and the partial pressure of the gases reaches equilibrium as soon as the blood leaves the lung capillaries. Thus the gas exchange process is modelled as a continuous process. The dynamic gas transportation due to the pulsatile blood flow is modelled by taking into consideration the blood volume change in each compartment.

Local regulation includes autoregulation of cerebral blood flow and global regulation of the chemoreflex are also included in the new model. The interaction between the chemoreflex and the baroreflex model is modelled based on the most recent published findings. The operating point of the baroreflex is reset by the stimulation of the peripheral chemoreflex while the gain of the sympathetic nerve activity is assumed to be reset by the central chemoreceptor.

Chapter 7 Validation of the cardiopulmonary model

7.1 Introduction

This chapter describes the validation of the model described in Chapter 6 by testing the interaction between the respiratory and the cardiovascular systems. The interactions between the two systems include the gas exchange process, the effect of breathing on the cardiovascular system and the blood gas contents on the hemodynamics as well as the chemoreflex and baroreceptor reflex.

In the cardiopulmonary model (Figure 7-1), the gases pass through the nose and mouth to the tracheo-bronchial tree model and the lung model where the gas exchange takes place. The brain detects the lung volume change and sends the required thoracic force to the pleural compartment. The pleural compartment then calculates the pleural pressure acting on the lung to stimulate the breathing. The gases are carried by the blood from the lung to other cardiovascular compartments. The left and right heart models, which have pressure and volume coupling between the two chambers, pump the blood through the whole body.

The interaction between the chemoreflex and the baroreflex models are shown diagrammatically in Figure 7-2. The peripheral chemoreceptor detects the change of P_{O2} and P_{CO2} in the brain artery and calculates the operating point for the baroreceptor model. The central chemoreceptor is sensitive to the brain arterial P_{CO2} and when it is stimulated, the gain of the sympathetic outflow is increased accordingly. The parasympathetic outflow and sympathetic outflow are sent to the effector sites which control the hemodynamic parameters including heart rate, cardiac contractility, venous unstressed volume and peripheral resistance.

In this chapter, parameters for the respiratory model and the chemoreceptor models are assigned. Then the model is used to simulate continuous breathing without the autonomic control to show how the systems interact at rest. The chemoreceptor models are then stimulated by hypoxia and hypercapnia and validated using the results from the most recent published data.

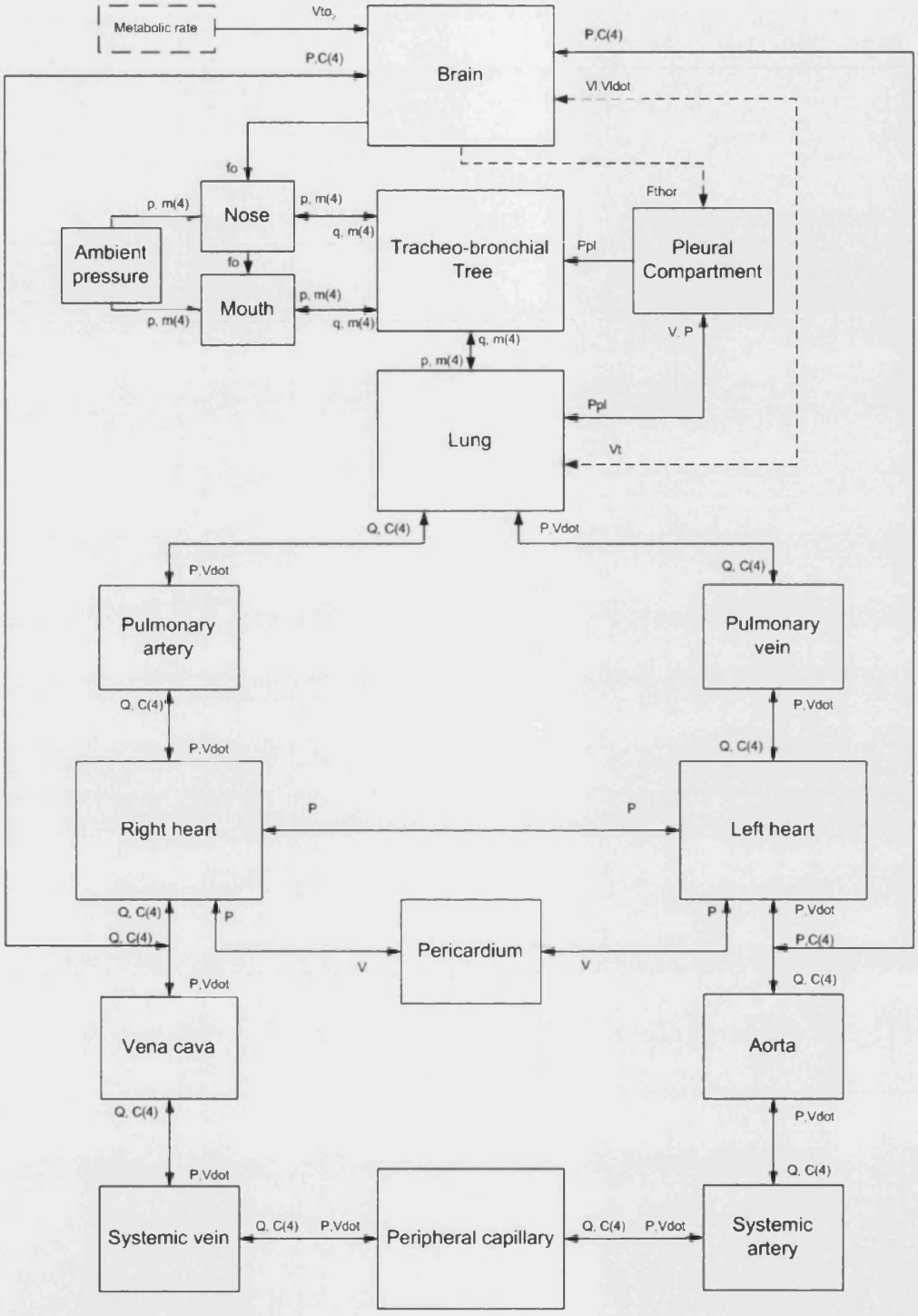

Figure 7-1 Simulation of human cardiopulmonary system block diagram (- -: signal; —: hydraulic or pneumatic pipes)

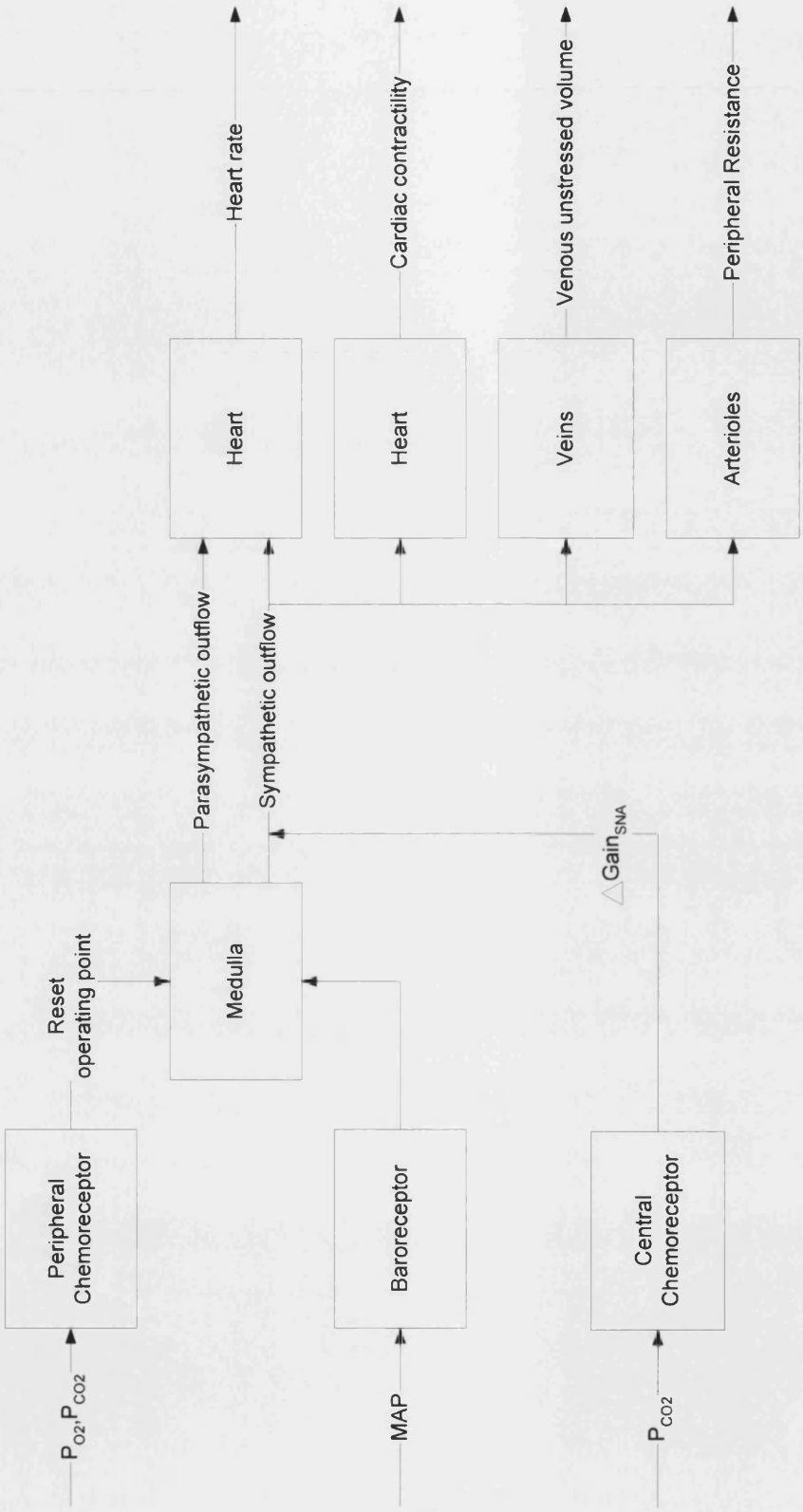

Figure 7-2 Simulation of human baroreflex and chemoreflex control system block diagram

7.2 Parameter identification

Table 7-1 shows the parameter values used in the respiratory and chemoreceptor models. The values for the respiratory model are taken from Lo (1995), the peripheral chemoreceptor values are from Rothe et al. (1990) and the central chemoreceptor values are from Lioy and Trzebski (1984).

Table 7-1 Parameters of the respiratory model and the chemoreceptor models

Variables	Value	Unit	Variables	Value	Unit
lung			**brain**		
residual volume	1.2	L	brain blood flow conductance	5.7	(L/min)/ bar
total lung capacity	6	L	brain oxygen consumption rate	0.05	L/min
functional residual capacity	2.4	L	brain respiratory quotient	0.8	
effective moving mass of lung	0.5	kg	total brain blood capillary volume	0.9	L
lung constant effective surface area	0.125	m^2	cardiac output time constant	6	seconds
lung minimum effective surface area	0.105	m^2	brain blood flow time constant	6	seconds
lung elastance when lung at un-stretched region	5	cm water/L	ratio between brain blood flow and cardiac output	0.15	
lung volume when lung stretched	5.5	L	inspiratory time chemical controller gain	0.062	
maximum lung elastance	10	cm water/L	expiratory time chemical controller gain	0.4	
viscous friction coefficient	500	N/(m/s)	thoracic force integral gain for inspiration	335	
polytropic index	1		thoracic force proportional gain for inspiration	6.7	
intra-pulmonary airway resistance	0.001	cm water/(L/s)	thoracic force integral gain for expiration	335	
fractional flow rate from right to left shunt	0.02		thoracic force proportional gain for expiration	50	
solubility coefficient of N2 in blood	0.013	L/(L blood atm)	time constant factor of demand lung profile	0.15	
solubility coefficient of He in blood	0.003	L/(L blood atm)	thoracic force derivative term gain	10^5	
saturated oxygen capacity in blood	0.2	L/L blood	minimum thoracic force	-700	N
saturated carbon dioxide capacity in blood	1	L/L blood	maximum thoracic force	700	N
nose			**mouth**		
equivalent diameter of nostril	22.5	mm	effective diameter of mouth	22.5	mm
width of linear flow region	0.0001	bar	width of linear flow region	10^{-4}	bar

.....continue

.....continue

Variables	Value	Unit	Variables	Value	Unit
trachea					
nominal radius of airway without traction	0.0001	m	number of tracheobronchial airway	16400	
addition airway radius with airway traction	0.0002	m	width of linear flow region	0.0001	bar
trachea wall stiffness	7000	N/m	closing lung volume	0.9	L
length of moving tracheobronchial wall	0.001	m	total lung capacity	6	L
minimum radius of extra-pulmonary airway	0	m	nominal radius of airway without traction	0.0001	m
maximum radius of extra-pulmonary airway	0.0003	m	addition airway radius with airway traction	0.0002	m
total volume of intra-thoracic zone	686		trachea wall stiffness	7000	N/m
total volume of extra-thoracic zone	0.052	L	length of moving tracheobronchial wall	0.001	m
	0.123	L	minimum radius of extra-pulmonary airway	0	m
peripheral chemoreceptor			**central chemoreceptor**		
peripheral chemoreceptor constant k1	-13.8		central chemoreceptor constant k4	1	
peripheral chemoreceptor constant k2	0.182		central chemoreceptor constant k5	-18.118	
peripheral chemoreceptor constant k3	828				

7.3 *Simulation results obtained using the cardiopulmonary model*

7.3.1 Continuous breathing test

Firstly the simulation results without the autonomic control from the brain are considered. This condition simulates a human at rest with quiet breathing and in the supine position. The heart rate is set to be 70 beats/min and the respiratory frequency to be 12 breaths/min.

Table 7-2 compares the model generated results to the published data. This shows that the values predicted by the model are close to the published data. Figure 7-3 shows the lung volume variation generated by the model and the partial pressures of CO_2 and O_2 in the alveolar, pulmonary vein and artery are shown in Figure 7-4 and Figure 7-5 respectively. The variation of the partial pressure with time also reflects a more realistic dynamic gas exchange process than the static process used by other researchers (Ben-Tal 2006;Liu et al. 1998;Lo 1995;Lu et al. 2001;Tilley et al. 2006;Tomlinson et al.

1994a). The partial pressure of the gases are in equilibrium at the end of pulmonary capillaries, where the partial pressure of O_2 in the alveolar compartment is slightly higher than that in the pulmonary vein due to the 2% pulmonary shunt for a healthy person at rest.

Table 7-2 Respiratory parameters generated by the model compared to the published data

	Tidal volume (L)	end tidal alveolar		Pulmonary artery		Pulmonary vein	
		P_{O2} (mmHg)	P_{CO2} (mmHg)	P_{O2} (mmHg)	P_{CO2} (mmHg)	P_{O2} (mmHg)	P_{CO2} (mmHg)
Published data (Berne & Levy 1988) and (Vander et al. 2001).	0.5	105	40	40	46	100	40
Modelled	0.495	108	40.9	42	45.5	102	40.9

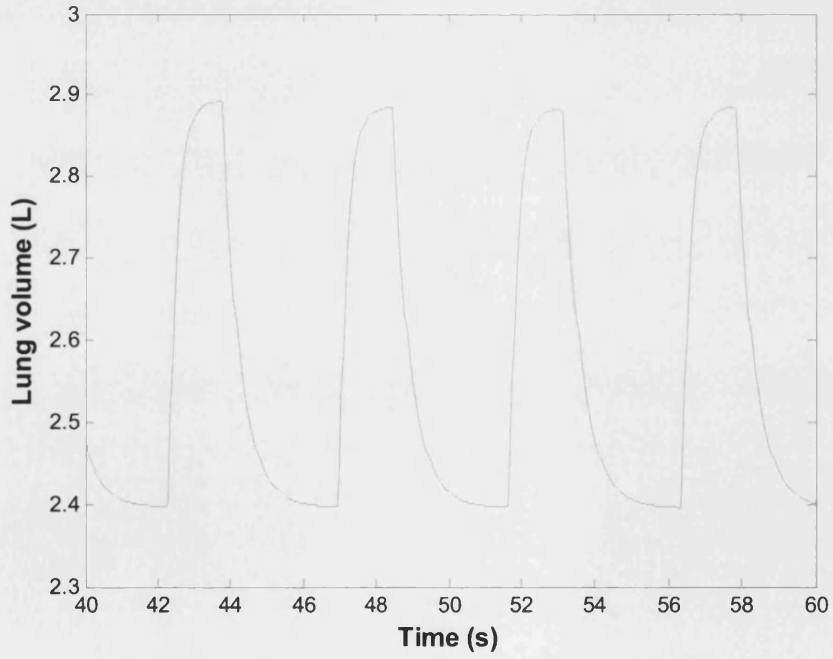

Figure 7-3 Lung volume at rest generated by the model

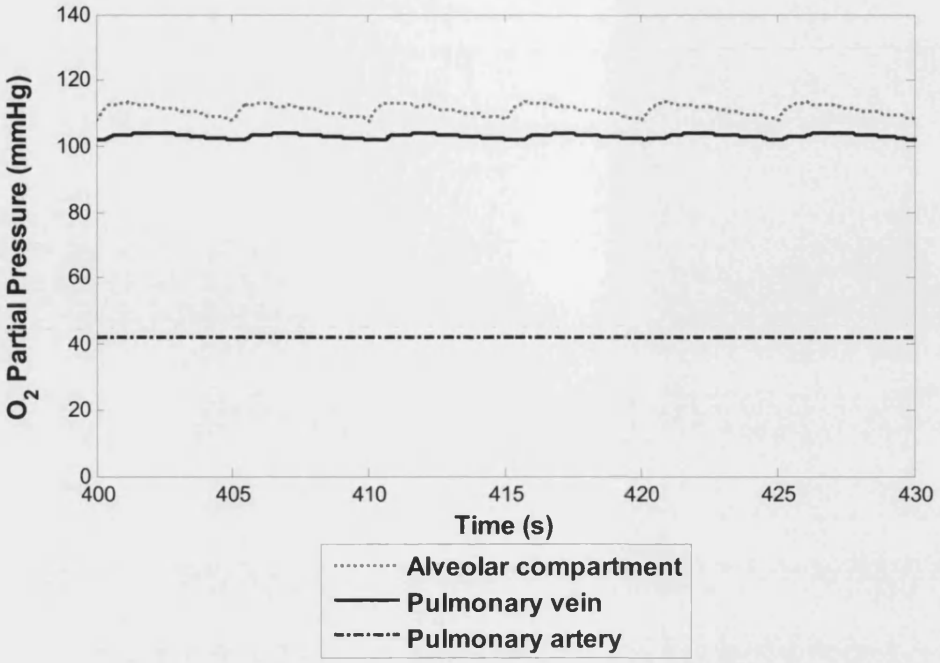

Figure 7-4 O_2 partial pressure of Alveolar compartment, Pulmonary vein and artery

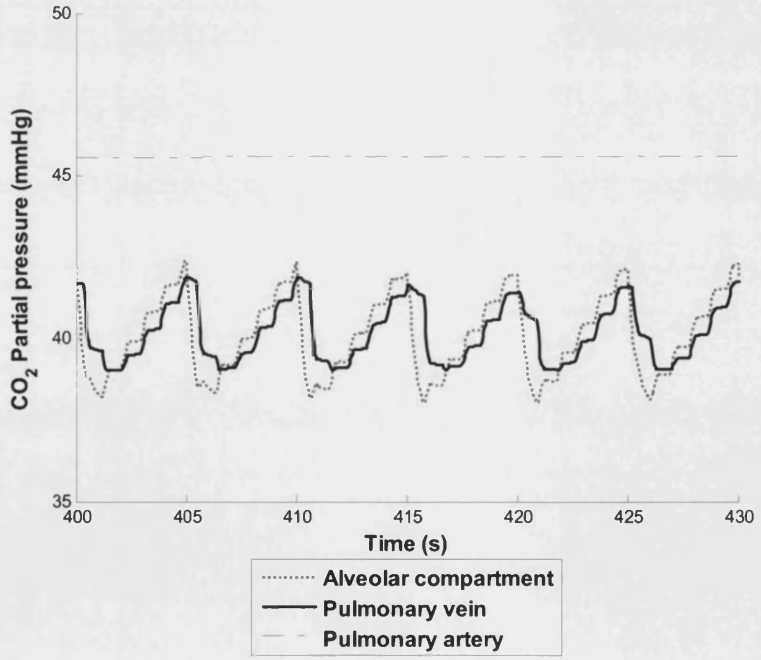

Figure 7-5 CO_2 partial pressure of Alveolar compartment, Pulmonary vein and artery

The diffusion rates of O_2 and CO_2 are shown in Figure 7-6 and Figure 7-7 respectively. As the gas exchange is a continuous process, the diffusion rate is calculated at every integration time step. Besides the rhythm of breathing, a secondary variation is also superimposed due to the variation in the blood flow. When the O_2 concentration in the pulmonary arterial blood decreases with blood flow (Figure 7-6), the pressure gradient between the two sides of the alveolar membrane becomes larger (Figure 7-4) which leads to a higher diffusion rate. Likewise, when the O_2 concentration increases with blood flow, the diffusion rate decreases to almost zero due to the pressure gradient reaching equilibrium. The rhythm of the breathing reflects clearly on the CO_2 diffusion rate (Figure 7-7). In this case, the diffusion rate is lower when exhaling and higher when inhaling due to changes in the gas content in the alveolar. Figures 7-6 and 7-7 also compare the diffusion rate and the overall consumption rate of CO_2 and O_2. The mean levels of the O_2 and CO_2 diffusion rates are the same as the overall consumption rate.

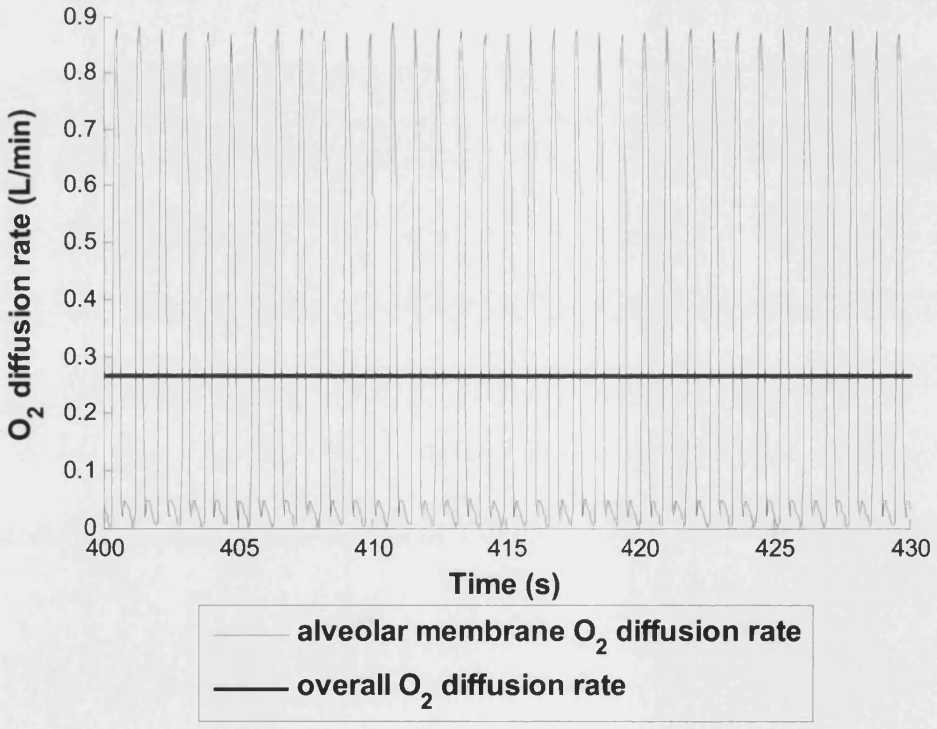

Figure 7-6 O_2 diffusion rate of alveolar membrane and overall O_2 consumption rate

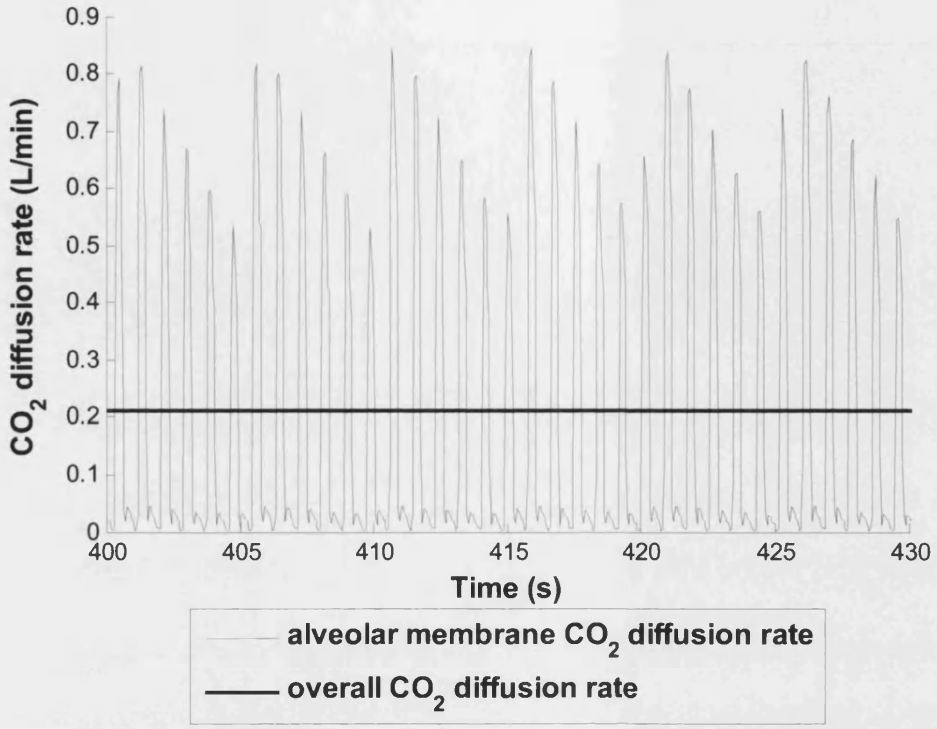

Figure 7-7 CO_2 diffusion rate of alveolar membrane and overall CO_2 consumption rate

The effect of intrathoracic pressure on arterial pressure was demonstrated in Chapter 3. Here, the effect of breathing on heart rate is simulated including the chemoreceptor and baroreceptor reflexes. Figure 7-8 shows sample records of the heart rate and tidal volume for a healthy human during quiet breathing (Hirsch & Bishop 1981). The heart rate increases during inhalation and decreases during exhalation with a certain time delay compared to the respiration. This phenomenon is known as respiratory sinus arrhythmia. The subjects used for the experiments by Hirsch et al.(Hirsch & Bishop 1981) had changes in heart rate ranging from 19.35 to 39.6 beats/min when the tidal volume was 1.5 L, due largely to the age and fitness of the subjects. The heart rate predicted by the model (Figure 7-9) shows similar behaviour to the experimental results (Figure 7-8), although the heart rate only varies by 12 beats/min for the same tidal volume.

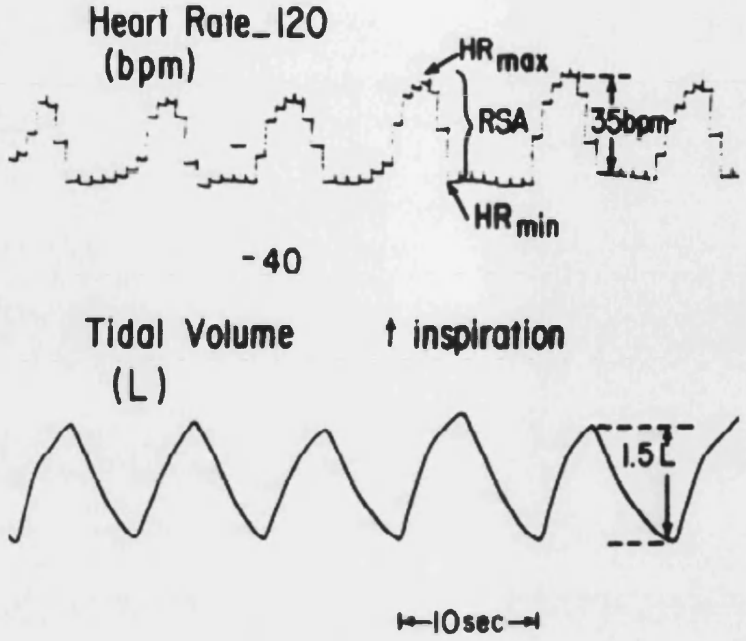

Figure 7-8 Records of heart rate (bpm: beats/min) and tidal volume (L) (Hirsch & Bishop 1981)

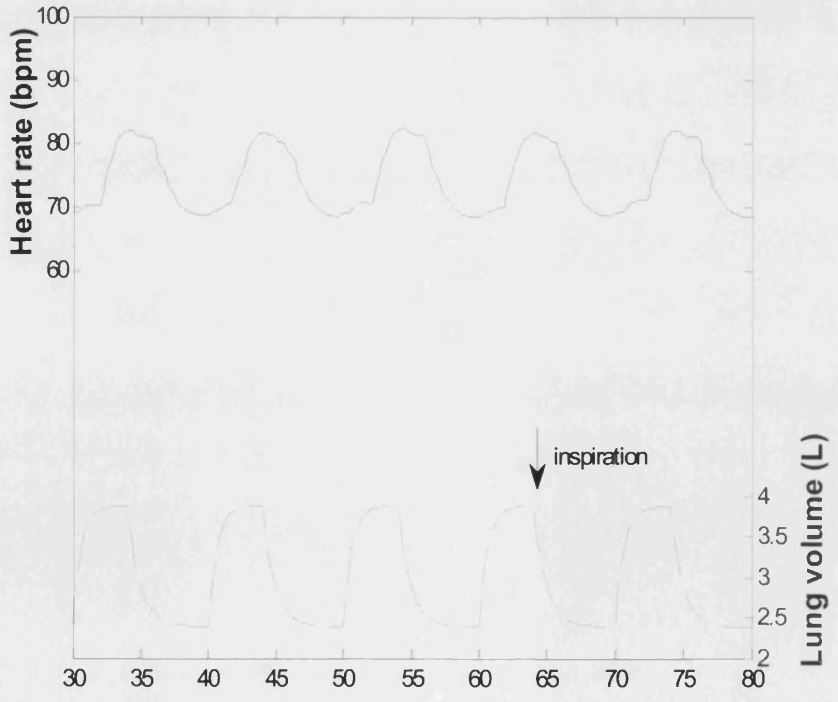

Figure 7-9 Model generated heart rate and lung volume; bpm: beats/min

7.3.2 Resetting of the baroreflex by the peripheral chemoreceptor

The reported central antagonistic interaction between the peripheral chemoreflex and arterial baroreflex was tested by activating the chemoreceptor and baroreceptor in the model. In order to isolate the effect of the lung stretch receptors on the cardiac responses, the breathing frequency and tidal volume were set to 12 breaths/min and 0.5 L throughout the simulation.

The first test was to determine the effect of resetting the baroreflex operating point by hypoxia. A step input in pressure from 40 to 160 mmHg was fed back to the baroreflex control loop to represent the controlled carotid sinus pressure in the experiment reported by Cooper et al.(2005). A hypoxic gas mixture of 12% O_2 and 88% N_2 was used as the inspired gas to stimulate the chemoreceptor.

Figure 7-10 shows the baroreflex resetting due to the chemoreceptor stimulation. The cardiac sigmoid curve during hypoxia shifts rightwards and slightly upwards. However, the change in the sensitivity and the operating point of the baroreflex were not significant, which is consistent with the observations from experiments (Cooper et al. 2005;Halliwill et al. 2003). The hypoxia caused the heart rate to increase by 21.0 beats/min compared with 20.9 to 24.4 beats/min obtained from actual experiments (Halliwill et al. 2003).

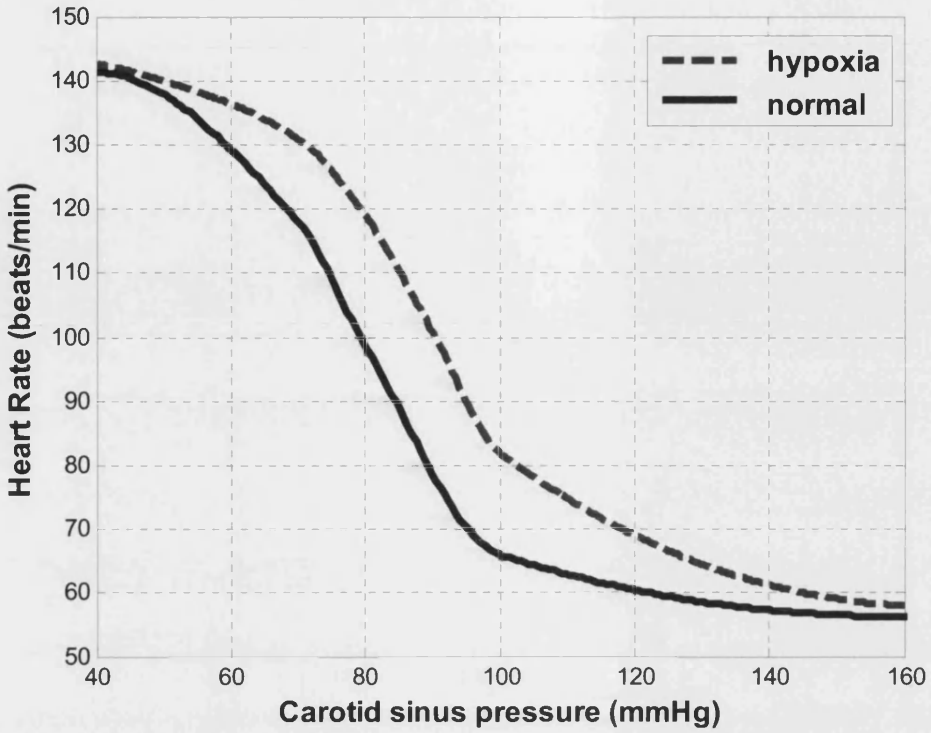

Figure 7-10 Baroreflex resetting due to the stimulation of peripheral chemoreceptor

7.3.3 The interaction between the baroreceptor and the chemoreceptor during hypoxia

The second test was undertaken to determine the antagonistic interaction between the baroreceptor and the chemoreceptor. The same hypoxic gas mixture (12% O_2, 88% N_2) was used to stimulate the chemoreceptor. The changes in the alveolar partial pressure of CO_2 and O_2 following the step input of the inspired gas mixture introduced at 100 seconds are shown in Figure 7-11.

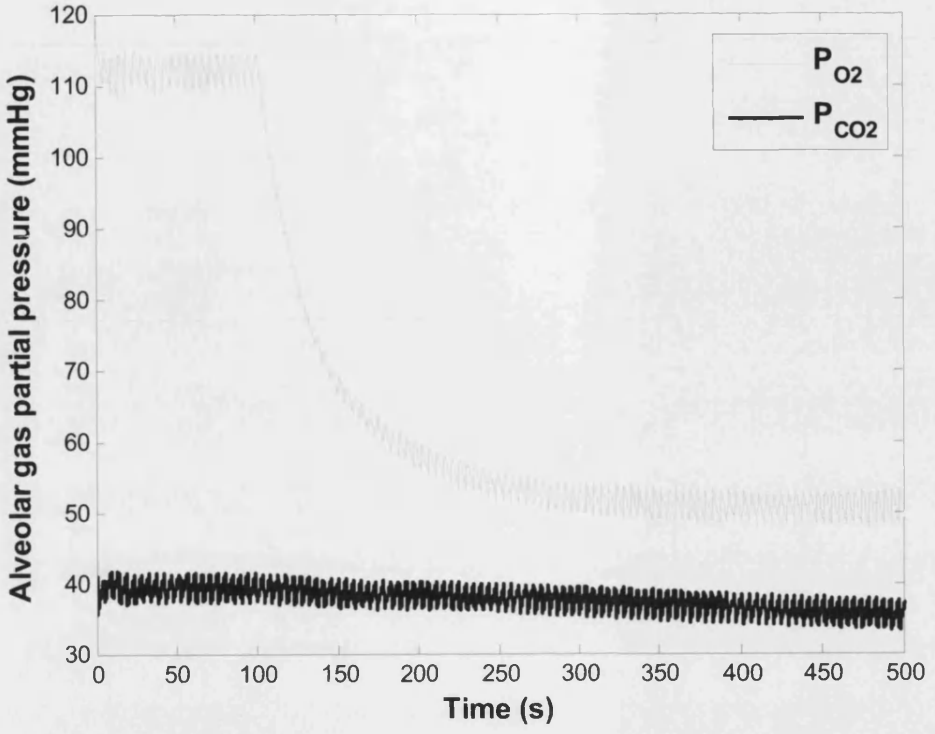

Figure 7-11 Alveolar P_{o2} and P_{co2} responses to hypoxia

During the denervation of the baroreceptor, the parasympathetic nerve outflow decreases and the sympathetic nerve outflow increases (Figure 7-12). This is inline with the expected result discussed in Chapter 6. The increased heart rate shown in Figure 7-13 is due to the predominance of the cardiac sympathetic over the cardiac vagal activation.

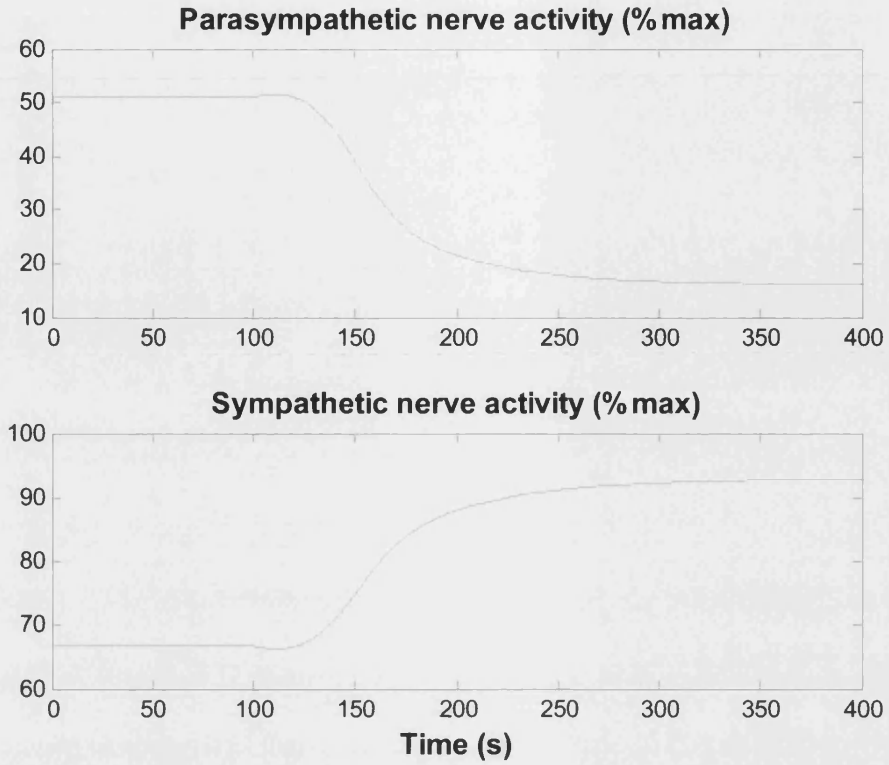

Figure 7-12 Response of efferent nerve activity responses to hypoxia when denervated baroreceptor

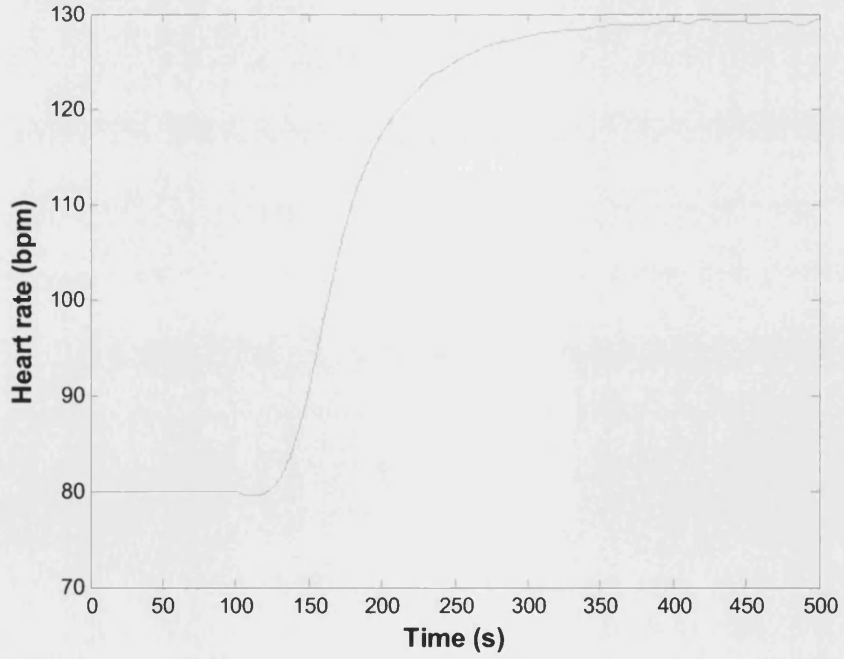

Figure 7-13 Response of heart rate responses to hypoxia when denervated baroreceptor

When the baroreceptor and the chemoreceptor both are innervated, the activation of the chemoreceptors inhibits baroreflex which leads to an increase of blood pressure (Figure 7-14). The activation of the baroreflex by the increased blood pressure blunts the change of the sympathetic outflow and parasympathetic outflow (Figure 7-15). Therefore the changes of the two autonomic division outflows are less than that of the denervation of the baroreceptor.

The cardiac responses agree with the observations obtained from experimentation (Dalymde et al. 1965;Karim et al. 1980). The Cardiac contractility (Figure 7-17) and heart rate (Figure 7-16) increased while the venous unstressed volume decreased (Figure 7-18). The total peripheral resistance basically remains unchanged (Figure 7-19). Figure 7-20 shows a quantitative comparison between the steady-state percentage change in heart rate, mean arterial pressure and total peripheral resistance with the experimental results by Cooper et al (2005) in humans during hypoxia. The agreement between the model and the experimental results is considered to be good although the changes obtained from the model are slightly higher than those obtained from experiment. The results presented in Figure 7-20 show that the model is capable of simulating the resetting of the baroreflex by activating the chemoreceptor and the dynamic interaction of the baroreceptor and chemoreceptor reflexes.

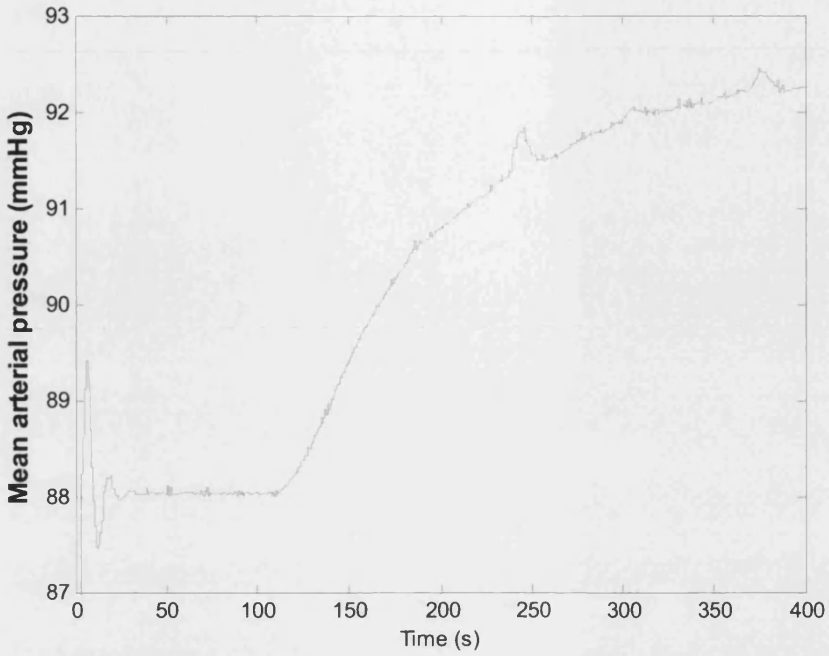

Figure 7-14 Response of mean arterial pressure responses to hypoxia when stimulating baroreceptor and chemoreceptor

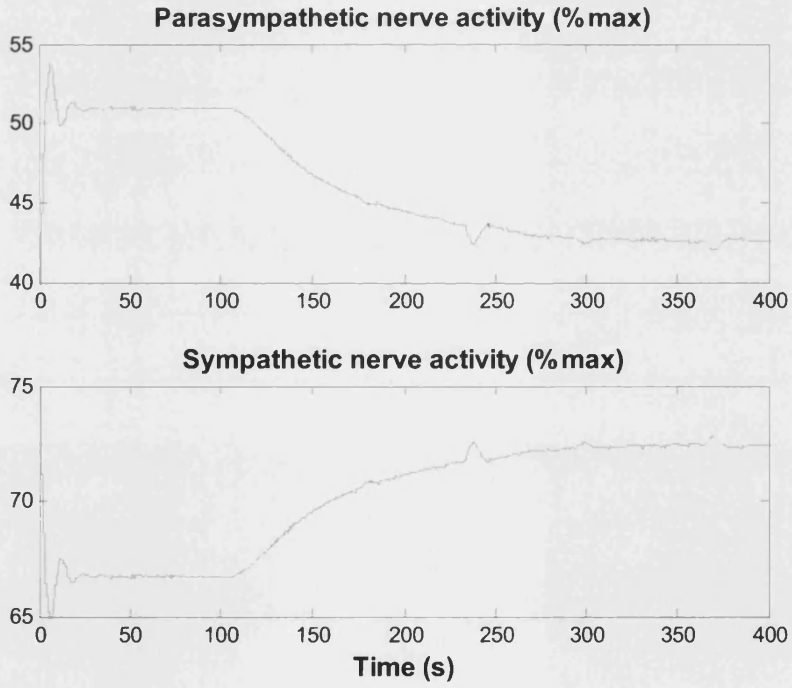

Figure 7-15 Response of nerve activity responses to hypoxia when stimulating baroreceptor and chemoreceptor

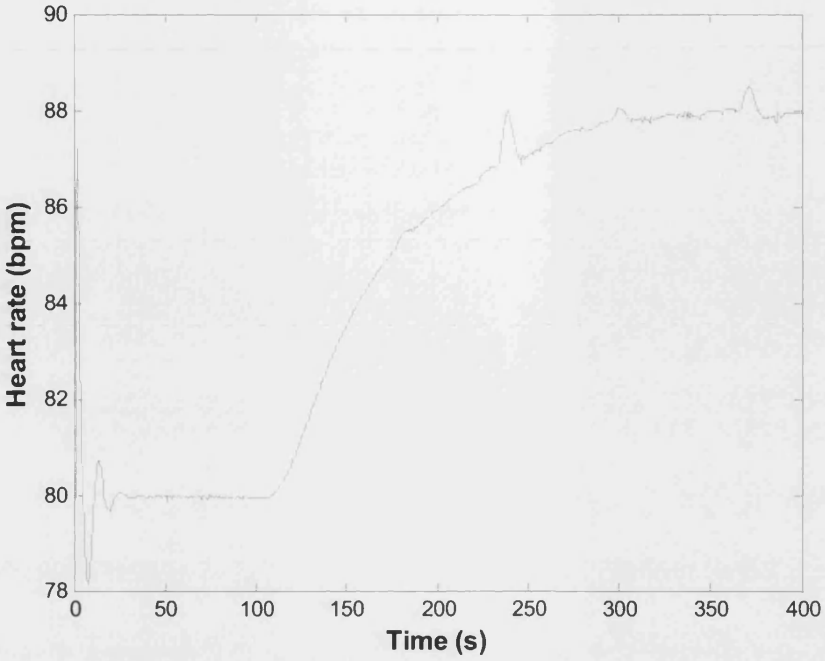

Figure 7-16 Response of heart rate responses to hypoxia when stimulating baroreceptor and chemoreceptor

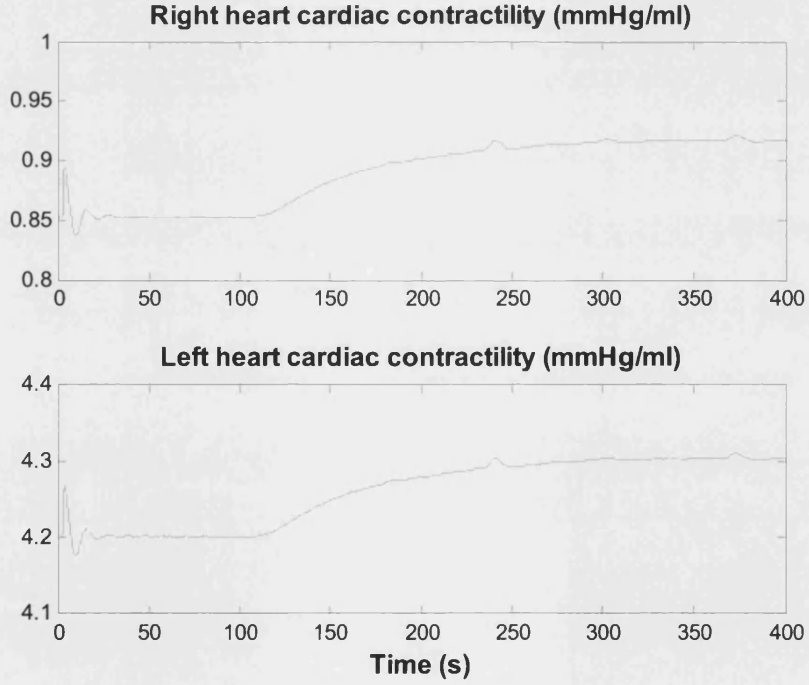

Figure 7-17 Response of cardiac contractility responses to hypoxia when stimulating baroreceptor and chemoreceptor

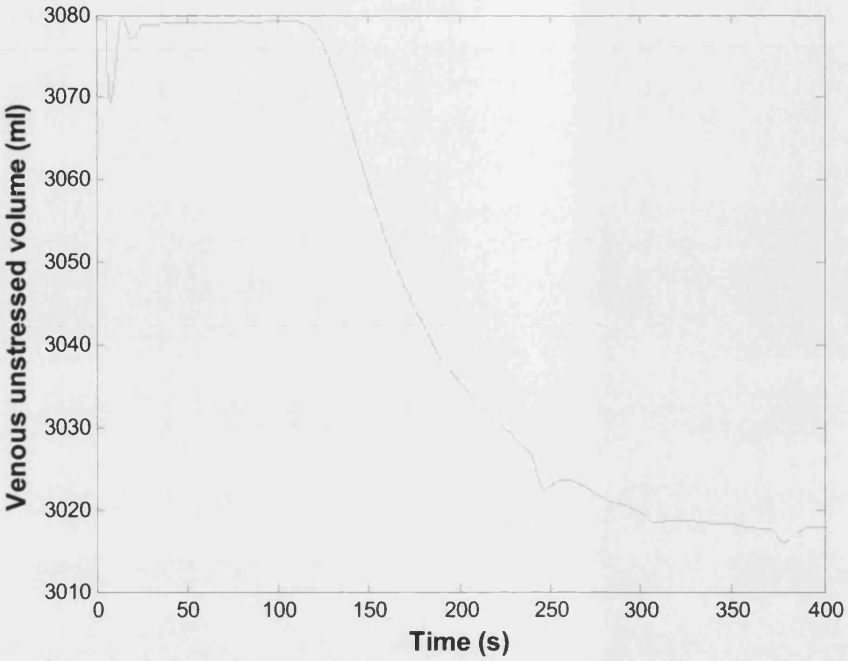

Figure 7-18 Response of venous unstressed volume responses to hypoxia when stimulating baroreceptor and chemoreceptor

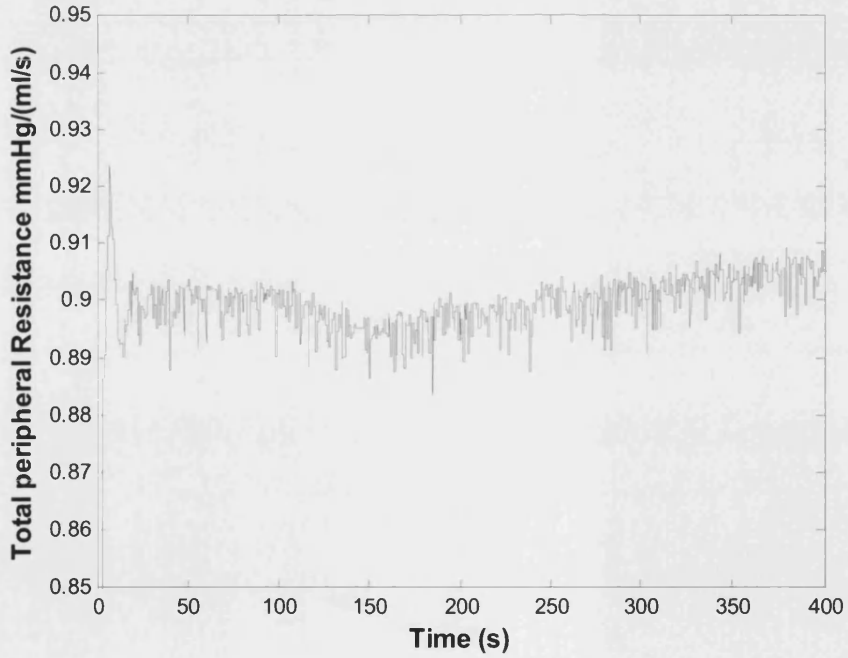

Figure 7-19 Response of total peripheral resistance responses to hypoxia when stimulating baroreceptor and chemoreceptor

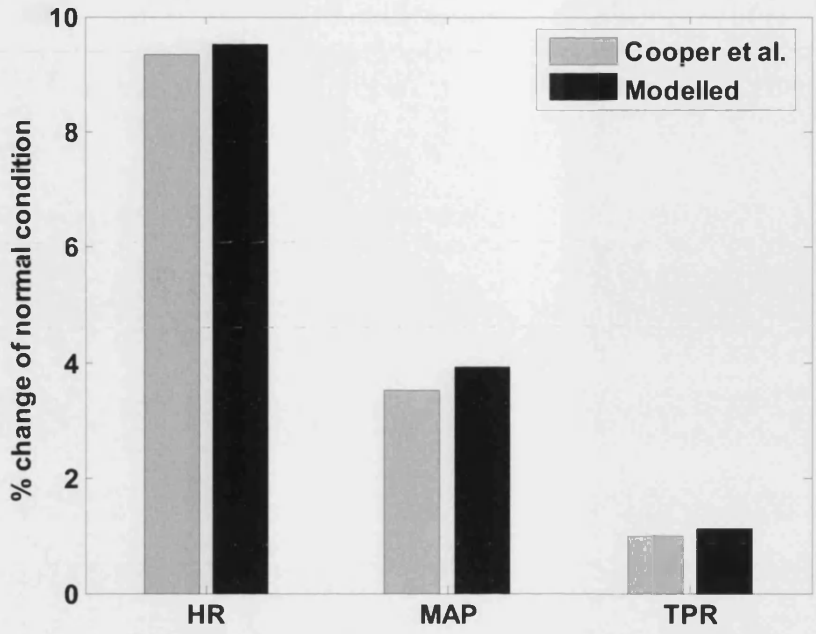

Figure 7-20 Normalized values of heart rate (HR), mean arterial pressure (MAP), total peripheral resistance (TPR) compared with experimental data (Cooper et al. 2005)

7.3.4 The interaction between the baroreceptor and the chemoreceptor during hypercapnia

The effects of hypercapnia were simulated by applying 5% CO2 and 95% O2 gas mixtures to the inspired gas when only the peripheral chemoreceptor was included in the model. The changes in heart rate, mean arterial pressure and total peripheral resistance obtained at this condition are compared with published data (Cooper et al. 2005) in Figure 7-21. It is clear that the model produces very different results to the experiment and the signs of the predicted changes are in the opposite direction to the measured data. However, when the central chemoreceptor is included, the model produces a much more satisfactory result (Figure 7-22) with the changes in the heart rate and the mean arterial pressure having similar values to the experimental data. Although the change in the predicted value for the total peripheral resistance is less than the average measured data, it should be noted that the measurements were subject to a $\pm$ 20% variation.

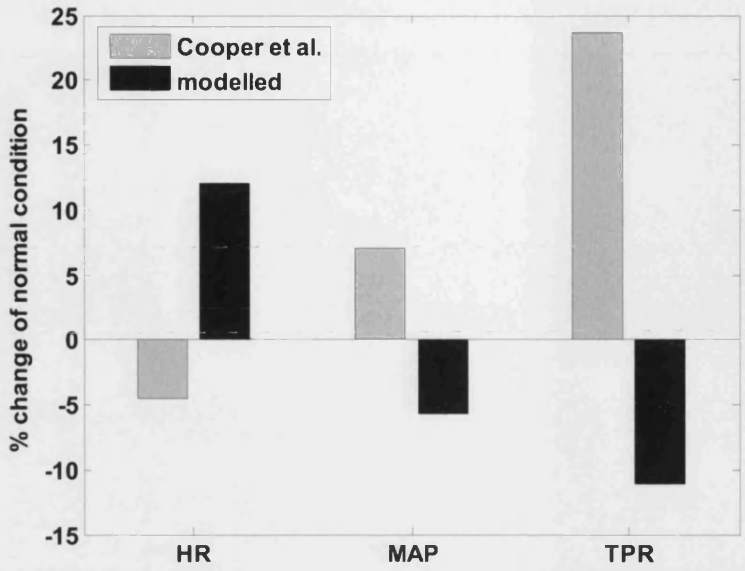

Figure 7-21 Model predicted heart rate (HR), mean arterial pressure (MAP), total peripheral resistance (TPR) compared with experimental data (Cooper et al. 2005) with denervated central chemoreceptor

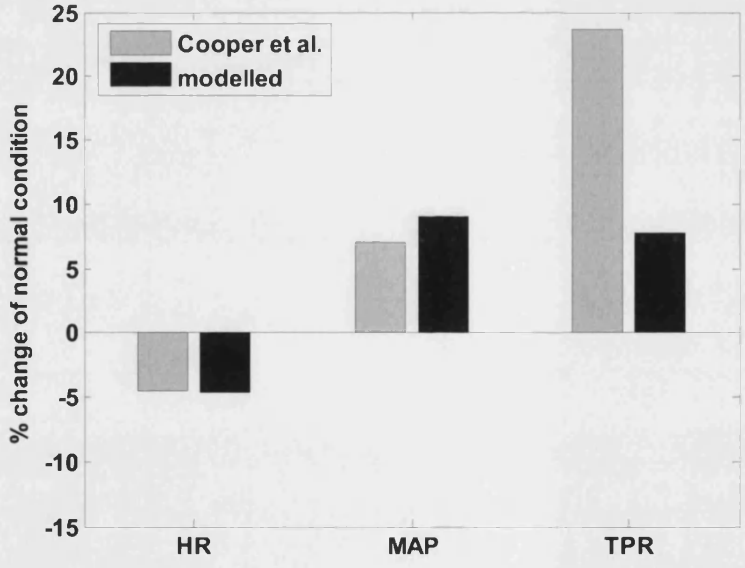

Figure 7-22 Model predicted heart rate (HR), mean arterial pressure (MAP), total peripheral resistance (TPR) compared with experimental data (Cooper et al. 2005) after innervated central chemoreceptor

7.4 Discussion

The cardiopulmonary model was developed by integrating the cardiovascular model with a respiratory model. For this reason, it was necessary to include the pulsatile blood flow generated in the cardiovascular model in the gas exchange process within the respiratory model. As the gas exchange process developed was represented as a continuous process, the variation of the gas partial pressures with time reflects the frequency of both breathing and blood flow.

The respiratory sinus arrhythmia was modelled by including both the chemoreceptor and baroreceptor reflexes. The heart rate variability due to the respiration predicted by the model shows a similar variation to the experimental data. The change in heart rate within each respiratory cycle occurs mainly as a result of the fluctuation of parasympathetic output to the heart. The action of the sympathetic outflow is suppressed in the model by the inclusion of a first order filter having a high time constant fitted to clinical data. The change in the predicted heart rate is not as significant as the experimental value due to the absence of lung stretch receptors in the current model.

The resetting of the baroreceptor by the peripheral chemoreceptor was investigated. Various pressures were fed into the baroreflex model stepwise to stimulate the baroreceptor while the peripheral chemoreceptor was stimulated by hypoxia. The operating point of the baroreflex due to the stimulation of the peripheral chemoreceptor shifts rightwards and upwards slightly. The shifting is consistent with the observations from Halliwill et al. (2003). Further hypoxia tests links the mean arterial pressure of the cardiovascular model to the baroreceptor model and shows that the model can predict the expected change in the cardiac responses. Firstly the mean arterial pressure increases because the peripheral chemoreceptor model shifts the operating point upwards. The increase of the mean arterial pressure activates the baroreceptor which leads to the increase of heart rate and cardiac contractility and the venous constriction. The change of the total peripheral resistance is not significant mainly because of the compensation of the local autoregulation of the brain.

The model for the central chemoreceptor is based on the assumption made by Simmons et al. (2007) that the central chemoreceptor alters the gain of the sympathetic nerve

activity and there is no influence on the parasympathetic nerve activity. A simulation is first performed by disconnecting the central chemoreceptor model and activating the peripheral chemoreceptor model by hypercapnia. The model produces rather different results to the experiments performed by Cooper et al. (2005). By including the central chemoreceptor model, the results improved significantly (Figure 7-22). The mean arterial pressure and the total peripheral resistance increase due to the increased sympathetic nerve activity via the central chemoreceptor. The decrease in the heart rate is mainly due to the increased parasympathetic nerve activity via the arterial baroreceptors in response to the rise in arterial pressure. The results produced here justify the assumption that the central chemoreceptor has an effect on the gain of the sympathetic nerve activity.

The baroreceptor and chemoreceptor models also show that the inclusion of the nonlinearity in the efferent compartment has the advantage that the interaction between the baroreceptor and other receptors can be developed. This was demonstrated by resetting the baroreceptor.

7.5 Closure

The cardiopulmonary model has been validated using a number of different test conditions. The interactions of the respiratory and cardiovascular systems including the gas exchange process, the effect of breathing on cardiovascular system and the blood gas contents on the hemodynamics are simulated and compared to publish data. The results produced by the model are in good agreement with experimental results obtained for humans.

The model is used to simulate the dynamic gas exchange process across the alveolar and the effect of the respiratory sinus arrhythmia. The effects of respiration on the blood flow and the gas exchange are clearly shown in the gas partial pressure waveforms and the heart rate variations. The model also shows the resetting of the baroreceptor operating point by the peripheral chemoreceptor model and the central chemoreceptor effects on the sympathetic outflow. The simulation of hypoxia and hypercapnia show

that the baroreceptor and chemoreceptor reflexes are capable of predicting similar cardiac responses found in the published data.

The cardiopulmonary model includes the detailed features of the cardiovascular and respiratory systems and a new control mechanism. With the model validated, the model can be used to predict human cardiac and respiratory responses under different conditions including cardiopulmonary disease and exercise.

Chapter 8 Applications of the cardiopulmonary model

8.1 Introduction

The model developed for the cardiopulmonary system is based on comprehensive cardiovascular and respiratory models and a new advanced control algorithm. The model can be used to predict human cardiac and respiratory responses under different physiological conditions. In this chapter, some possible applications of the model are demonstrated by predicting the cardiopulmonary responses of patients with lung and cardiovascular disease, together with those of healthy subjects during exercise.

8.2 Lung disease

Diffusion impairment is a common cause for lung disease such as chronic obstructive pulmonary disease. Diffusion impairment results from thickening of the alveolar membranes or a decrease in their surface area (Vander et al. 2001). It causes failure of equilibration of blood P_{O2} with alveolar P_{O2}, although the effect on CO_2 does not always exist because CO_2 tends to diffuse readily. P_{CO2} might be reduced if it is hypoxemia (inadequate oxygen in the blood) as this stimulates ventilation.

The mathematical description of the diffusion impairment is described by including fractional lung damage in the gas exchange process as following:

$$P_{puc,O2} = (1 - D_m) \cdot P_{alv,O2} \tag{8-1}$$

$$P_{puc,CO2} = (1 - D_m) \cdot P_{alv,CO2} \tag{8-2}$$

The fractional lung damage D_m can be regarded as the fraction of alveoli that are damaged in a diseased lung. The pulmonary capillary diffusion impairment can be modelled by altering the value of D_m and D_m is set to be 0.25 to model a mild lung disease. Figure 8-1 shows the partial pressure of O_2 difference across the lung membranes. Because the diffusion capacity of the lung decreases, the amount of gas that diffuses across the alveoli decreases leading to a decrease in the gas partial pressure in the blood. For example, for the healthy lung result shown previously in Figure 7-4, both

pressures were above 100 mmHg compared to a maximum level of around 76 mmHg for the diseased lung. The partial pressure of CO_2 does not decrease as much as O_2 because the CO_2 diffuses more quickly than O_2 (Figure 8-2). The $\dot{V}/Q$ ratio decreases from 1 for a normal lung to 0.875 for a disease lung (Figure 8-3).

Tilley et al. (2006) modelled patients with acute lung disease in an intensive care unit using a multi-compartment lung model. The diffusion impairment was modelled by localized variations in the $\dot{V}/Q$ ratio. This method uses more realistic findings obtained from a diseased lung which has different local $\dot{V}/Q$ ratios in the lung. On the other hand, the method for a single compartment lung model presented in this research represents the effect of the disease by the thickening of the capillary surface. Thus this single compartment lung model is capable of modelling a diseased lung. Compared to Tilley's method, this method is more accessible because it does not require a $\dot{V}/Q$ ratio lookup table derived from experiments. However, the method inevitably can only simulate the average value of $\dot{V}/Q$ ratio of the lung due to its single compartment nature.

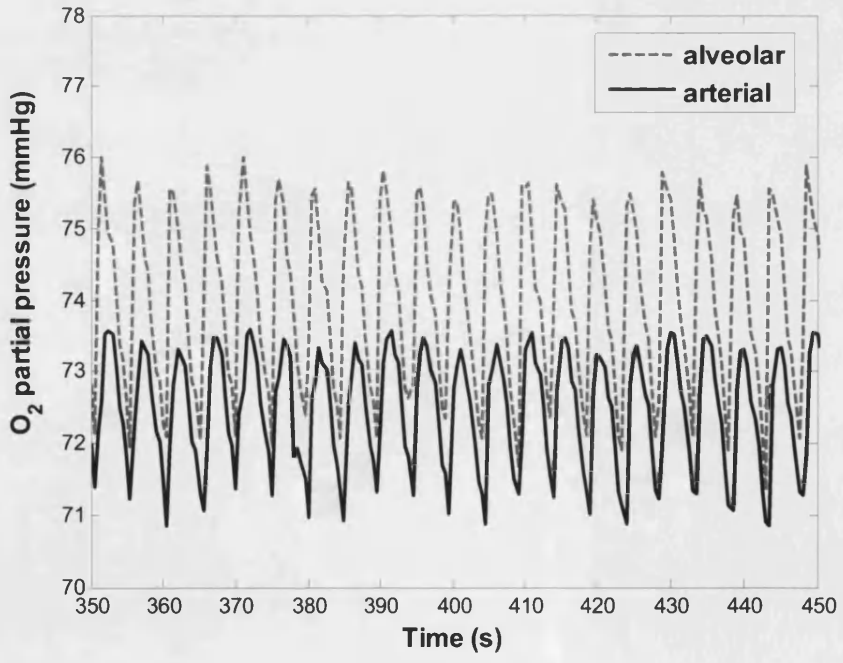

Figure 8-1 Model generated alveolar and arterial P_{O2}

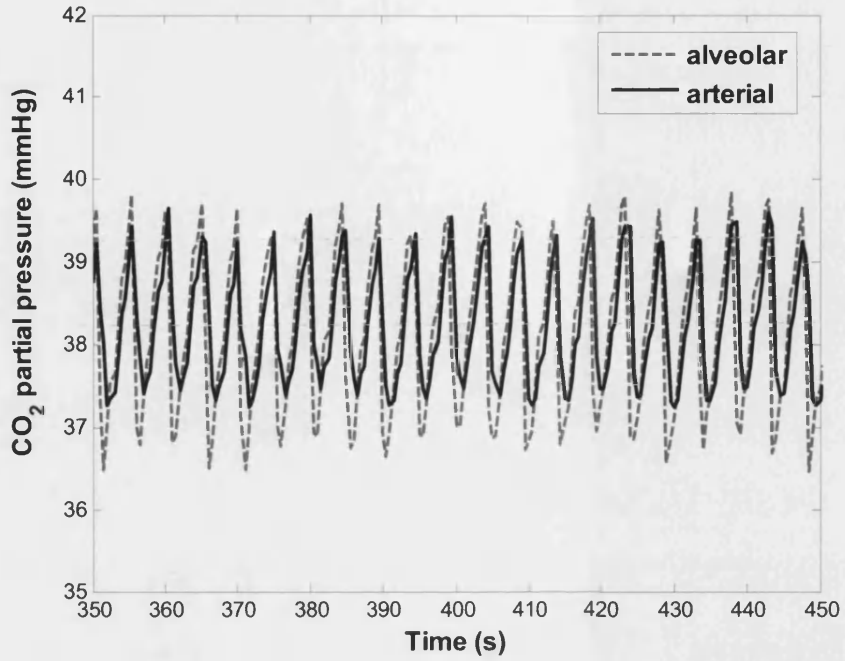

Figure 8-2 Model generated alveolar and arterial P_{CO2}

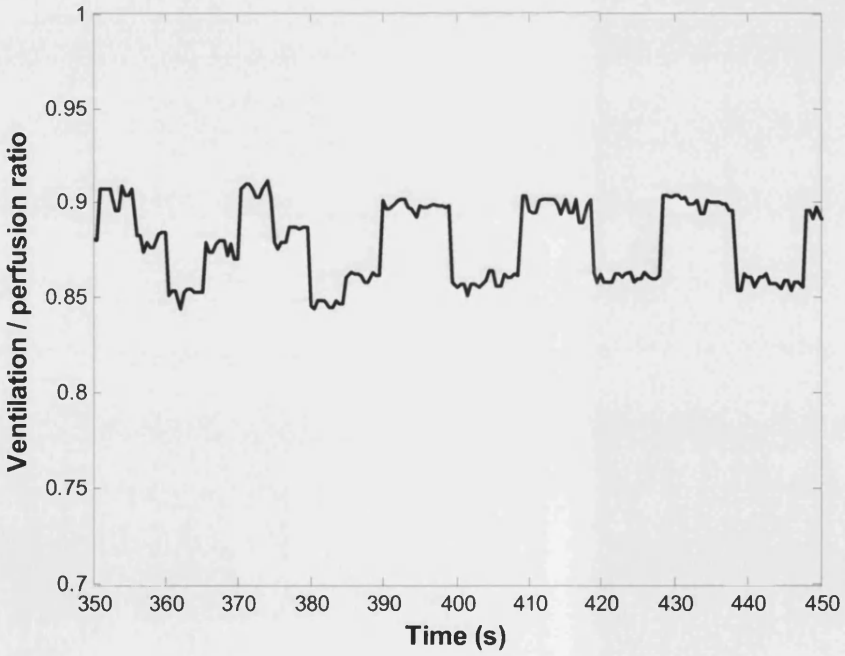

Figure 8-3 Model generated $\dot{V}$ / Q ratio

8.3 Mitral valve stenosis

Mitral stenosis is one of the most common disorders in valvular heart disease. Mitral stenosis is a narrowing or blockage of the opening of the mitral valve, which separates the atrium and the ventricle in the left heart. This prevents the correct amount of blood flowing between the chambers. Obstruction of the mitral orifice causes a left ventricular filling disturbance. In order to maintain the left ventricular filling volume, the left atrial pressure is elevated, which produces a left atrioventricular pressure gradient at end diastole. The elevated left atrial pressure in turn raises the pulmonary venous, capillary, and arterial pressures, resulting in pulmonary congestion and right heart failure. In normal subjects, a mitral orifice area is usually 4 to 6 cm^2 while patients with mitral valve stenosis have a mitral orifice area of less than 2 cm^2 (Sugawara et al. 1989). Therefore, mitral stenosis can be simulated by changing the mitral valve area A_{mv} in the model from 4 cm^2 for normal to 2 cm^2 for a mild mitral stenosis or to 1 cm^2 for a severe mitral stenosis.

Mitral flow in the case of mitral stenosis shows a distinctive feature as it is injected through a narrower orifice. Figure 8-4 shows the model generated mitral flow in a healthy person and patients with mitral stenosis compared to doppler recordings of transmitral flow from Tamai et al. (1990). In a healthy subject, the mitral flow rate shows a biphasic pattern. Immediately after opening of the mitral valve, the flow accelerates to achieve the first peak, and then decelerates to nearly zero during the rapid filling phase in early diastole. This is followed by another peak of the flow due to the atrial contraction, which is usually larger than the first peak. In the case of mitral stenosis, the initial increase in flow velocity is more rapid than in the healthy subject. From the maximal velocity, the flow decelerates more slowly and linearly toward the baseline, followed by a second increase due to the atrial contraction. This second rise in velocity sometimes achieves a higher peak than the first.

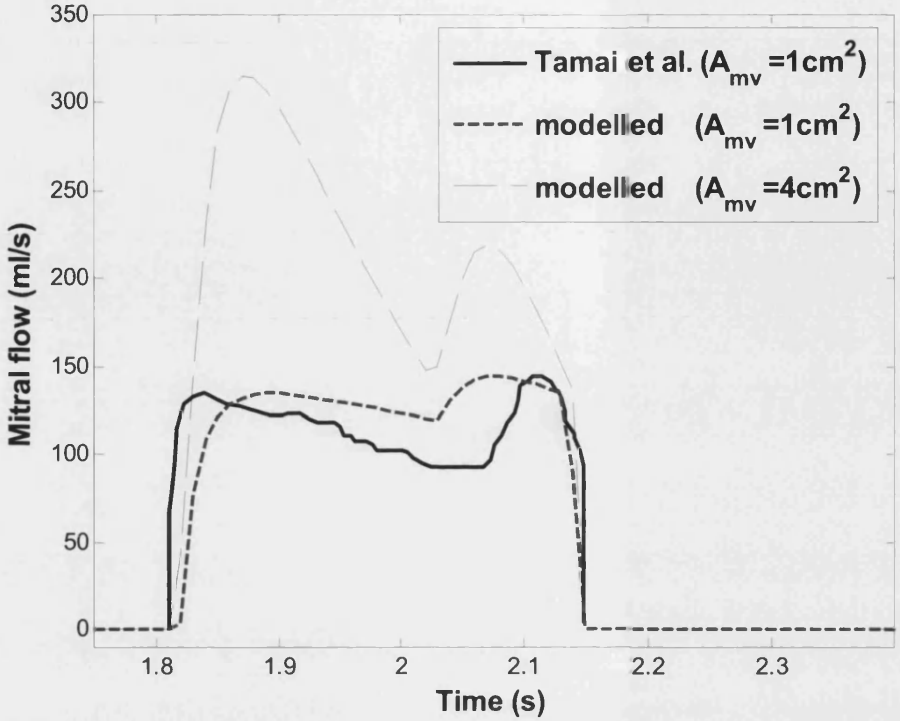

Figure 8-4 Model generated mitral flow in healthy person and patients with mitral stenosis compared to doppler recordings of transmitral flow from Tamai et al. (1990)

Figure 8-5 shows the oscillographic records from two conscious, instrumented dogs. Figure 8-6 shows the model generated pressure waveform for a mitral stenosis patient which shows similar trends to Figure 8-5. The pressure of the left atrium in the stenosis patients is higher and flatter compared to a normal person. Table 8-1 gives a comparison of the model generated respiratory and hemodynamic parameters in normal people and in patients with mitral stenosis. The loss of atrial contraction causes a decrease in cardiac output. The reduced cardiac output causes pulmonary venous congestion and fatigue leads to the main symptom of mitral stenosis dyspnea (difficulty in breathing). The higher pressure in the left atrium due to mitral stenosis is transmitted to the pulmonary veins and the pulmonary capillaries producing a resultant rise in pressure.

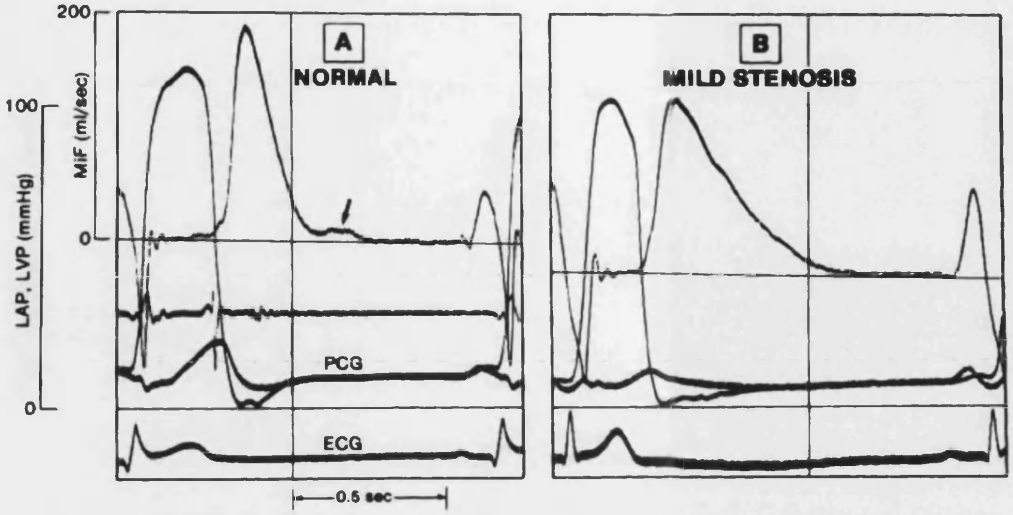

Figure 8-5 Oscillographic records from two conscious, instrumented dogs. The pressure-flow pattern in A is normal, whereas the pattern in B suggests a relatively mild mitral stenosis. MiF = mitral flow; LVP, LAP = left ventricular, left atrial pressure; PCG = intracardiac phonocardiogram; ECG = lead II electrocardiogram. (Keren et al. 1986)

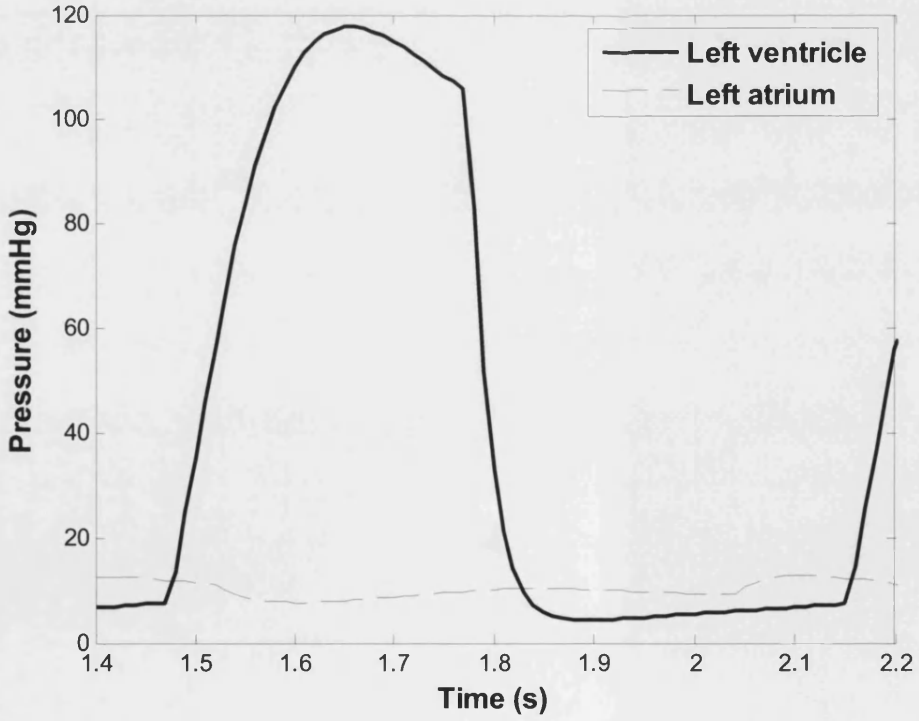

Figure 8-6 Model generated pressure of left ventricle and left atrium in patients with mitral stenosis

Table 8-1 Model generated respiratory and hemodynamic parameters for mild stenosis

	P_{puc} (mmHg)	P_{puv} (mmHg)	Cardiac Output (L/min)	Heart Rate (beats/min)	Ventilation Rate (L/min)
Normal	12.28	8.87	5.8	80.8	6.11
Mitral stenosis	16.5	12.4	5.57	84.8	6.31

8.4 Heart failure

Heart failure may be acute or chronic. Acute heart failure may be caused by toxic quantities of drugs and anaesthetics or by certain pathological conditions, such as coronary artery occlusion. Chronic heart failure may occur in conditions such as hypertension or ischemic heart disease. In these forms of heart failure, myocardial contractility is impaired.

Acute severe left heart failure was modelled by decreasing the left heart contractility by 50%. The change in contractility of any ventricles will alter the distribution of blood volume in the two vascular systems, pulmonary or systemic systems. Some of the systemic blood shifts to the pulmonary reservoir (Figure 8-7). During left ventricular failure, the left ventricle pumps a diminished flow. If the right ventricle is not affected, the right ventricle will continue to pump the normal flow to the pulmonary system. The inequality in the right and left ventricular outputs will result in a progressive increase in left atrial pressure and a progressive decrease in the right atrial pressure as Figure 8-8 shows. Therefore left ventricular output will increase toward the normal value and the right ventricular output will fall below the normal value. This process will continue until the outputs of two ventricles become equal to each other again. At this new equilibrium condition, the outputs of the two ventricles will be subnormal. The elevated left atrial pressure will be accompanied by an equally elevated pulmonary venous pressure, which can have serious clinical consequences.

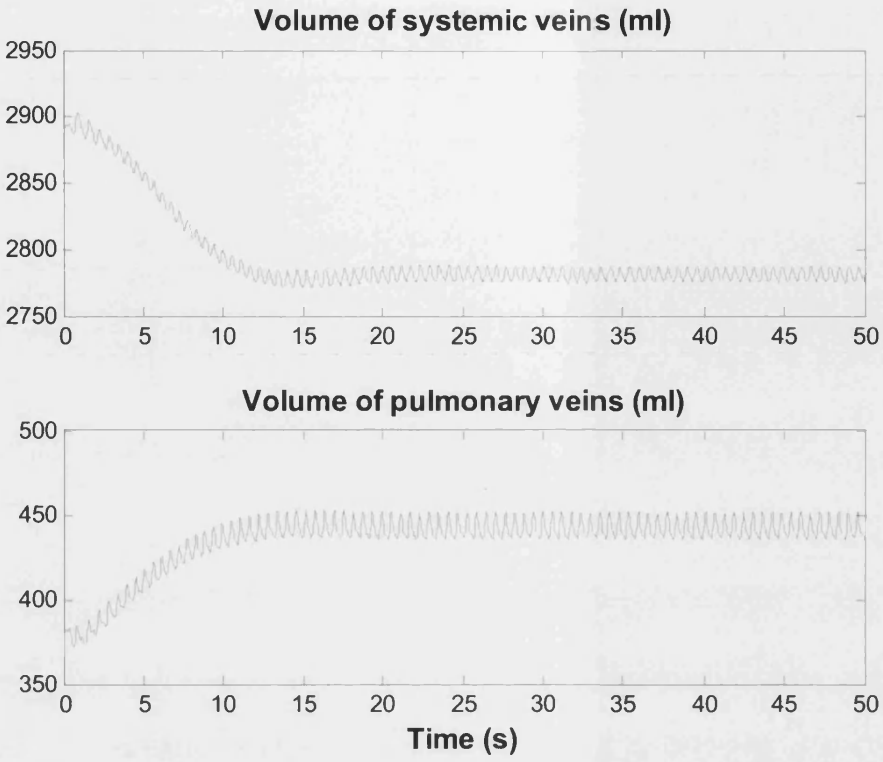

Figure 8-7 Volume of systemic veins and pulmonary veins during left heart failure

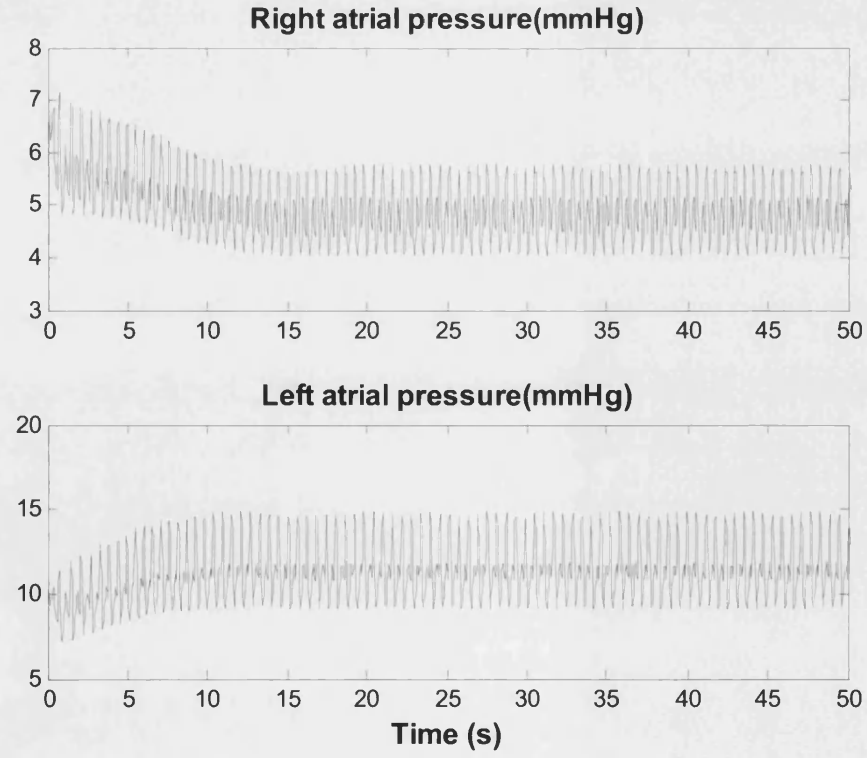

Figure 8-8 Right atrial and left atrial pressure during left heart failure

The changes of the hemodynamic parameters for a patient with severe left heart failure are shown in Table 8-2. Restricted cardiac output is an essential feature of heart failure. The heart rate increases as one of the compensatory ways of maintaining adequate cardiac output. Ventilation frequency increases due to the retarded gas exchange in the lung.

Table 8-2 Change of the hemodynamic parameters due to left heart failure

	Heart Rate (beats/min)	Cardiac Output (L/min)	Ventilation Frequency (Breaths/min)	Mean arterial pressure (mmHg)
Changes from experimental data (Hambrecht et al. 2000) and (Grassi et al. 1995)	+15~+22	-0.8 ~ -1.1	+0.9 ~ +5.3	-2.5 ~ -10.5
Model predicted changes	+20.5	-0.9	+0.8	-10.4

8.5 Exercise

The cardiovascular and respiratory adjustments in exercise consist of a combination and integration of neural and local (chemical) factors (Berne & Levy 2001). Chapter 5 shows the effect of the baroreflex on the cardiovascular system at the onset of exercise by shifting the operating point of the baroreflex and locally induced vasodilatation in the exercising muscles. The cardiopulmonary models can predict the cardiovascular and respiratory responses during exercise. For light work exercise, the O_2 uptake rate is approximately 0.9 L/min. The vascular resistance reduces to 0.6 mmHg s/ml during exercise. These values were used in the flowing simulation studies.

Figures 8-9 to 8-15 show the results predicted by the model, where the exercise starts at 50 seconds and lasts for 20 seconds. During the first few seconds of exercise, the ventilation increases rapidly before showing a slower increase over the next few seconds (Figure 8-9). When exercise is stopped, there is an immediate decrease in ventilation followed by a slower exponential decrease towards the resting value. The rapid changes in the ventilation are due to the neural mechanism (the central command

and mechanoreceptors in the skeletal muscles) while the slower changes are due to the humoral mechanism (acting via central and peripheral chemoreceptors) (Green 1990). The central command and mechanoreceptors both react to exercise very quickly. The mechanoreceptor react to vasodilatation can be modelled by decreasing the peripheral resistance based on a time constant of 5.5 seconds (Elstad et al. 2002). This is very rapid compared with the chemoreceptor response whose time constant is 30 seconds.

Figure 8-16 shows a comparison of the predicted results with the experimental data. The model initiates the exercise by changing the O_2 consumption rate of the active muscle and the muscle blood flow resistance. For this reason, experimental data obtained from passive

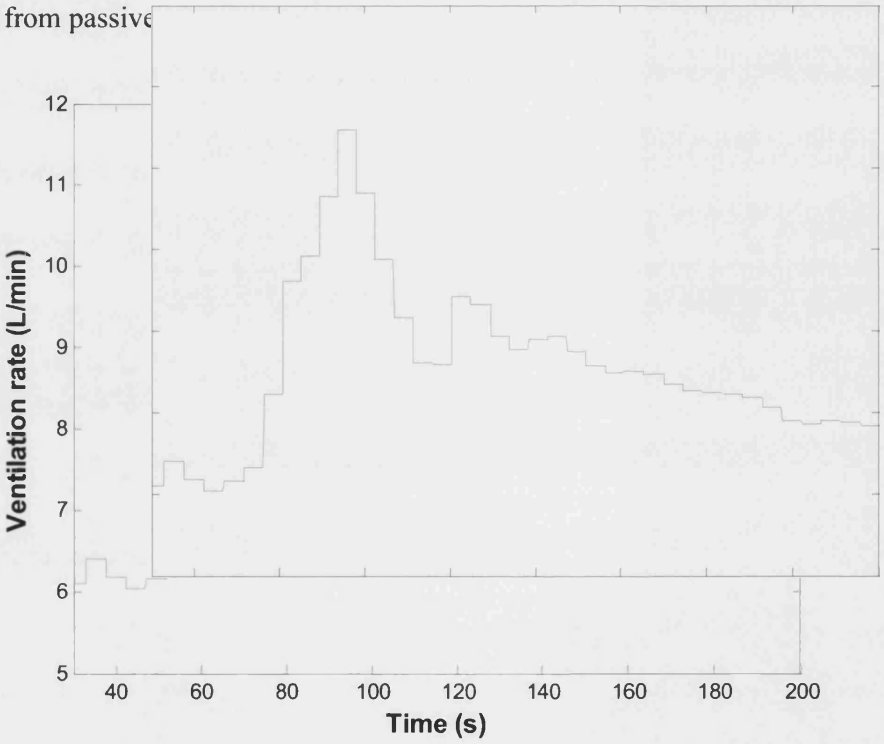

Figure 8-9 Ventilation rate before, during and after exercise

After the onset of exercise, the heart rate increases rapidly before decreasing slowly back to the resting level (Figure 8-10). Cardiac output increases during exercise (Figure 8-11). Because of the low resistance and great dispensability of the pulmonary vascular bed, the increase in pulmonary blood flow (Figure 8-12) is accompanied by only a small rise in pulmonary vascular pressure (Figure 8-13). More capillaries are opened in the lung and the area available for gas diffusion increases and, as a consequence, the diffusing capacity for both O_2 and CO_2 rises (Figure 8-14 and Figure 8-15). As can be

seen, the gas exchange in the lung is slower when responding to the exercise compared to cardiovascular responses. Even after exercise, the O_2 diffusion rate remains high to compensate for the high O_2 consumption in the active muscle during exercise.

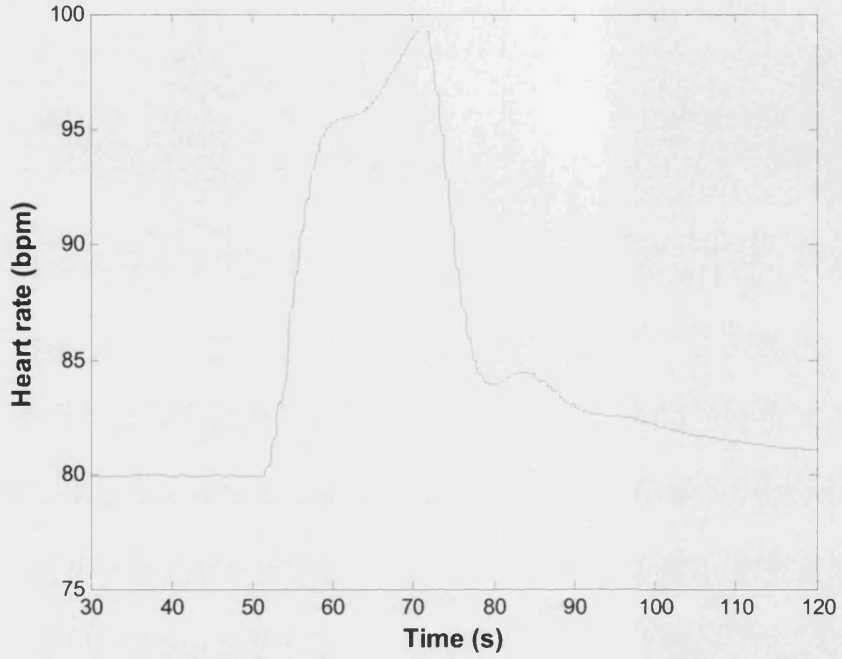

Figure 8-10 Heart rate before, during and after exercise

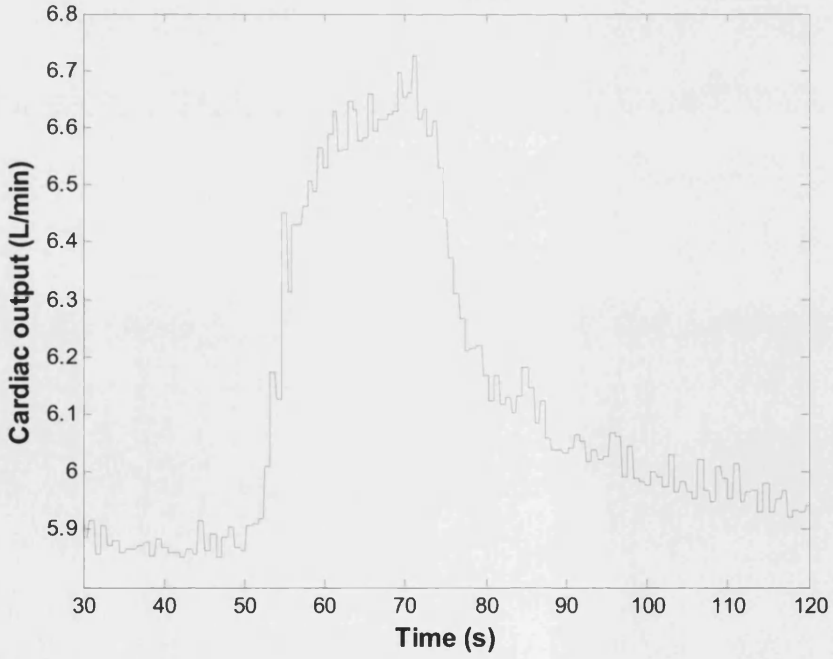

Figure 8-11 Cardiac output diffusion rate before, during and after exercise

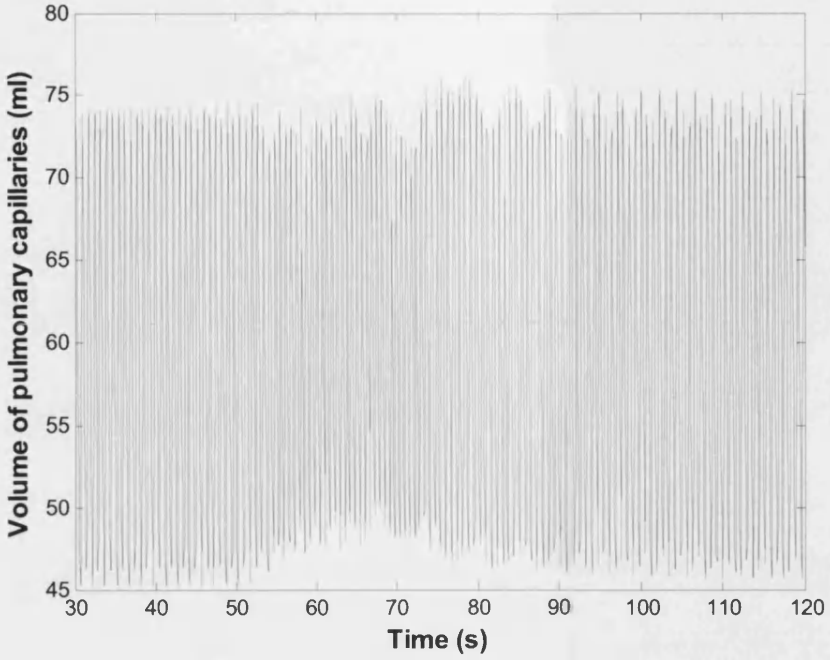

Figure 8-12 Volume of pulmonary capillaries before, during and after exercise

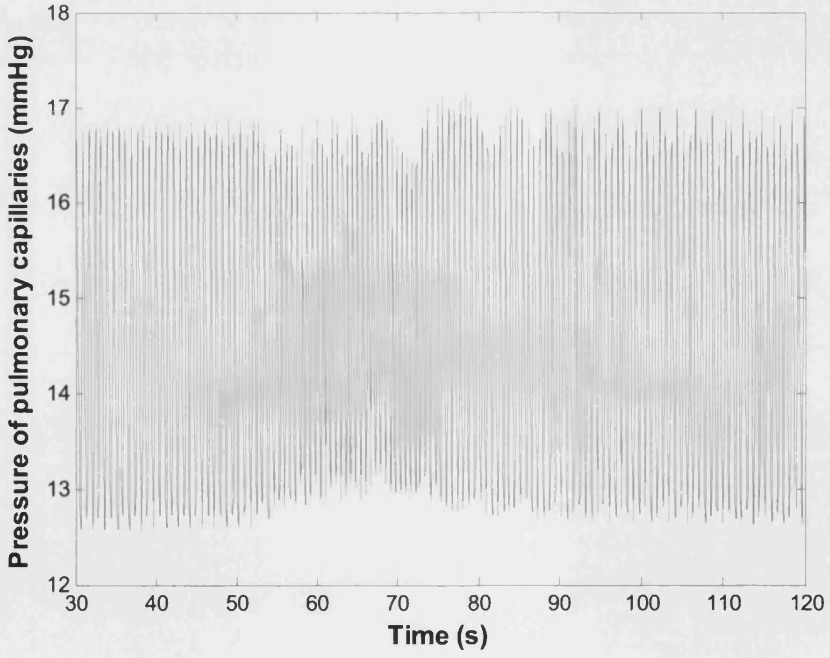

Figure 8-13 Pressure of pulmonary capillaries before, during and after exercise

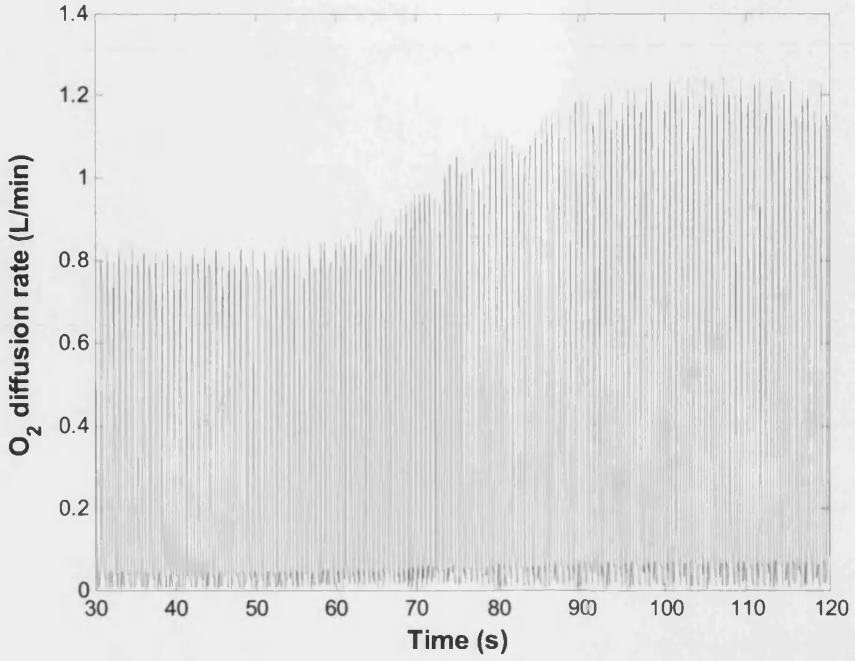

Figure 8-14 O_2 diffusion rate before, during and after exercise

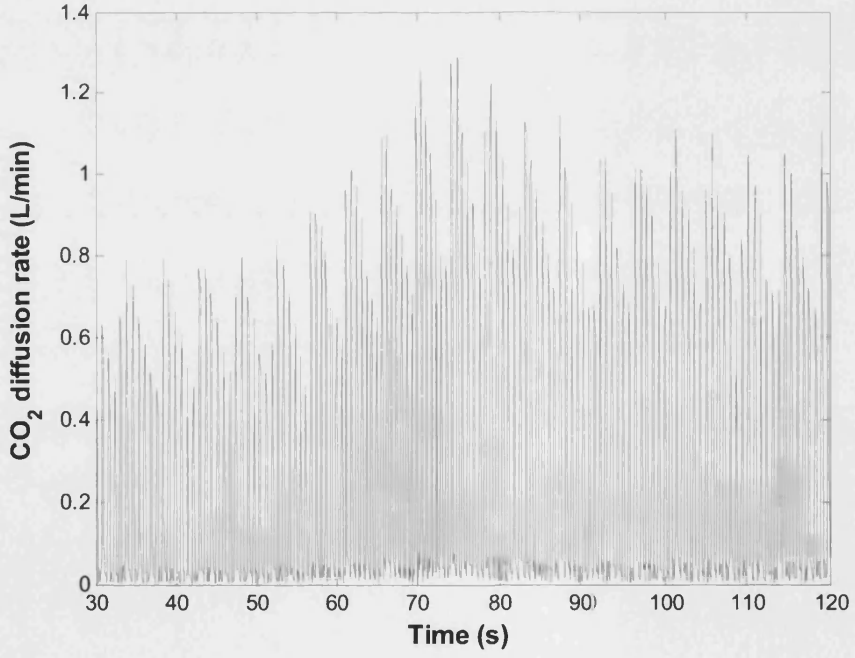

Figure 8-15 CO_2 diffusion rate before, during and after exercise

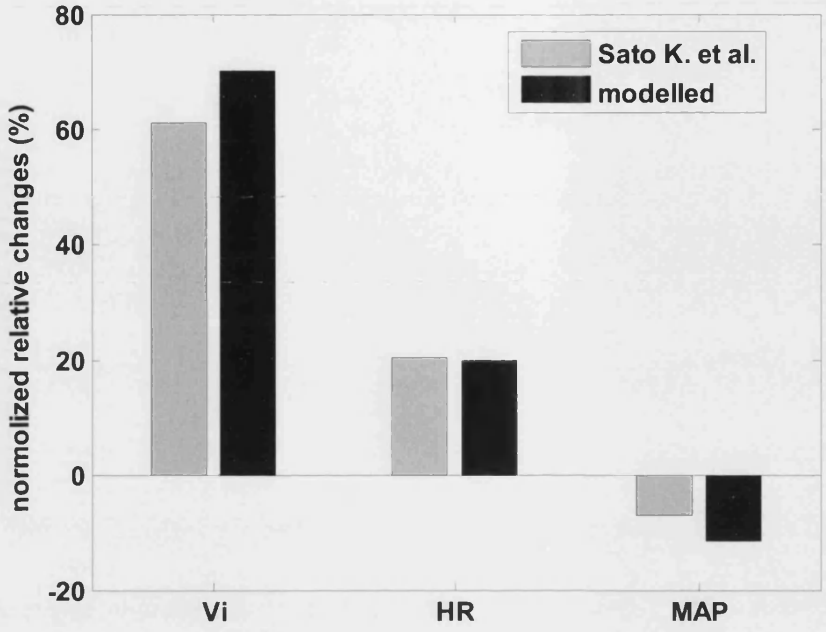

Figure 8-16 Comparison of changes of Vi (ventilation rate), HR(heart rate) and MAP (mean arterial pressure) between experiments from passive exercise (Sato et al. 2004) and model predicted

8.6 Closure

The cardiopulmonary model developed in this research has been used successfully to simulate the system responses due to respiratory and cardiovascular diseases as well as exercise.

Pulmonary capillary diffusion impairment, the common cause for a lung disease, is simulated by altering the fractional lung damage. The inequality of the ventilation/perfusion ratio caused by such damage is shown in the simulation. This shows that the single compartment lung model developed in this research is capable of modelling a diseased lung. Compared to the multi-compartment lung model, the method for the single compartment lung model presented here is more accessible because it does not require a $\dot{V}/Q$ ratio lookup table derived from experiments. Instead, this method models the cause of the disease in a physically realistic manner which is the thickening of the capillary surface. However, the method inevitably can only simulate the average value of $\dot{V}/Q$ ratio of the lung due to its single compartment nature.

The comprehensive cardiovascular model also allows the simulation of cardiovascular diseases. Mitral stenosis is one of the most common disorders in valvular heart disease. This is easily simulated by altering the mitral valve area in the heart model. The mitral flow and pressure waveforms generated by the model are close to the recordings from experiments. Furthermore, the increased ventilation rate predicted by the model indicates the main symptom of mitral stenosis dyspnea.

Acute severe left heart failure is another type of common cardiovascular disease. It can be modelled by decreasing the left heart contractility in the heart model. The blood volume re-distribution due to heart failure is clearly shown in the simulation results and the changes of the hemodynamic and respiratory parameters due to this disease are in good agreement with published data.

The cardiovascular and respiratory adjustments in exercise are easily simulated due to the inclusion of a complete regulation model. The baroreflex motivates the fast adaptation of the hemodynamic and respiratory responses while the peripheral and central chemoreflexes simulates the slower responses to exercise. The pulmonary circulation and the gas exchange process in the lung are also adjusted accordingly.

It is considered that the cardiopulmonary model can be useful in clinical demonstration and education as well as supporting research in other areas including sport sciences.

Chapter 9 Conclusions and Future Work

9.1 Conclusions

This thesis describes the development of a comprehensive mathematical model of the human cardiopulmonary system that combines respiratory and cardiovascular aspects and their associated control actions.

A review has been undertaken of the different approaches used to model the cardiovascular system. This showed a wide variation in complexity of the model and, in many cases, the application was limited to a particular physiological function or clinical disease. After establishing the important features of the cardiovascular system, a mathematical model has been developed that contains 13 segments including the blood vessels and heart chambers. The heart serves as a hydraulic pump and the vessels are distensible pipes configured in a serial and parallel arrangement. Specifically, the heart is represented by a four-chamber model and the chambers, ventricles and atria, were modelled as time-varying elastance components. The action of the heart valves was represented using Bernoulli's equation. The heart model also includes the interactions between the left and right heart together with the interventricular septum and the pericardium. Blood vessels were represented by capacitance, resistance, viscoelastance and inertance terms. The capacitance is nonlinear and represented by an exponential pressure-volume relationship. The interaction between the respiratory system and the cardiovascular system was accounted for by applying the intrathoracic pressure on the blood vessels inside the thoracic cavities.

A sensitivity study undertaken using realistic parameter values obtained from literature, provided a guide regarding the tuning of the parameter values necessary to achieve specific physiological conditions. The characteristic atrial and ventricular pressure and flow waveforms were generated by the time-varying elastance hemodynamics. The exponential pressure-volume equation effectively represents the non-linearity property of the arteries. By the inclusion of features, such as the interventricular septum, the heart valves and the pericardium, a model was developed that is capable of predicting a number of clinical or physiological phenomena. For example, valvular stenosis was modelled by changing the area of the heart valve and the shift of the ventricular pressure

was modelled by changing the effective septal elastance. The constraint of the pericardium to the heart's sudden overdistension was shown by altering the pericardial pressure. Simulations also showed the blood pressure to vary with the intrathoracic pressure. The accurate representation of the hemodynamics and the good agreement with published pressure and flow waveforms provided confidence for the incorporation of the baroreflex control model and the respiratory model.

The cardiovascular regulation system is very complex. Many models have been developed by researchers in order to understand the cardiovascular regulation system. This has mainly concentrated on modelling the baroreceptors because the baroreflex action is the most important short-term regulator for the arterial pressure and cardiovascular function. An improved baroreceptor reflex model has been developed based on a three-compartment model - afferent compartment, central compartment and efferent compartment. A sigmoid function was included in the efferent compartment to produce sympathetic and parasympathetic nerve outflow to the effector sites. The effector model for the heart rate was enhanced by including the interaction between the two autonomic nerve divisions. The baroreflex model was represented in a physiological manner and provides a clearer picture of how the baroreflex system works.

Simulation results presented show the ability of the model to predict the static and dynamic hemodynamic responses to environmental disturbances. Two open loop tests, artificial heart pacing and a drug induced blood pressure change, were performed to assess the response of the baroreflex control algorithm. Artificial heart pacing was modelled by applying an external input to the heart rate and the predicted cardiac output and stroke volume showed good agreement with published data. The biphasic changes of the cardiac output with heart rate were also demonstrated by the artificial heart pacing. Over the lower frequency range, the reduction in stroke volume was found to be proportionately less than the increase in heart rate, causing the cardiac output to increase. At high pacing frequency, the increments in heart rate decrease the cardiac output because the decrement in stroke volume exceeded the increment in heart rate over this high range of pacing frequencies. Drug induced blood pressure changes were used to assess the steady state response of the baroreceptor regulation. The relationship between the predicted heart rate and mean arterial pressure obtained had a sigmoid shape which is in line with published data.

Tests were also performed to assess the model's transient response. From the power spectrum of the generated heart rate, two peaks were found at 0.08 Hz and 0.2 Hz, both being in the frequency range observed from measured data. The low frequency value was due to the combined effect of vagal and sympathetic nerve activity while the high frequency value resulted from the influence of respiration on the cardiovascular system. The change in the peaks was useful in the evaluation of the parasympathetic and sympathetic activities. This was demonstrated by varying the gain of the two autonomic divisions. The high and low peaks of the heart rate spectrum were both more sensitive to the change of the sympathetic gain although parasympathetic outflow had a dominant effect on the heart rate control. This was caused by the sympathetic outflow having a large influence on the vascular resistance which adjusts the baroreflex input - mean arterial pressure. The influence of the respiration on the cardiovascular system was also demonstrated by simulating a Valsalva manoeuvre. The baroreceptor regulation produced a realistic arterial waveform similar to what would be expected from such a manoeuvre. Hemodynamic responses at the onset of exercise were also modelled. The predicted results showed the same trend as published experimental data and successfully demonstrated the contribution of the baroreceptor regulation during exercise.

A respiratory model was then developed and integrated with the cardiovascular model to form a complete cardiopulmonary model. The respiratory model includes the mechanics of breathing, gas exchange process and the regulation of the respiratory system. The gases passing from the nasal passageways through the trachea to the alveolar were modelled using the mass conservation equation. The lung and the trachea tree were modelled as a mechanical device and a Windkessel model. As the mechanical model gave more realistic results, this approach was used as the basic for the lung model. The gas exchange in the alveolar was assumed to take place at the end of the lung capillaries and the partial pressure of the gases reach equilibrium as soon as the blood leaves the lung capillaries. Thus the gas exchange was modelled as a continuous process. The dynamic gas transportation due to the pulsatile blood flow was modelled by including the blood volume change in each compartment. Local regulation included autoregulation of the cerebral blood flow and the global regulation of the chemoreflex were also included in the new model. The interaction between the chemoreflex and the baroreflex was accounted for according to the most recent clinical findings. The operating point of the baroreflex was reset by the stimulation of the peripheral

chemoreflex while the gain of the sympathetic nerve activity was assumed to be reset by the central chemoreceptor.

The cardiopulmonary model has been validated using a number of different test conditions. The interactions of the respiratory and cardiovascular systems including the gas exchange process, the effect of breathing on the cardiovascular system and the blood gas contents on the hemodynamics were simulated and compared to published data. The results produced by the model were in good agreement with the experimental results obtained for humans. The effects of respiration on the blood flow and the gas exchange were clearly shown in the gas partial pressure waveforms and the heart rate variations. The simulation of hypoxia and hypercapnia validates the model of the baroreflex and the chemoreflex as similar cardiac responses prediction were obtained to those found in the published data.

Possible applications of the model have been demonstrated by predicting the cardiopulmonary responses of patients with lung and cardiovascular disease, together with those of healthy people during exercise. Pulmonary capillary diffusion impairment, the common cause for a lung disease, was simulated by altering the fractional lung damage. The inequality of the ventilation/perfusion ratio caused by such damage was shown in the simulation. This confirms that the single compartment lung model is capable of representing a diseased lung. Compared to the multi-compartment lung model, the method for the single compartment lung model presented here is more accessible because it does not require a $\dot{V}/Q$ ratio lookup table derived from measurements. Instead, this approach models the cause of the disease which is the thickening of the capillary surface. However, it can only simulate the average value of $\dot{V}/Q$ ratio of the lung due to its single compartment nature.

The comprehensive cardiovascular model also allows the simulation of cardiovascular disease. Mitral stenosis is one of the most common disorders in valvular heart disease. This was simulated simply by altering the mitral valve area in the heart model. The mitral flow and pressure waveforms generated by the model were similar to the recordings from measurements on patients. Furthermore, the increased ventilation rate predicted by the model indicated the main symptom of mitral stenosis, dyspnea. Acute

severe left heart failure is another type of common cardiovascular disease. This was modelled by decreasing the left heart contractility. The blood volume re-distribution due to heart failure was shown in the simulation results and the changes of the hemodynamic and respiratory parameters due to this disease were in good agreement with published data.

The cardiovascular and respiratory adjustments in exercise were easily simulated due to the inclusion of a complete regulation model. The baroreflex motivated the fast adaptation of the hemodynamic and respiratory responses while the peripheral and central chemoreflexes simulated the slower responses to exercise. The pulmonary circulation and the gas exchange process in the lung were also adjusted accordingly.

The simulations presented in this thesis show that the cardiopulmonary model is capable of predicting the complex interactions between the cardiovascular system and the respiratory system. In general, it has the following advantages compared to other published cardiopulmonary models:

1. Both cardiovascular and respiratory models are modelled in detail which allows the interaction between the two systems to be simulated under diseases and other physiological conditions.

2. The gas exchange process is modelled as a continuous process which allows the modelling of the mismatch ventilation/perfusion ratio due to lung damage using a one-compartment lung model.

3. The advanced regulation algorithm explains the regulation of the cardiopulmonary system in a more physiological manner and allows further neuro-hormonal regulation mechanism to be easily integrated in the future.

It is considered that the cardiopulmonary model can be a useful tool in clinical demonstration and education as well as supporting research in areas including sport sciences.

9.2 Recommendations for future work

9.2.1 The cardiovascular model

The cardiovascular model does not take account of orthostatic stress. This limits the possibility to model the effects of human posture and altitude on the cardiovascular system. Including this feature should widen the scope of the model to include deep water diving and high altitude applications.

The cerebral circulation is always an important feature in local circulation studies. The cerebral circulation is simplified to be a blood vessel in the current model. However in reality, the cerebral circulation works in a very complicated manner and the cerebral autoregulation is far more complex than what it is modelled here. The current model does not include this feature because only the global circulation was of interest. It would be interesting to include the cerebral circulation and to investigate its effect on the global model. This would also extend the analysis to include the coronary circulation for the heart which supplies blood to the heart and the renal circulation which supplies blood to the kidneys.

9.2.2 The respiratory model

Although the respiratory model is comprehensive, it is difficult to model lung disease such as chronic obstructive pulmonary disease as the dead space and pulmonary shunt are assumed to remain constant. However this is not the case for a diseased lung and the values change with the end-tidal partial pressure of CO_2. Hence, future improvement could include converting these constant parameters into variables.

As the respiratory model is based on a mechanistic approach, some of the parametric data entries involve terms that are inappropriate for use by clinicians and physicians. Therefore, further effort is needed to ensure that all of the parameters are based on meaningful physiological terms.

9.2.3 The cardiopulmonary regulation model

The cardiopulmonary control model includes both baroreflex and chemoreflex models. The peripheral chemoreflex model resets the baroreflex operating point to a higher pressure without changing the baroreflex sensitivity. Currently, to researchers working in this area, whether the sensitivity is also changed by the activation of chemoreceptors is unclear. This is an area that can be addressed when more clinical data becomes available.

Large differences have been observed in clinical tests when the response to hypoxia and hypercapnia is compared in different species with spontaneous or artificially controlled ventilation. These differences suggest that the lung stretch receptors may play a primary role in the hypoxic or hypercapnia state. However, there is the possibility that these differences are caused by the anaesthetic agents used. Therefore, the effect of lung stretch receptors on the cardiovascular system is an area for further investigation.

The human thermoregulation is another interesting aspect for future study. For example, how the performance of an athlete is affected by temperature changes in the body and in the environment is an issue in sport science. During exercise, the heat produced by the fast metabolism is released by an increase in the skin blood flow and the evaporation of sweat. The ambient temperature has a large influence on the rate of heat production and sweating response. Although a model representing thermoregulation is still far from being complete, the operating point concept has been applied (Green 1990) using a similar concept to that used in the cardiopulmonary regulation model. Therefore, the inclusion of thermoregulation in the current model is feasible as the ambient temperature is included and the autonomic control algorithm already incorporates the operating point concept.

References

AL-DAHAN, M. I., LEANING, E. R., CARSON, D. W. H., & FINKELSTEIN, L. (1985). The validation of complex unidentifiable models of the cardiovascular system. *Proc.IFAC Symposium* , 1213-1218.

AVULA, X. J. & OESTREICHER, H. L. (1978). Mathematical model of the cardiovascular system under acceleration stress. *Aviat.Space Environ.Med.* 49(1 Pt. 2), 279-286.

BACCANI, B., DOMENICHINI, F., PEDRIZZETTI, G., & TONTI, G. (2002). Fluid dynamics of the left ventricular filling in dilated cardiomyopathy. *J.Biomech.* 35(5), 665-671.

BELLVILLE, J. W., WHIPP, B. J., KAUFMAN, R. D., SWANSON, G. D., AQLEH, K. A., & WIBERG, D. M. (1979). Central and Peripheral Chemoreflex Loop Gain in Normal and Carotid Body-Resected Subjects. *Journal of Applied Physiology* 46(4), 843-853.

BEN-TAL, A. (2006). Simplified models for gas exchange in the human lungs. *Journal of Theoretical Biology* 238(2), 474-495.

BENEKEN, J. & DEWIT, B. (1967). A physical approach to hemodynamic aspects of the human cardiovascular system. In *Physical Bases of Circulatory Transpport: Regulation and Exchange* (Eds E. Reeve & A. Guyton), pp. 1-45. Philadelphia: PA: Saunders.

BERNE, R. M. & LEVY, M. N. (2001). *Cardiovascular Physiology*. the United States of America: Mosby,Inc.

BERNE, R. M. & LEVY, M. N. (1988). *Physiology*. the USA: The C.V.Mosby Company.

BEYAR, R., HAUSKNECHT, M. J., HALPERIN, H. R., YIN, F. C., & WEISFELDT, M. L. (1987). Interaction between cardiac chambers and thoracic pressure in intact circulation. *AJP - Legacy* 253(5 Pt 2), H1240-H1252.

BOWMAN, A. W., FRIHAUF, P. A., & KOVACS, S. J. (2004). Time-varying effective mitral valve area: prediction and validation using cardiac MRI and Doppler echocardiography in normal subjects. *AJP - Heart and Circulatory Physiology* 287(4), H1650-H1657.

BOYERS, D. G., LUETSCHE.JA, & CUTHBERT.JG (1972). Simulation of Human Cardiovascular System - Model with Normal Responses to Change of Posture, Blood Loss, Transfusion, and Autonomic Blockade. *Simulation* 18(6), 197-206.

CHUNG, D. C., NIRANJAN, S. C., CLARK, J. W., JR., BIDANI, A., JOHNSTON, W. E., ZWISCHENBERGER, J. B., & TRABER, D. L. (1997). A dynamic model of ventricular interaction and pericardial influence. *Am.J.Physiol* 272(6 Pt 2), H2942-H2962.

COOPER, V. L., PEARSON, S. B., BOWKER, C. M., ELLIOTT, M. W., & HAINSWORTH, R. (2005). Interaction of chemoreceptor and baroreceptor reflexes by hypoxia and hypercapnia - a mechanism for promoting hypertension in obstructive sleep apnoea. *The Journal of Physiology* 568(2), 677-687.

CORNISH, K. G., BARAZANJI, M. W., YONG, T., & GILMORE, J. P. (1989). Volume expansion attenuates baroreflex sensitivity in the conscious nonhuman primate. *AJP - Legacy* 257(3 Pt 2), R595-R598.

CROSTON, R. C. & FITZJERRELL, D. G. (1974). Cardiovascular model for the simulation of exercise, lower body negative pressure, and tilt experiments. *Proceedings of the Fifth Annual Pittsburgh Conference* 5, 471-476.

CUNNINGHAM, D. J., PETERSEN, E. S., PICKERING, T. G., & SLEIGHT, P. (1972). The effects of hypoxia, hypercapnia, and asphyxia on the baroreceptor-cardiac reflex at rest and during exercise in man. *Acta Physiol Scand.* 86(4), 456-465.

DALY, M. D. B. & SCOTT, M. J. (1958). The effects of stimulation of the carotid body chemoreceptors on heart rate in the dog. *The Journal of Physiology Online* 144(1), 148-166.

DALYMDE, B., HAZZLEDINE, J. L., & HOWE, A. (1965). REFLEX RESPIRATORY AND PERIPHERAL VASCULAR RESPONSES TO STIMULATION OF THE ISOLATED PERFUSED AORTIC ARCH CHEMORECEPTORS OF THE DOG. *J.Physiol* 177, 300-322.

DAVIDSON, N. S., GOLDNER, S., & MCCLOSKEY, D. I. (1976). Respiratory modulation of barareceptor and chemoreceptor reflexes affecting heart rate and cardiac vagal efferent nerve activity. *The Journal of Physiology Online* 259(2), 523-530.

DOWNING, S. E. & SIEGEL, J. H. (1963). Baroreceptor and chemoreceptor influences on sympathetic discharge to the heart. *AJP - Legacy* 204(3), 471-479.

DU, Y. H. & CHEN, A. F. (2007). A "love triangle" elicited by electrochemistry: complex interactions among cardiac sympathetic afferent, chemo-, and baroreflexes. *Journal of Applied Physiology* 102(1), 9-10.

ELSTAD, M., TOSKA, K., & WALLOE, L. (2002). Model simulations of cardiovascular changes at the onset of moderate exercise in humans. *Journal of Physiology-London* 543(2), 719-728.

FIORE, G. B., GRIGIONI, M., DANIELE, C., D'AVENIO, G., BARBARO, V., & FUMERO, R. (2002). Hydraulic functional characterisation of aortic mechanical heart valve prostheses through lumped-parameter modelling. *J Biomech.* 35(10), 1427-1432.

FLANAGAN, T. C. & PANDIT, A. (2003). Living artificial heart valve alternatives: a review. *Eur.Cell Mater.* 6, 28-45.

FOGLIARDI, R., DI, D. M., & BURATTINI, R. (1996). Comparison of linear and nonlinear formulations of the three-element windkessel model. *Am.J.Physiol* 271(6 Pt 2), H2661-H2668.

FUNG, Y. C. (1984). *Biodynamics: Circulation.* New York: Springer-Verlag.

GRASSI, G., SERAVALLE, G., CATTANEO, B. M., LANFRANCHI, A., VAILATI, S., GIANNATTASIO, C., DEL BO, A., SALA, C., BOLLA, G. B., POZZI, M., & MANCIA, G. (1995). Sympathetic Activation and Loss of Reflex Sympathetic Control in Mild Congestive Heart Failure. *Circulation* 92(11), 3206-3211.

GREEN, J. F. & MILLER, N. C. (1973). A model describing the response of the circulatory system to acceleration stress. *Ann.Biomed.Eng* 1(4), 455-467.

GREEN, J. H. (1990). *The Autonomic Nervous System and Exercise*. Padstow, Cornwall,Great Britain: T.J.Press Ltd.

GRODINS, F. S., BUELL, J., & BART, A. J. (1967). Mathematical analysis and digital simulation of the respiratory control system. *J.Appl.Physiol* 22(2), 260-276.

GRODINS, F. S., GRAY, J. S., SCHROEDER, K. R., NORINS, A. L., & JONES, R. W. (1954). Respiratory Responses to CO2 Inhalation. A Theoretical Study of a Nonlinear Biological Regulator. *Journal of Applied Physiology* 7(3), 283-308.

GROOD, E. S., MATES, R. E., & FALSETTI, H. (1974). Model of Cardiac-Muscle Dynamics. *Circulation Research* 35(2), 184-196.

GUYTON, A. C. (1991). *Textbook of Medical Physiology*. Philadelphia: W.B. Saunders Company.

HALLIWILL, J. R., MORGAN, B. J., & CHARKOUDIAN, N. (2003). Peripheral chemoreflex and baroreflex interactions in cardiovascular regulation in humans. *The Journal of Physiology Online* 552(1), 295-302.

HAMBRECHT, R., GIELEN, S., LINKE, A., FIEHN, E., YU, J., WALTHER, C., SCHOENE, N., & SCHULER, G. (2000). Effects of Exercise Training on Left Ventricular Function and Peripheral Resistance in Patients With Chronic Heart Failure: A Randomized Trial. *JAMA: The Journal of the American Medical Association* 283(23), 3095-3101.

HELDT, T., SHIM, E. B., KAMM, R. D., & MARK, R. G. (2002). Computational modeling of cardiovascular response to orthostatic stress. *J.Appl.Physiol* 92(3), 1239-1254.

HILL, A.V. (1938). Heat of shortening and the dynamic constants of muscle. Proc.R.soc.Lond. (Biol.) 126,136-195

HIRSCH, J. A. & BISHOP, B. (1981). Respiratory sinus arrhythmia in humans: how breathing pattern modulates heart rate. *AJP - Heart and Circulatory Physiology* 241(4), H620-H629.

HORTON, S. (2001). *Bathfp Modelling of the Cardiovascular and Respiratory system*. University of Bath.

HSING-HUA, F. & KHOO, M. C. K. (2002). PNEUMA - a comprehensive cardiorespiratory model. *Volume 2* (, pp. 1533-1534.

HYNDMAN, B. W. (1972). A digital simulation of the human cardiovascular system. *Infor.J.* 10, 8-35.

ITANI, T. F. & KOUSHANPOUR, E. (1989). A mathematical Model of the Arterial Baroreceptors. Proceedings of the Annual International Conference of the IEEE Engineering in Medicine and Biology Society. pp. 289-299.

JANICKI, J. S. & WEBER, K. T. (1980). The Pericardium and Ventricular Interaction, Distensibility, and Function. *American Journal of Physiology* 238(4), H494-H503.

JARON, D., MOORE, T. W., & CHU, C. L. (1984). A cardiovascular model for studying impairment of cerebral function during +Gz stress. *Aviat.Space Environ.Med.* 55(1), 24-31.

JOHN, D. & MACARTHUR, C. T. Heart Rate Variability. http://www.macses.ucsf.edu/Research/Allostatic/notebook/heart.rate.html . 2-6-1997. 10-6-2007.

KARIM, F., HAINSWORTH, R., SOFOLA, O. A., & WOOD, L. M. (1980). Responses of the heart to stimulation of aortic body chemoreceptors in dogs. *Circ.Res.* 46(1), 77-83.

KAWADA, T., YANAGIYA, Y., UEMURA, K., MIYAMOTO, T., ZHENG, C., LI, M. H., SUGIMACHI, M., & SUNAGAWA, K. (2003). Input-size dependence of the baroreflex neural arc transfer characteristics. *American Journal of Physiology-Heart and Circulatory Physiology* 284(1), H404-H415.

KEREN, G., MEISNER, J. S., SHEREZ, J., YELLIN, E. L., & LANIADO, S. (1986). Interrelationship of mid-diastolic mitral valve motion, pulmonary venous flow, and transmitral flow. *Circulation* 74(1), 36-44.

KING, M. J., CORDEN, J., DAVID, T., & FISHER, J. (1996). A three-dimensional, time-dependent analysis of flow through a bileaflet mechanical heart valve: comparison of experimental and numerical results. *J.Biomech.* 29(5), 609-618.

KOLLAI, M., JOKKEL, G., BONYHAY, I., TOMCSANYI, J., & NASZLADY, A. (1994). Relation between baroreflex sensitivity and cardiac vagal tone in humans. *Am.J Physiol* 266(1 Pt 2), H21-H27.

KOLLAI, M. & KOIZUMI, K. (1989). Cardiac Vagal and Sympathetic-Nerve Responses to Baroreceptor Stimulation in the Dog. *Pflugers Archiv-European Journal of Physiology* 413(4), 365-371.

KONO, A., MAUGHAN, W. L., SUNAGAWA, K., HAMILTON, K., SAGAWA, K., & WEISFELDT, M. L. (1984). The use of left ventricular end-ejection pressure and peak pressure in the estimation of the end-systolic pressure-volume relationship. *Circulation* 70(6), 1057-1065.

KORNER, P. I. (1971). Integrative neural cardiovascular control. *Physiol Rev.* 51(2), 312-367.

LAI, Y. G., CHANDRAN, K. B., & LEMMON, J. (2002). A numerical simulation of mechanical heart valve closure fluid dynamics. *J.Biomech.* 35(7), 881-892.

LAUSTED, C. G. & JOHNSON, A. T. (1999). Respiratory resistance measured by an airflow perturbation device. *Physiol Meas.* 20(1), 21-35.

LEANING, M. S., PULLEN, H. E., CARSON, E. R., & FINKELSTEIN, L. (1983). Modelling a complex biological system: the human cardiovascular system. 2. Model validation reduction and development. *Transactions on Instrumentation, Measurement, and Control* 5, 87-98.

LEVY, M. N. & ZIESKE, H. (1969). Autonomic control of cardiac pacemaker activity and atrioventricular transmission. *Journal of Applied Physiology* 27(4), 465-470.

LIOY, F. & TRZEBSKI, A. (1984). Pressor effect of CO2 in the rat: different thresholds of the central cardiovascular and respiratory responses to CO2. *J.Auton.Nerv.Syst.* 10(1), 43-54.

LIU, C. H., NIRANJAN, S. C., CLARK, J. W., JR., SAN, K. Y., ZWISCHENBERGER, J. B., & BIDANI, A. (1998). Airway mechanics, gas exchange, and blood flow in a nonlinear model of the normal human lung. *J.Appl.Physiol* 84(4), 1447-1469.

LO, J. K. W. (1995). *Mathematical modelling of mixed gas breathing equipment and associated system.* University of Bath.

LU, K., CLARK, J. W., JR., GHORBEL, F. H., WARE, D. L., & BIDANI, A. (2001). A human cardiopulmonary system model applied to the analysis of the Valsalva maneuver. *Am.J.Physiol Heart Circ.Physiol* 281(6), H2661-H2679.

MARUYAMA, Y., ASHIKAWA, K., ISOYAMA, S., KANATSUKA, H., INOOKA, E., & TAKISHIMA, T. (1982). Mechanical Interactions Between 4 Heart Chambers with and Without the Pericardium in Canine Hearts. *Circulation Research* 50(1), 86-100.

MAUGHAN, W. L., SUNAGAWA, K., & SAGAWA, K. (1987). Ventricular systolic interdependence: volume elastance model in isolated canine hearts. *AJP - Legacy* 253(6 Pt 2), H1381-H1390.

MCKINLEY, M. & O'LOUGHLIN, V. (2005). *Human Anatomy.* McGraw-Hill Science.

MELBIN, J., DETWEILER, D. K., RIFFLE, R. A., & NOORDERGRAAF, A. (1982). Coherence of Cardiac-Output with Rate Changes. *American Journal of Physiology* 243(4), H499-H504.

MELCHER, A. & DONALD, D. E. (1981). Maintained ability of carotid baroreflex to regulate arterial pressure during exercise. *AJP - Heart and Circulatory Physiology* 241(6), H838-H849.

MELCHIOR, F. M., SRINIVASAN, R. S., & CHARLES, J. B. (1992). Mathematical modeling of human cardiovascular system for simulation of orthostatic response. *AJP - Legacy* 262(6 Pt 2), H1920-H1933.

MIGLIAVACCA, F., PENNATI, G., DUBINI, G., FUMERO, R., PIETRABISSA, R., URCELAY, G., BOVE, E. L., HSIA, T. Y., & DE LEVAL, M. R. (2001). Modeling of the Norwood circulation: effects of shunt size, vascular resistances, and heart rate. *AJP - Heart and Circulatory Physiology* 280(5), H2076-H2086.

NEUMANN, P. & HEDENSTIERNA, G. (2001). Ventilation-perfusion distributions in different porcine lung injury models. *Acta Anaesthesiologica Scandinavica* 45(1), 78-86.

OIKAWA, S., HIRAKAWA, H., KUSAKABE, T., NAKASHIMA, Y., & HAYASHIDA, Y. (2005). Autonomic cardiovascular responses to hypercapnia in conscious rats: the roles of the chemo- and baroreceptors. *Auton.Neurosci.* 117(2), 105-114.

PATTERSON, J. L., JR., GOETZ, R. H., DOYLE, J. T., WARREN, J. V., GAUER, O. H., DETWEILER, D. K., SAID, S. I., HOERNICKE, H., MCGREGOR, M., KEEN, E. N., SMITH, M. H., JR., HARDIE, E. L., REYNOLDS, M., FLATT, W. P., & WALDO, D. R. (1965). Cardiorespiratory dynamics in the ox and giraffe, with comparative observations on man and other mammals. *Ann.N.Y.Acad.Sci.* 127(1), 393-413.

PENNATI, G., BELLOTTI, M., & FUMERO, R. (1997). Mathematical modelling of the human foetal cardiovascular system based on Doppler ultrasound data. *Med.Eng Phys.* 19(4), 327-335.

PENNATI, G., FIORE, G. B., LAGANA, K., & FUMERO, R. (2004). Mathematical modeling of fluid dynamics in pulsatile cardiopulmonary bypass. *Artif.Organs* 28(2), 196-209.

PETZOLD, L. (1983). Automatic Selection of Methods for Solving Stiff and Nonstiff Systems of Ordinary Differential-Equations. *Siam Journal on Scientific and Statistical Computing* 4(1), 136-148.

PITSIKOULIS, C., GATES, G. J., BARTELS, M., & DEMEERSMAN, R. (2007). The central chemoreceptor contribution to autonomic outflow. *The FASEB Journal* 21(6), A921-A92a.

POTTER, E. K. (1981). Inspiratory inhibition of vagal responses to baroreceptor and chemoreceptor stimuli in the dog. *The Journal of Physiology Online* 316, 177-190.

RAJABALLY, T. E. (1999). *BATHfp Modelling of the Human Heart and In-Flight Respiration Simulation.* University of Bath.

ROTHE, C. F., MAASS-MORENO, R., & FLANAGAN, A. D. (1990). Effects of hypercapnia and hypoxia on the cardiovascular system: vascular capacitance and aortic chemoreceptors. *Am.J.Physiol* 259(3 Pt 2), H932-H939.

ROWELL, L. B. & OLEARY, D. S. (1990). Reflex Control of the Circulation During Exercise - Chemoreflexes and Mechanoreflexes. *Journal of Applied Physiology* 69(2), 407-418.

RUSHMERE, R. F. (1970). *Cardiovascular Dynamics.* London: W.B. Saunders Company.

SATO, K., MATSUO, H., KATAYAMA, K., ISHIDA, K., HONDA, Y., KATSUMATA, K., & MIYAMURA, M. (2004). Ventilatory and circulatory responses at the onset of voluntary exercise and passive movement in sprinters. *Eur.J.Appl.Physiol* 92(1-2), 196-203.

SEGERS, P., VERDONCK, P., StERGIOPULOS, N., WESTERHOF, N., WOUTERS, P., and KOLH, P. (2003). Systematic and pulmonary hemodynamics assessed with a lumped-parameter heart-arterial interaction model. Journal of Engineering Mathematics, 47(3-4), 185-199.

SHERWOOD, L. (2001). *Human Physiology: From Cells to Systems.* Pacific Grove, CA: Brooks/Cole (Thomson Learning).

SIMMONS, G. H., MANSON, J. M., & HALLIWILL, J. R. (2007). Mild central chemoreflex activation does not alter arterial baroreflex function in healthy humans. *J.Physiol* 583(Pt 3), 1155-1163.

SNYDER, M. F. & RIDEOUT, V. C. (1969). Computer simulation studies of the venous circulation. *IEEE Trans.Biomed.Eng* 16(4), 325-334.

SOMERS, V. K., MARK, A. L., & ABBOUD, F. M. (1991). Interaction of baroreceptor and chemoreceptor reflex control of sympathetic nerve activity in normal humans. *J.Clin.Invest* 87(6), 1953-1957.

STYS, A. & STYS, T. (1998). Current clinical applications of heart rate variability. *Clinical Cardiology* 21(10), 719-724.

SUD, V. K., SRINIVASAN, R. S., CHARLES, J. B., & BUNGO, M. W. (1993). Mathematical modelling of the human cardiovascular system in the presence of stenosis. *Phys.Med.Biol.* 38(3), 369-378.

SUGA, H. (1971). Theoretical Analysis of A Left-Ventricular Pumping Model Based on Systolic Time-Varying Pressure/Volume Ratio. *Ieee Transactions on Biomedical Engineering* BM18(1), 47-&.

SUGAWARA, M., KAJIYA, R. D., KITABATAKE, A., & MATASUO, H. (1989). *Blood Flow in the heart and Large Vessels.* Tokyo: Springer-Verlag.

SUN, Y. (1991). Modeling the dynamic interaction between left ventricle and intra-aortic balloon pump. *AJP - Legacy* 261(4 Pt 2), H1300-H1311.

SUN, Y., BESHARA, M., LUCARIELLO, R. J., & CHIARAMIDA, S. A. (1997). A comprehensive model for right-left heart interaction under the influence of pericardium and baroreflex. *Am.J.Physiol* 272(3 Pt 2), H1499-H1515.

SUN, Y. & GEWIRTZ, H. (1988). Estimation of intramyocardial pressure and coronary blood flow distribution. *AJP - Legacy* 255(3 Pt 2), H664-H672.

SUN, Y., SJOBERG, B. J., ASK, P., LOYD, D., & WRANNE, B. (1995). Mathematical model that characterizes transmitral and pulmonary venous flow velocity patterns. *AJP - Legacy* 268(1 Pt 2), H476-H489.

TAMAI, J., NAGATA, S., AKAIKE, M., ISHIKURA, F., KIMURA, K., TAKAMIYA, M., MIYATAKE, K., & NIMURA, Y. (1990). Improvement in mitral flow dynamics during exercise after percutaneous transvenous mitral commissurotomy. Noninvasive evaluation using continuous wave Doppler technique. *Circulation* 81(1), 46-51.

TANG, Y., TURNER, M. J., & BAKER, A. B. (2005). Effects of alveolar dead-space, shunt and V/Q distribution on respiratory dead-space measurements. *British Journal of Anaesthesia* 95(4), 538-548.

TENVOORDE B.J. & KINGMA R. (2000). A baroreflex model of short term blood pressure and heart rate variability. *Stud Health Technol Inform* 71, 179-200.

THOMSON HEALTHCARE. Heart valve disease. http://www.pdrhealth.com/patient_education/BHG01CA16.shtml . 2004.

TILLEY, D. G., MILES, A. W., MURPHY, C. M., BROOK, B. S., WILSON, A. J., & BREEN, D. Computer Modelling of the Human Respiratory system in Adult Intensive Care,I-Mathematical Modelling. 2006. Unpublished Work

TJEN, A. L., BONHAM, A., & LONGHURST, J. (1997). Interactions between sympathetic and vagal cardiac afferents in nucleus tractus solitarii. *AJP - Heart and Circulatory Physiology* 272(6), H2843-H2851.

TOMLINSON, S. P., LO, J., & TILLEY, D. G. (1993). Time Transient Gas-Exchange in the Respiratory System. *Ieee Engineering in Medicine and Biology Magazine* 12(3), 64-70.

TOMLINSON, S. P., LO, J. K. W., & TILLEY, D. G. (1994a). Computer simulation of human interaction with underwater breathing equipment. *Proceedings of the Institution of Mechanical Engineers, Part H: Journal of Engineering in Medicine* 208(4), 249-261.

TOMLINSON, S. P., TILLEY, D. G., & BURROWS, C. R. (1994b). Computer-Simulation of the Human Breathing Process. *Ieee Engineering in Medicine and Biology Magazine* 13(1), 115-124.

TOSKA, K. & ERIKSEN, M. (1994). Peripheral Vasoconstriction Shortly After Onset of Moderate Exercise in Humans. *Journal of Applied Physiology* 77(3), 1519-1525.

TSAKIRIS, A. G., GORDON, D. A., PADIYAR, R., & FRECHETTE, D. (1978). Relation of mitral valve opening and closure to left atrial and ventricular pressures in the intact dog. *AJP - Legacy* 234(2), H146-H151.

URSINO, M. (2000). Modelling the interaction among several mechanisms in the short-term arterial pressure control. *Stud Health Technol Inform* 71, 139-161.

URSINO, M. & MAGOSSO, E. (2003). Role of short-term cardiovascular regulation in heart period variability: a modeling study. *American Journal of Physiology-Heart and Circulatory Physiology* 284(4), H1479-H1493.

URSINO, M., MAGOSSO, E., & AVANZOLINI, G. (2001a). An integrated model of the human ventilatory control system: the response to hypercapnia. *Clinical Physiology* 21(4), 447-464.

URSINO, M., MAGOSSO, E., & AVANZOLINI, G. (2001b). An integrated model of the human ventilatory control system: the response to hypoxia. *Clinical Physiology* 21(4), 465-477.

VANDER, A., SHERMAN, J., & LUCIANO, D. (2001). *Human Physiology: The Mechanisms of Body Function.*

WAGNER, P. D. & WEST, J. B. (1972). Effects of diffusion impairment on O 2 and CO 2 time courses in pulmonary capillaries. *Journal of Applied Physiology* 33(1), 62-71.

WALGENBACH, S. C. & DONALD, D. E. (1983). Inhibition by Carotid Baroreflex of Exercise-Induced Increases in Arterial-Pressure. *Circulation Research* 52(3), 253-262.

WARNER, H. R. & COX, A. (1962). A mathematical model of heart rate control by sympathetic and vagus efferent information. *Journal of Applied Physiology* 17(2), 349-355.

WARNER, H. R. & RUSSELL, R. I. C. H. (1969). Effect of Combined Sympathetic and Vagal Stimulation on Heart Rate in the Dog. *Circulation Research* 24(4), 567-573.

WEST, J. B. & WAGNER, P. D. (1977). Pulmonary Gas Exchange. In *Bioengineering aspects of the lung* (Ed J. B. West), pp. 361-457: Marcel Dekker, Inc.

YAMAMOTO, W. S. (1978). A mathematical simulation of the hyperneas of metabolic CO2 production and inhalation. *Am.J.Physiol* 235(5), R265-R278.

YAMAMOTO, W. S. (1980). Computer simulation of ventilatory control by both neural and humoral CO2 signals. *Am.J.Physiol* 238(1), R28-R35.

ZACEK, M. & KRAUSE, E. (1996). Numerical simulation of the blood flow in the human cardiovascular system. *J Biomech.* 29(1), 13-20.